The Use of Thermal Modelling in Improving Rural Subsistence Aquaculture

by

Dylan Francis Bailey

Submitted in fulfilment for the requirements for the degree *Magister Scientiæ* in the Faculty of Science at the Nelson Mandela Metropolitan University

Submitted on: 5 January 2007

Supervisor: Dr. P. E. D. Winter

Zoology Department

Abstract

There has been a long history of attempts to promote subsistence rural aquaculture within South Africa. Many of these attempts have failed due to inadequate support from government and support agencies. There has been a recent revived interest in promoting rural aquaculture development. Presented in this project are six scenarios demonstrating the potential application of thermal modelling techniques to improving subsistence rural aquaculture. These scenarios were based on a model validated against a real life system, and run with environmental data for the year 2005. Bovine manure, grass thatch, cereal straw and *Typha* spp. water reeds were tested for thermal performance. These results were then applied to the scenarios. The open and kraal enclosed pond scenarios yielded the widest deviation in temperatures throughout the year, with an average temperature of 3.8^{o}C and 6.0^{o}C above ambient and a temperature range of 10.6^{o}C and 12.4^{o}C for the year respectively. Eliminating solar radiation and reducing wind speed resulted in an average difference of 1.5^{o}C below ambient and a temperature range of 7.5^{o}C for the year. When completely enclosed in a well-sealed traditional Xhosa style hut, the pond had an average difference of 5.6^{o}C below outside ambient temperature, with a range of 7.8^{o}C for the year. A passive solar heating scenario added to the sealed hut scenario, which when run continuously maintained an average difference of 34.7^{o}C above outside ambient temperatures, with a range of 56^{o}C for the year. When a hypothetical 25^{o}C temperature control was included in the model, the system maintained an average of 7.1^{o}C above ambient outside temperatures, with a temperature range of 0.8^{o}C throughout the year. The wider range of temperatures made available through the use of thermal modelling approaches provides a more diverse range of species available for subsistence rural aquaculture at any site, significantly improving its potential.

Key Words: Thermal; Modelling; Subsistence; Rural; Aquaculture; Temperature; MatLab

Table of Contents

The Use of Thermal Modelling in Improving Rural Subsistence Aquaculture

1. Introduction

1.1. Aquaculture in Africa: The Cottage Fallacy

Aquaculture in South Africa is still an emerging technology. South Africa's contribution to the industry is some 5% of Africa's total, which in turn contributes 0.56% to that of the world total. Aquacultural development in sub-Saharan Africa has been hindered because of lack of appropriate skills and resources, relatively large expense when compared to traditional farming techniques and general lack of African-oriented techniques and technology (Hecht 1995).

Anthropogenic development is increasing the pressure put on natural resources. As these resources become exhausted there will be a growing demand for alternative sources of nutrition. Aquaculture is poised to be the next major source of protein during the course of the 21st century. Unfortunately, Africa's current rate of aquaculture development compared to the rate of human population expansion does not appear very promising from this aspect. There have been many attempts to introduce aquaculture and aquaculture techniques to sub-Saharan African rural communities but the majority of these efforts have been in vain. Hecht (1995) and Hecht and Britz (1990) have pointed out that the problems with foreign aided aquaculture development centre on the lack of understanding by the general international community of the rural situation that exists in sub-Saharan Africa. They have shown that small-scale rural subsistence ventures are unfeasible since they will always ultimately run at a loss, although their primary aim was to provide a source of alternative protein for rural family nutrition (the cottage fallacy). It has been shown that since the motivation by governments or participating organizations to develop small-scale rural set-ups to a more viable commercial scale is ineffective, the ventures either run at a loss or cease to operate. Reasons for the ineffectiveness of rural aquaculture include lack of

skills and development, inefficiencies of small scale aquaculture farms, profit or sustenance output does not balance with resource inputs, output fluctuates and is not guaranteed, and purchased sustenance is cheaper and more readily available. If successful, however, these ventures can provide job opportunities and access to essential skills and training.

1.2. Subsistence rural aquaculture improvement using thermal modelling

The foremost critical factor in any aquaculture system is temperature. This parameter is the single most important factor in selecting species for culture and is a strong governor of productivity (Huguenin and Colt 1989; Zhu, Wang and Deltour 2000; Klemetson and Rogers 1985). In this study the use of thermal modelling to improve the potential of aquaculture ventures in rural areas is investigated. Through effective thermal modelling it may be possible to reduce energy and resource requirements for aquaculture developments both in the initial set up stages as well as during the long term. Thermal modelling has been used previously in rural aquaculture assessments, although primarily for determining suitable site locations in areas with little or no available data (Kapetsky and Nath, 1997).

Thermal models were developed that aided in determining the thermal performance of selected organic materials available to rural farmers, and determining the thermal performance of aquaculture ponds in various scenarios. These scenarios included:

- Open ponds
- Ponds sheltered from wind
- Ponds sheltered from wind and sun
- Ponds enclosed in a sealed structure, sheltered from wind, sun and ambient temperature
- Ponds with solar heating

The sealed structures represented traditional Xhosa-style huts, which are traditionally constructed using thatch for the roofing, wattle and daub, water

reed or straw for the wall fillings and mud and manure mixtures to seal the walls. The Xhosa-style traditional structure scenarios were not intended to reflect actual potential set-ups as described, but rather to demonstrate the effectiveness of utilizing rural technologies for aquaculture. Xhosa-style traditional structures provide a convenient source of data, and together with the models demonstrated in this project, illustrate the potential of blending modern aquaculture approaches with traditional rural techniques. The final engineering application of these techniques to physical set-ups is beyond the scope of this project, but through the results of these models can be shown to be a potentially viable approach.

Models were developed in the MatLab computing environment. Materials were tested in a specially constructed environment and measured using a known thermal system model of that environment. This process was also used to develop the basic theory for the final thermal models.
Although the primary aim of this project was to investigate modelling techniques to aid in viability analysis and construction considerations in rural aquaculture situations, the outcomes of the project will no doubt yield benefits in other facets of rural or self-subsistence life. The project concentrated primarily on the use of materials of organic origin that are abundant in rural areas and which have not fallen under the scope of previous aquaculture-related thermal modelling projects.

1.3. Traditional Construction Materials in Rural Life

Materials were selected based on background literature reviews on materials accessible to rural communities with some form of use in traditional architecture.

- Cow Manure
- Cereal Straw
- Thatch (Elephant Grass)
- Water Reed (*Typha* spp)

Cattle manure is known to have been used in traditional building in southern Africa since before the 1600's (Walton 1956), although primarily as a reinforcing agent for clay housing. Cattle manure is usually very fibrous in nature, owing primarily to the indigestible nature of the cellulose, lignins, and crude fibre in their diet (van Soest 1982). This distinct characteristic of herbivorous manure gives it a high thermal insulative property. The thermal performance, however, will vary according to the type of digestion within the animal (rumination, fermentation), and the types of vegetable matter ingested.

Walton (1956) gives an account of traditional life amongst Sotho-Tswana and Bantu tribes. The traditional construction of huts amongst these tribes consists primarily of mud walls reinforced with cow manure for strength. The roof is thatched using elephant grass or woven reeds. Some original settlements had rock rubble walls that were plastered with a clay / manure mixture which is renewed periodically. The thickness of these walls varies from 22 to 30 inches. This is gradually thickened during the course of renewals.

Spence and Cook (1983) reviewed traditional building techniques in 3rd world developing countries with emphasis on selection of locally available material for building purposes. Of particular relevance are the materials and methods employed in the construction of sub-saharan African architecture:

1. Mud and sticks used for walls, floors and roofs
2. Grass thatch (Elephant Grass) for walls and roofs, lasts up to 25 years
3. Timber walls and roofs
4. Bamboo and split bamboo supporting framework
5. Tree branch pole supporting framework
6. Bush/water reeds (*Phragmites*) walls and roofs, lasts up to 70 years

Common thatching materials include water reed (*Phragmites sp.*), cereal straws (oats, barley, wheat and rye), and Elephant grass (West 1987, Spence and Cook 1983). Thatch is regarded as an excellent insulator of heat.

2. Thermal Modelling Approach

2.1. Theory of Heat Transfer and Heat Transfer Modelling

The following descriptions were adopted from Cengel (2002), Rohsenow and Choi (1961), Brown and Marco (1958), Jakob and Hawkins (1957), and Incropera and DeWitt (2002).

2.1.1. Thermal Modelling Techniques

In thermal modelling approaches, real world problems are broken into smaller more manageable systems or compartments. For example, a wall of several layers is broken down into each layer, and then the properties of each layer are defined along with its thermal behaviour. These compartments are then assembled once again numerically and then tested. Various scenarios can be run on the models to determine their thermal performance, and conclusions drawn on calculated prediction.

2.1.1.1. Steady-state and transient-state modelling

The movement of thermal energy within space and time can be modelled using several methods. Heat transfer can be described in either its "steady-state" or "transient-state". In the "steady-state" the inputs and outputs of thermal energy and temperatures are constant. In this state, the system in question has attained its energy equilibrium, whereby all of the inputs and outputs have balanced and no further changes will occur. This method is useful as simple numeric calculations can be used in modelling the thermal performance of materials in their intended end application.

In the "transient-state", the system is undergoing continuous change over time. The inputs and outputs may vary as a function of time and temperature. In practice, a system is never at rest, and in transient thermal modelling a thermal balance can theoretically never be achieved. For example, a temperature in a compartment of a system with steady inputs and outputs may approach a final steady-state temperature, but will do so at an exponentially decaying rate. Mathematically, the temperature will reach its final steady-state temperature as time approaches infinity. For practical

reasons a boundary condition or limit is drawn, based on the slope of the tangent to the temperature profile, to define when the temperature has reached its steady state.

2.1.1.2. Representations of thermal models

It is often convenient to describe models or processes in a graphic format. This makes a system easier to comprehend and allows for broader understanding of the intended outcome of the model. A convenient method for representing thermal systems which is particularly popular is an "R-C Thermal Network". This approach breaks thermal behaviour down into its two most basic processes: Storage and Flux.

Storage of thermal energy occurs when a compartment accumulates energy, much like a canister of collecting water. This compartment will have a finite storage capacity dependent on its properties. This behaviour is not unlike an electrical capacitor that accumulates electrical energy over time.

Flux of thermal energy occurs when energy is transported between compartments. This flux is often determined by the thermal properties of the compartment and the amount of energy stored in the two adjacent compartments, defined as the potential gradient or difference between compartments. This behaviour is not unlike an electrical resistor, which limits the amount of current passing through it depending on the potential difference on either side.

These concepts put forward an important analogy, thermal and electrical capacitors, and thermal and electrical resistors. These concepts can be applied to graphic representations of such systems, resulting in the classic "R-C" or Resistor-Capacitor Thermal Network Model, as represented in Figure 2.1.

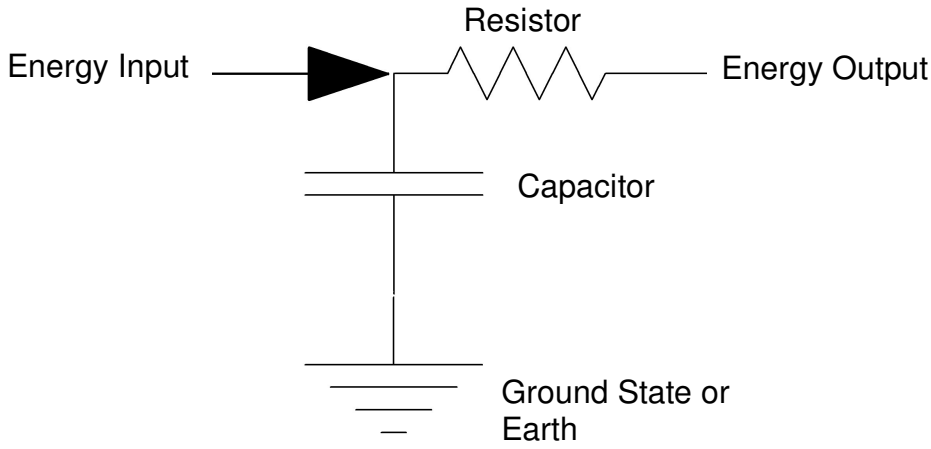

Figure 2.1 - Classic representation of the R-C Thermal Network Model

The earth symbol represents the systems relative potential to the "ground state". This is the state the system would attain if all inputs and outputs are removed and the system lost all of its positive energy potential. In most thermal modelling cases this represents the ambient environment in which that system is located. It often also represents absolute zero, as this is the theoretical ground state of the universe in a thermodynamics sense.

2.1.1.3. Compartment Lumping

Many thermal systems are complex in nature. Representing these systems mathematically can be complex and often impractical. A convenient method for reducing the complexity of the system is through a process known as "lumping". This involves combing the properties of similar materials in sequential contact with each other. Resistances can be added in series and capacitances can be added in parallel. The result is a cumulative number for resistance and capacitance. This can only apply to similar materials in contact with each other, in most cases only solids. It can be applied to gases and liquids, but only in a few cases, and is often not advisable due to the complexity of thermal interactions in fluids.

2.1.2. General Heat Transfer Theory

2.1.2.1. Thermal Conductivity

Thermal conduction is the flow or transfer of thermal energy by molecular motion within a single body or between two distinct bodies in contact with each other. Thermal resistance is the reciprocal of thermal conduction. The rate of conduction is determined by the difference in temperature and conductivity of the body, as defined within the Fourier equation:

$$q = -kA\frac{dt}{dL}$$

where:

q is the rate of heat transmission in *W*
k is the thermal conductivity of the material in *W/m.K*
A is the area of the material in m^2
dt is the temperature difference between the two sides of the material in *K*
dL is the length or thickness of the material in *m*

2.1.2.2. Thermal Capacity

Thermal capacity is the amount of thermal energy a given body can hold per unit of temperature change, measured as unit energy per unit temperature (*J/K*). The specific heat capacity of a substance is the amount of thermal energy a given material of a specific mass (the product of volume and density) can hold per unit of temperature change, measured as unit energy per unit mass per unit temperature (*J/kg.K*).

2.1.2.3. Thermal Diffusivity

Thermal diffusivity is the rate of change in temperature a given body will experience given the rate of thermal conduction and its thermal capacity. The thermal diffusivity of a given body is determined by the dividend of the thermal conductance and the product of the specific heat and material density:

$$\alpha = \frac{k}{\rho.C_p}$$

where:

α is the thermal diffusivity in $J/m^2.s$
k is the thermal conductivity in *W/m.K*
ρ is the density of the material in kg/m^3
C_p is the specific heat of the material in *J/kg.K*

2.1.2.4. Thermal Radiation

Thermal radiation is a phenomenon identical to the emission of light. Radiant energy is a form of electromagnetic wave motion, and is significant over all wavelengths. During radiation thermal energy is transferred through empty space in the form of electromagnetic radiation. The Stefan-Boltzmann law determines the amount of thermal radiation that is transmitted by a black body at a given temperature, known as *emissivity*:

$$e_b = \sigma T^4$$

where:

e_b is the energy emitted by a black body in W/m^2
σ is the *Stefan-Boltzmann* constant: $5.67 \times 10^{-8}\ W/m^2.K^4$
T is the temperature of the body in K

This law also determines the amount of thermal radiation a given object will absorb at a specific temperature, known as *absorptivity*.

2.1.3. Fluid Dynamics

2.1.3.1. Properties of fluids

Heat transfer in fluids behaves very differently to that of heat transfer in solids, due to the motility of the fluid molecules. There are several important physical properties of fluids that distinguish their behaviours in a given system. In addition to thermal conductivity, specific heat and thermal diffusivity, these are:

1. **Density (ρ):** The mass of fluid contained in a given volume, measured as unit mass per unit volume: kg/m^3
2. **Viscosity:** The ability of the fluid to resist shear deformation due to cohesion and interaction between molecules. This determines the rate at which a fluid can free flow.
    a. The **Coefficient of Dynamic Viscosity (μ)** is the shear force per unit area required to move a layer of fluid of a given unit velocity past another layer a unit distance away, measured as unit mass per unit length per unit time: *kg/m.s*

   b. The **Kinematic Viscosity (ν)** is the ratio of dynamic viscosity to mass density, measured in unit area per unit time: m^2/s
3. **Coefficient of Thermal Expansion (β):** The change in density caused by molecular expansion as a function of temperature at a constant pressure.

2.1.3.1.1. Convection

As a given body is heated, its density becomes less as it expands. With fluids, this process increases the buoyancy of the fluid, which is pushed upwards as it is displaced by denser fluids, resulting in a thermally induced flow called convection.

2.1.3.1.2. Boundary Layer

As fluid passes over a given surface, a film will develop between the main stream and the surface. The film will be almost stationary where it is in direct contact with the surface, and its velocity will increase with distance from the surface, until it reaches the velocity of the main fluid stream. The characteristics of this film are determined by the nature of the fluid such as its viscosity and flow characteristics.

2.1.3.2. Dimensionless Numbers

Certain physical behaviours of fluids affecting heat transfer have been explored experimentally and summarised using various dimensionless numbers, named after their respective founders. Since these numbers are dimensionless, they can be applied to problems of any dimension. There are five important dimensionless numbers related to heat transfer:

1. Reynolds Number
2. Grashof Number
3. Prandtl Number
4. Rayleigh Number
5. Nusselt Number

2.1.3.2.1. Reynolds Number

The Reynolds number demonstrates the turbulent behaviour of fluids at a given boundary layer at various velocities during forced convection, which is determined by the ratio of inertia forces to viscous forces:

$$\mathrm{Re} \approx \frac{\rho V L}{\mu}$$

where:

Re is the dimensionless Reynolds Number
ρ is the density of the fluid in kg/m^3
V is the velocity of the fluid in *m/s*
L is the characteristic length of the boundary surface in *m*
μ is the Coefficient of Dynamic Viscosity in *kg/m.s*

At low *Re* values, viscous forces keep disturbances within the boundary layer small and the flow remains fairly laminar. At larger values of *Re*, inertia forces begin to overwhelm viscous forces and larger disturbances develop within the boundary layer, thus increasing the turbulence of the flow. The point at which laminar flow changes to turbulent flow is regarded as the *critical Reynolds number*. The Reynolds number also significantly influences the boundary layer, causing it to decrease in thickness as *Re* increases.

2.1.3.2.2. Grashof Number

The Grashof number demonstrates the turbulent behaviour of fluids at a given boundary layer at various velocities during free or natural convection, which is determined by the ratio of fluid buoyancy forces to fluid viscosity forces:

$$Gr = \frac{g\beta d^3 (T_i - T_a)}{\mu^2}$$

where:

Gr is the dimensionless Grashof number
g is the acceleration of gravity in *m/s*
β is the Coefficient of Thermal Expansion
T_i is the temperature of the solid in *K*
T_a is the temperature of the fluid in *K*
μ is the dynamic viscosity of the fluid in *kg/m.s*
d is the length in *m*

At low *Gr* values, viscous forces keep disturbances within the boundary layer small and the flow remains fairly laminar. At larger values of *Gr*, fluid bouyancy forces begin to overwhelm viscous forces and larger disturbances develop within the boundary layer, thus increasing the turbulence of the flow. The Grashof number also significantly influences the boundary layer, causing it to decrease in thickness as *Gr* increases.

2.1.3.2.3. Prandtl Number

The Prandtl number is the ratio of kinematic viscosity to thermal diffusivity of a given fluid. It is essentially the ratio of the fluid velocity boundary layer thickness to that of the thermal boundary layer thickness, and is used in convection calculations to determine the rate of thermal diffusion between a surface and a flowing fluid:

$$\mathrm{Pr} = v / \alpha$$

where:

Pr is the dimensionless Prandtl Number
v is the kinematic viscosity of the fluid in m^2/s
α is the thermal diffusivity of the fluid in m^2/s

2.1.3.2.4. Rayleigh Number

The Rayleigh number is the product of the Grashof and Prandtl numbers and is used to determine the onset of natural convection in a fluid:

$$Ra = Gr \cdot \mathrm{Pr}$$

When the values of *Ra* are low, the heat transfer in a fluid is primarily due to conduction. When the values of *Ra* are high, the heat transfer in a fluid is significantly influenced by the free convection of the fluid. The onset of free convection occurs at a critical Rayleigh number, denoted Ra_c.

Generally speaking, Ra_c value is usually around 1100 for an open surface. In a Bénard configuration, where a horizontal bottom plate of a temperature greater than a parallel horizontal top plate is separated by a distance *d*, resulting in a constant temperature gradient, the Ra_c value is usually around 1700.

2.1.3.2.5.Nusselt Number

The Nusselt number determines the ratio of actual heat transfer into a fluid from given surface when influenced by convection, in other words, the ratio of heat transfer by conduction and convection. It can be determined by one of two formulas:

$$Nu = \frac{hL}{k}$$

or

$$Nu = (\frac{Ra}{Ra_c})^{\frac{1}{3}}$$

where:

Nu is the dimensionless Nusselt number
h is the convective heat transfer coefficient in $W/m^2.K$
k is the coefficient of heat transfer in *W/m.K*
L is the characteristic length in *m*
Ra is the dimensionless Rayleigh number
Ra_c is the dimensionless critical Rayleigh number

2.2. Controlled Environment for Modelling Experiments

2.2.1. Requirements

During the initial planning stages of the project it became apparent that there were no suitable environmental chambers within the facility. The environmental chambers that were available were either not of suitable size, not accurate enough or did not posses the level of control required for the project. It was decided to design and construct a simple environmental chamber from available resources that could be under exclusive computer control.

The thermal control within the chamber was designed based on similar design as described by Wangaard, McDonell, Burger and Wilmot (1991). The chamber was situated within a thermally controlled environmental room, which maintained the ambient temperature at 20 ^{o}C +/- 2 ^{o}C. This ensured the accuracy and stability of the environmental chamber, while allowing samples to acclimate to the experiment start up temperature of 20 ^{o}C before commencement of an experiment. A large precision environmental chamber was thus constructed that could accurately control its internal temperature within a range of 15 ^{o}C to 25 ^{o}C +/- 0.2 ^{o}C.

2.2.1.1. Environmental Chamber Design

2.2.1.1.1. Chamber Shell

The size of the chamber needed to be sufficient to accommodate the flux box. Various options were explored from a cost and practicality perspective. An old shell of a chest freezer was found that was of suitable size and in good condition. The door was refitted with new seals and the old compressor and condenser coils were removed. The newly acquired “chamber” was placed on its side on a sturdy table that allowed its door to swing open downwards. Initially a small latch was used, but was later replaced by an electric winch motor that could seal the door tightly and open it automatically at the end of an experiment to allow the chamber and flux box to vent.

2.2.1.1.2.Thermal Control

A heat exchanger consisting of a heating and cooling coil was placed within the chamber with an air circulation fan. Calculated pulsing of pumps from a heat sink and heat source reservoir kept at 10 °C and 30 °C respectively controlled the temperature within the chamber via the heat exchanger (Figure 2.2). The pulse width was set to exchange all water within the coils per single pulse. A calibration procedure was run where each heat pump is pulsed at progressively increasing intervals while the temperature was recorded. A 3rd degree polynomial equation of the form $y = ax^3 + bx^2 + cx + d$ was fitted to the temperature measurements by regression. The interval required between pulses to obtain a desired temperature was thus determined by using the solution to the 3rd degree polynomial equation, in other words, a cubic polynomial formula (taken after the Cardano formula as described by Schechter (2006)):

$$x = \sqrt[3]{\left(\frac{-b^3}{27a^3} + \frac{bc}{6a^2} - \frac{d}{2a}\right) + \sqrt{\left(\frac{-b^3}{27a^3} + \frac{bc}{6a^2} - \frac{d}{2a}\right)^2 + \left(\frac{c}{3a} - \frac{b^2}{9a^2}\right)^3}} + \sqrt[3]{\left(\frac{-b^3}{27a^3} + \frac{bc}{6a^2} - \frac{d}{2a}\right) + \sqrt{\left(\frac{-b^3}{27a^3} + \frac{bc}{6a^2} - \frac{d}{2a}\right)^2 + \left(\frac{c}{3a} - \frac{b^2}{9a^2}\right)^3}} + \frac{b}{3a}$$

One distinctive limitation to using this formula is that it cannot accept negative numbers in its square roots. Although the calibration of the chamber did result in negative numbers, these were treated as positive integers in the cubic formula with the same results at the end. The chamber was calibrated against a South African Bureau of Standards calibrated alcohol thermometer.

The use

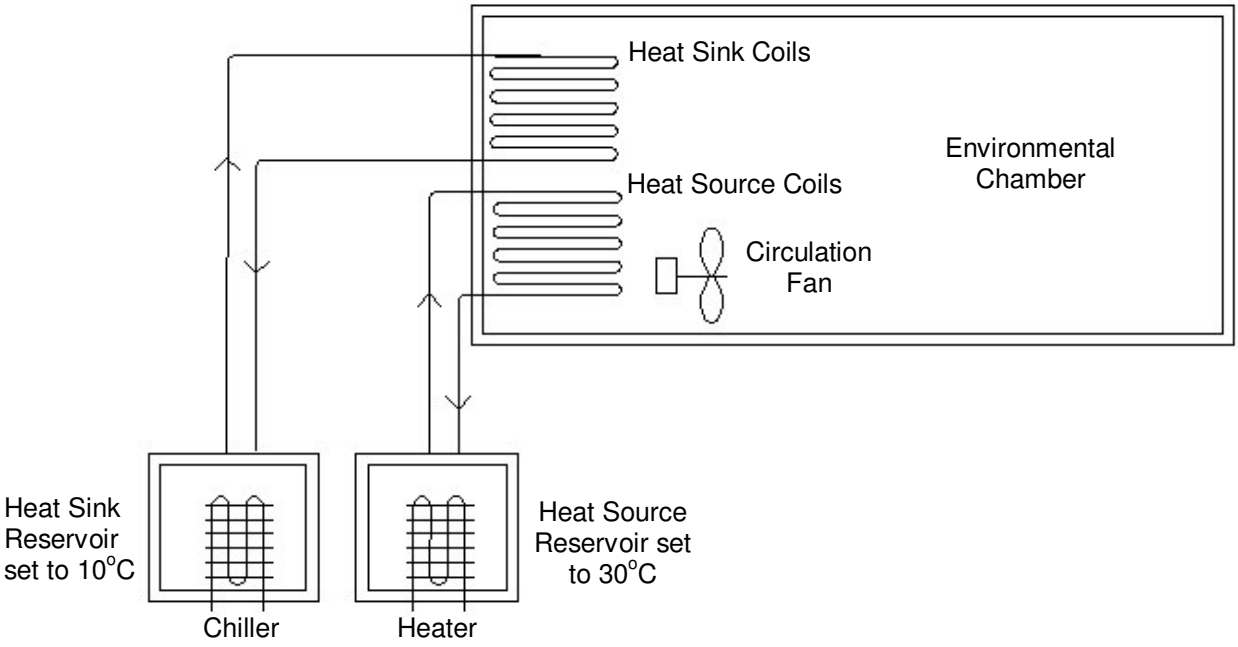

Figure 2.2 - Schematic of the environmental chamber and thermal control system

2.3. The Flux Box

2.3.1. Principal of operation

The flux box was based upon the “Hot Box” (Rose and Svendsen 2004) as used in the building industry to measure the thermal properties of insulation materials (Figure 2.3). This box served as a controlled thermal environment allowing heat passage in only one direction through a given sample. The principal difference was that the “Hot Box” measures heat moving horizontally through a given sample, while the flux box measures heat moving vertically through a sample. The heat from the heat source was conditioned to flow in a uniform manner through the sample. This allows for greater accuracy in a simple single dimensional modelling approach.

The sample was held between two reference plates of high thermal conductivity. The inner reference plate was exposed to the conditioned heat source within the box, while the outer plate was exposed to the ambient environment of the flux box. The flux box was held within the environmental chamber at a fixed temperature. This kept any thermal leakage from the flux box constant, which could be easily compensated for should the need arise.

2.3.2. Components and construction

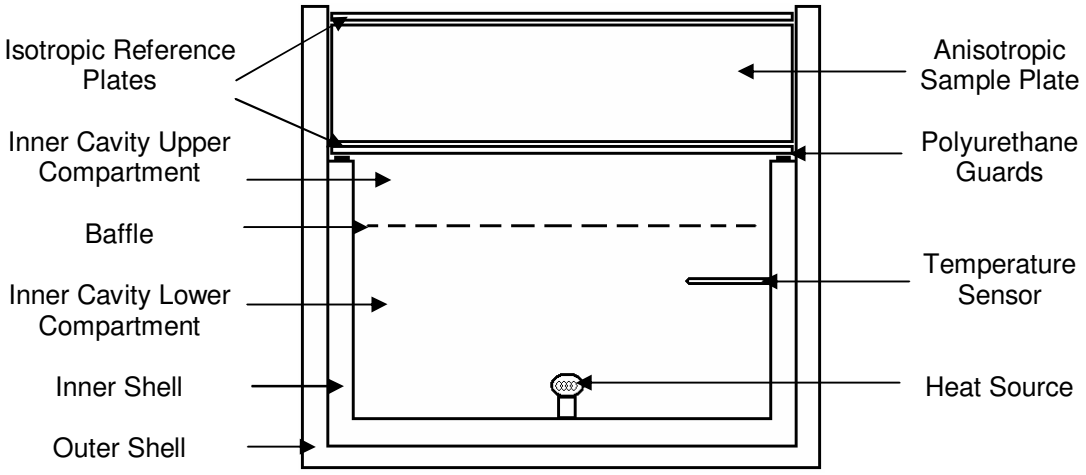

Figure 2.3 – Flux Box Construction

2.3.2.1. Box shell

The walls of the box were constructed from 39mm thick low density expanded polystyrene sheets. Sheets were secured using silicone adhesive. An outer shell of 500mm width by 500mm length by 500mm height was constructed. A second inner shell of 422 mm width by 422 mm length by 224 mm height was constructed and secured within the outer shell. This created a wall thickness of 78mm around the inner cavity and a ledge step within the outer shell on which the inner reference plate rested. The ledge step was lined with polyurethane strips to minimize thermal leakage. The distance between the ledge step and the top of the box, subtracting the total thickness of the two reference plates, allowed for a maximum sample thickness of 60mm. A lid for the outer shell of 50mm width by 50mm length with a square hole of 345mm width by 345mm length was constructed to minimise air movement over the top reference plate.

2.3.2.2. Reference Plates

The reference plates consisted of two 6mm thick aluminium sheets 422mm wide by 422mm length. Polystyrene spacers 15mm width by 407mm length by 15mm height were used to separate the plates to the correct sample thickness. These spacers were placed end to end around the edges and also served as additional insulation guards to minimize any lateral movement of heat out of the sample. A total of 16 spacers were constructed which when stacked allowed for a maximum sample thickness of 60mm. The size accommodation for the sample plates was thus 392mm by 392mm.

2.3.2.3. Heat Source

The heat source was placed in the middle bottom of the inner box cavity. This heat source comprised of a standard 230 volt 15 watt incandescent lamp on a plastic bayonet base. A 1mm thick perforated fibreglass baffle of 30mm width by 30mm length was suspended 50mm above the heat source. This baffle served to uniformly distribute the convection currents generated by the heat source across the bottom reference plate, eliminating hotspots and heating the plate in a uniform manner. The baffle also served to minimize radiation generated by the heat source from falling on the reference plate. This created

a condition whereby all energy from the heat source would be only carried into the bottom reference plate by thermal conduction and convection alone.

2.3.2.4. Temperature Sensor

The temperature sensor consisted of a PT100 thermocouple within a stainless-steel outer jacket. The sensor was placed through the middle of one of the inner box walls, 90mm below the bottom reference plate.

2.3.2.5. Vent

In order to minimize the delay between sample runs, a forced aspirator was attached to vent the box after each sample run, returning the inner cavity temperature back to the ambient set point. The aspirator consisted of a 12-volt centrifugal blower with the vacuum port connected to the bottom of the inner box cavity. The blower was restricted to prevent undesirable thermal leakage. A restricted vent pipe on the opposite corner of the box was attached for air inflow.

2.4. Flux Box Sample Preparation and Experiments

2.4.1. Sample Plates

The flux box was designed to accommodate plate sizes of 392mm by 392mm with progressive sample thickness of 15mm, 30mm, 45mm and 60mm. As samples were acquired from natural sources, preparation was needed before the samples could be loaded into the Flux Box. Five repetitions of each sample thickness were prepared. This yielded a total of 20 samples per material tested. A constant volume to mass ratio was adhered to to ensure consistent sample densities.

2.4.1.1. Manure Sample Preparation

The bovine manure sample needed to be packed into plates of the required size and thickness and then dried for each experiment. Wooden frames 15mm thick were constructed with an internal length and width of 392mm by 392mm. This provided the base mould for the manure plates. The frames could be stacked to provide increasing thickness in 15mm increments.

The moulds were placed onto a drying mesh rack. The manure plates were prepared by placing fresh manure into the moulds lined with plastic. The moulds were then removed and the plates placed into a drying oven. The oven was set to 45^{o}C and the samples left for one week to dry. The drying temperature was chosen based on the recommendations of van Soest (1982) on manure sample preparation. Higher drying temperatures would lead to inconsistent drying and the development of artefacts within the manure plate.

An initial 60mm sample was prepared first to determine the mass of manure required to fill the subsequent plates. The calculated masses required for the 15mm, 30mm, 45mm and 60mm plates were 3kg, 6kg, 9kg, and 12kg respectively. Once the plates were dried, the dry mass was measured (Table 2.1).

Table 2.1 – Prepared manure sample properties

Thickness	Average Dry Mass(g)	Std Dev	Dry Mass %	Moisture %
60mm	1889.00	98.24	15.74	84.26
45mm	1314.40	139.79	14.60	85.40
30mm	913.60	23.08	15.23	84.77
15mm	457.80	10.16	15.26	84.74

2.4.1.2. Thatch, Cereal Straw and Typha Reeds Sample Preparation

The thatch and cereal straw was pre-dried upon acquisition. The Typha reeds were acquired fresh and were air dried for two weeks before use. The thatch and Typha reeds were cut into 392mm lengths. The Typha reeds, thatch and cereal straw samples were then packed into initial 60mm plates to determine the masses of the subsequent plates. The measured masses were then simply divided by four to obtain the required masses of the subsequent thickness.

Table 2.2 – Prepared thatch, cereal straw, and typha reeds properties

	Thatch		Cereal Straw		Typha Reeds	
Thickness	Avg. Mass (g)	Std. Dev.	Avg. Mass (g)	Std. Dev.	Avg. Mass (g)	Std. Dev.
60mm	1494.80	16.08	352.20	3.27	455.40	3.44
45mm	1125.00	18.51	264.60	4.56	341.20	3.27
30mm	751.80	18.44	176.40	3.36	225.80	2.77
15mm	377.40	19.89	87.86	2.41	112.80	2.49

2.4.2. Flux Box Measurements

The samples were allowed time to acclimate to the starting temperature of the experiment. Each sample was then loaded into the flux box on top of the bottom reference plate. The edges were lined with the polystyrene spacers and the top reference was loaded and secured using wire ties. The flux box was then loaded into the environmental chamber and the experiment commenced. The heat source was switched on automatically five seconds after the door was sealed. The heat source then ran until the target temperature of 45^{o}C was met, after which the chamber door was

automatically opened, the heat source was shut off and the flux box was vented. During the experiment temperature measurements of the inner cavity of the flux box and the environmental chamber were sampled once per second to an MS Access database.

2.4.3. Flux Box Data Preparation

The data acquired from the Flux Box experiments was filtered and processed before further analysis took place. The objective of the preparation procedure was to:

- Import the data into Matlab
- Separate the data into data sets and generate tables synchronized with the data sets:
    - Experiment starting times
    - Data set sizes
- Identify and determine the pattern of any anomalies in the data
- Filter the data by removal of the anomalies and interpolating

2.4.3.1. Data Import

Data was imported from the MS Access database by using Dynamic Data Exchange (DDE) calls to MS Access. Since the data needed only be imported once, this was the simplest and least time consuming approach. The data consisted of the following components, each stored in an individual field within the database:

- **Thermal Variable Data:** All acquired thermal values in ^{o}C.
- **Data Markers:** Markers stored by the logger indicating the status of various data:
    - **"B"** indicates the beginning of an experiment or data set
    - **"E"** indicates the end of an experiment or data set
    - Other status indicators representing the status of the logging system, etc. were ignored.
- **Date and Time Stamps:** Date and time of the data snapshot.

Each field was directly imported into their own single column matrix within Matlab.

2.4.3.2. Data set separation

All values imported from the database were stored within a single field. The data was separated into data sets by using the data markers to flag the beginning and end of a data set. The data would be separated into the following matrices:

- Thermal variable data was separated into a **Thermal Variable Matrix** with individual columns for data sets.
- Date and Time data would be separated into a **Data Set Start Time Matrix**.
- The length of each data set in samples would be stored in a **Data Set Length Matrix**.

A program loop was developed in Matlab that would scan through and separate the imported matrices. Every time a “B” marker was encountered:

- The time and date at that occurrence was stored in the Data Set Start Time Matrix and denoted the starting time of the experiment
- A new Thermal Variable Matrix column was used for all thermal variable data until the “E” marker occurrence.
- The value of a separate loop counter in the program loop was stored to the Data Set Length Matrix and reset.

Since the Thermal Variable Matrix needed to be square by MatLab standards, and the data set lengths varied, an initial m-by-n not-a-number (NaN) matrix based on the maximum data sets encountered was generated. Once the thermal variable data was filled, all missing data values were represented by NaN values.

2.4.3.3. Filtering the data

The data was visually inspected for any unusual anomalies that may be encountered. One anomaly that was evident was negative spikes occurring at apparently random intervals (Figure 2.4). It became apparent that the switching of the pumps on the environmental chamber caused these spikes. Upon closer inspection, the pattern was evidently repetitive: spikes were always negative and spanned no more than five samples each time.

Since the spikes were easily detectable it was a simple procedure to scan and remove them. A program loop was developed in MatLab that would scan through the data sets and detect any sudden negative spike that exceeded a preset threshold value. The program then removed five samples from the beginning of the spike detection.

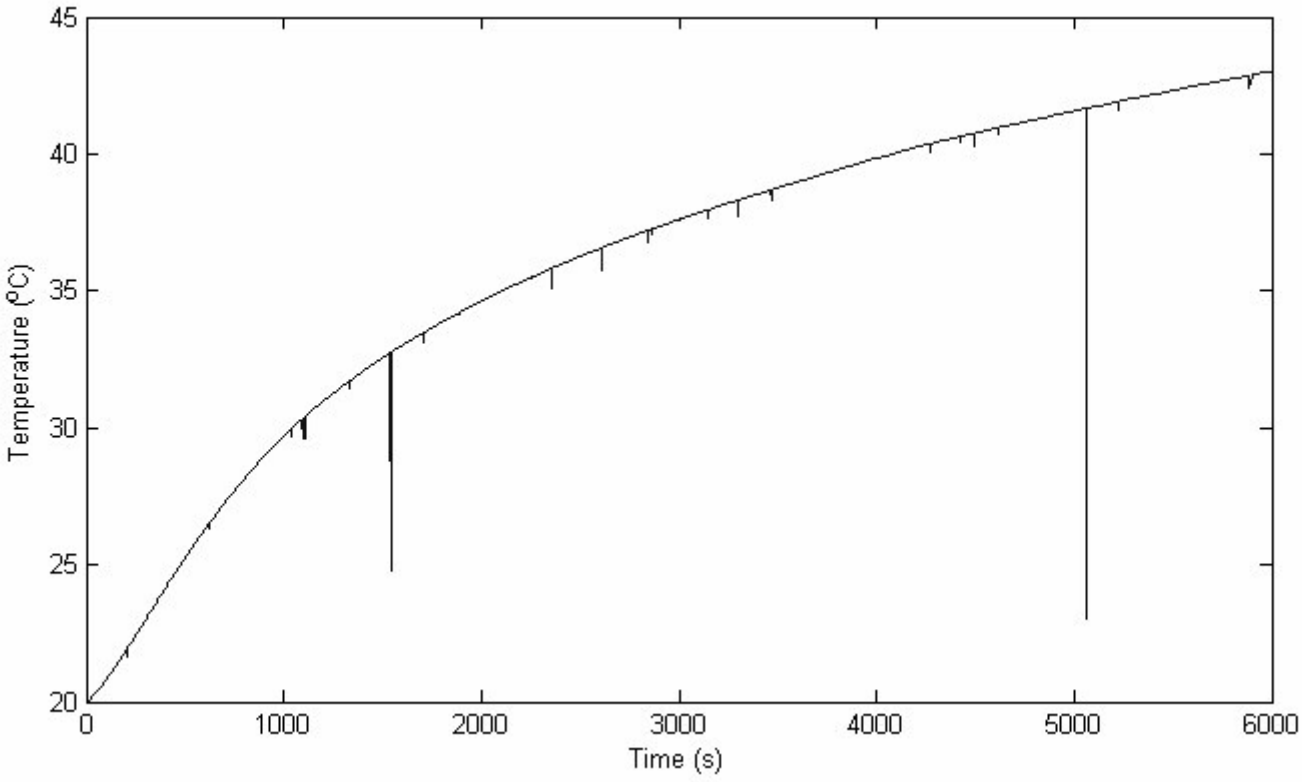

Figure 2.4 – Sample data set showing negative spike anomalies before filtering

Upon removal of the anomalies, the gaps left in the data series were filled using linear interpolation. This was necessary as all proceeding functions used within MatLab did not accept NaN data and would not return results if they were encountered. Since the gaps were small, the effect on the final data set was negligible. The final data set was then ready for further processing (Figure 2.5).

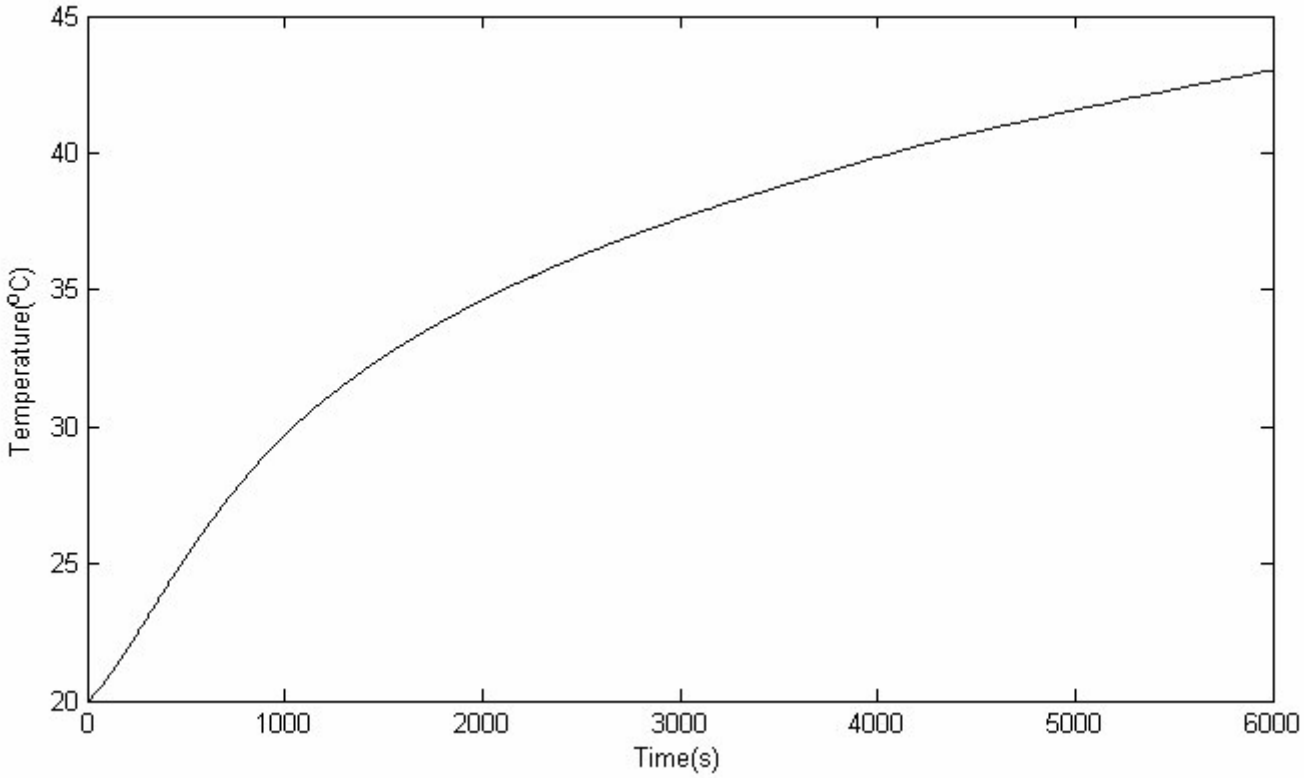

Figure 2.5 - Sample data set after filtering

3. Thermal Model Development

3.1. Basic thermal model development and investigation using the Flux Box

The flux box was designed to investigate the three primary processes of thermal transfer in natural systems, namely conduction through solids, convection through fluids and radiation through empty space. The inner cavity of the flux box contained the heat source that would induce convection of the air and emit radiation. Heat flux out of the box occurred through conduction through two isotropic layers sandwiching a single anisotropic layer. The temperature sensor within the inner cavity was exposed to the convection and radiation of the heat source.

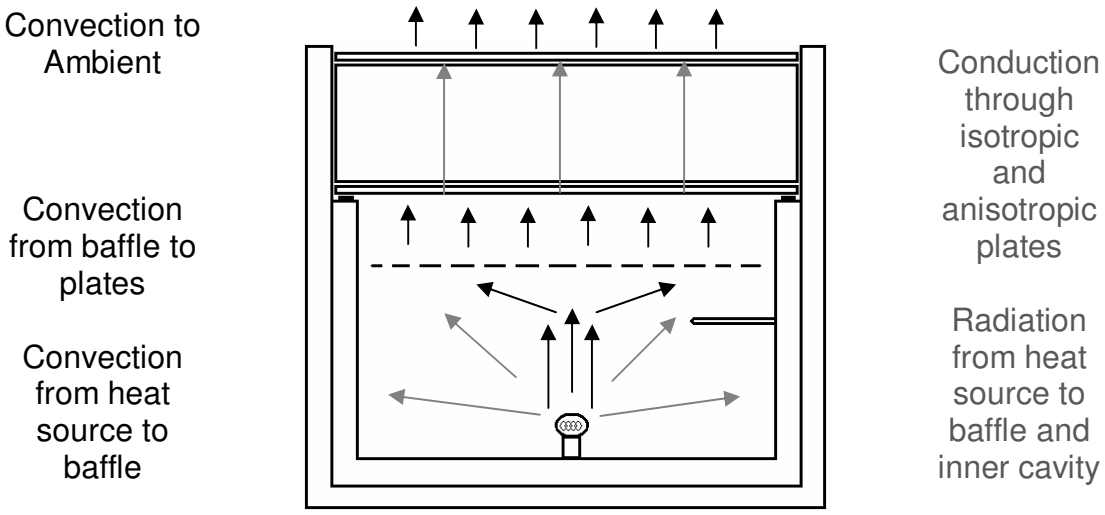

Figure 3.1 – Heat transfer fluxes within the Flux Box

3.1.1. The Flux Box Model

3.1.1.1. Model Development

The flux box mathematical model was based on a one-dimensional node oriented system of linear differential equations. Each node represents each component within the flux box.

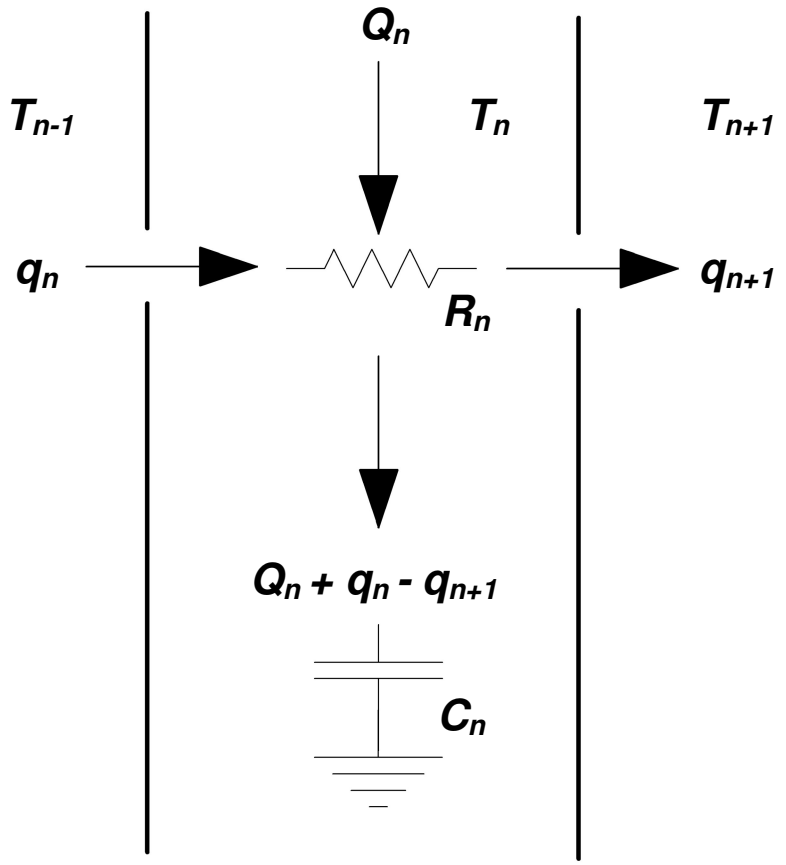

Figure 3.2 – Schematic representation of a single thermal node

Each node accepts thermal flux inputs from other nodes (q) as well as external heat sources (Q). The energy balance of each node is presented:

Rate of change of energy in node: $C_n \frac{d}{dt} T_n$	=	Net flow rate of energy into node: $q_n - q_{n+1}$	+	External energy flow rate into node: Q_n

For each node as represented in Figure 3.2, the rate of temperature increase of the node ($\frac{d}{dt}T_n$) can be expressed as a function of the incoming thermal energy flux (q_n), the external energy input (Q_n) and the outgoing thermal energy flux (q_{n+1}):

$$q_{n+1} = \frac{T_n - T_{n+1}}{R_n} \tag{3.1}$$

$$\frac{d}{dt}T_n = \frac{Q_n + q_n - q_{n+1}}{C_n} \tag{3.2}$$

The classic thermal network representation of (1) and (2) in differential equation form:

$$(\rho c V)_i \frac{d}{dt}T_i = \sum_j \frac{T_j - T_i}{R_{ij}} + Q_i \tag{3.3}$$

where

T is the temperature in *K*
Q is the heat input in *J/s*
R is the thermal resistance in *K/J.s*
c is the specific heat in *J/kg.K*
ρ is the density in kg/m^3
V is the volume in m^3
q is the node thermal flux in *J/s*
C is the node thermal capacitance in *J/K*

3.1.1.2. Model Components

Table 3.1 shows the processes and assumptions for each Flux Box Model component. Within the flux box numerical model, each node represents a component of the flux box.

Table 3.1 – Flux Box Model Components and Assumptions

Component	Processes	Assumptions
Heat Source	Conduction	Only conduction occurs. Influence of radiation considered negligible.
Inner Cavity	Conduction, Convection, Radiation	All radiation converted to conductive thermal energy before reaching plates.
Bottom Reference Plate	Conduction	Purely isotropic.
Sample Plate	Conduction	Any convection is considered negligible.
Top Reference Plate	Conduction	Purely isotropic.
Ambient	Conduction, Convection, Radiation	Ambient environment infinite in size.

Table 3.2 – Model component inputs and outputs

Component	**Energy Flux Input (q_n)**	**External Energy Flux Input (Q_n)**	**Energy Flux Output (q_{n+1})**
Heat Source	Non	Input Power Conduction	Inner Cavity
Inner Cavity	Heat Source	Input Power Radiation	Bottom Reference Plate
Bottom Reference Plate	Inner Cavity	Non	Sample Plate
Sample Plate	Bottom Reference Plate	Non	Top Reference Plate
Top Reference Plate	Sample Plate	Non	Ambient

Table 3.3 – Model component elements

Component	**Thermal Resistances (R)**	**Thermal Capacitances (C)**
Heat Source	Filament, Gas, Glass Envelope	Filament, Gas, Glass Envelope
Inner Cavity	Convection	Dry Air, Air Moisture
Bottom Reference Plate	Isotropic Metal	Isotropic Metal
Sample Plate	Air Pocket Convection, Organic Fibres, Moisture	Air Pockets, Organic Fibres, Moisture
Top Reference Plate	Isotropic Metal	Isotropic Metal
Ambient	Convection	Not Applicable / Infinite

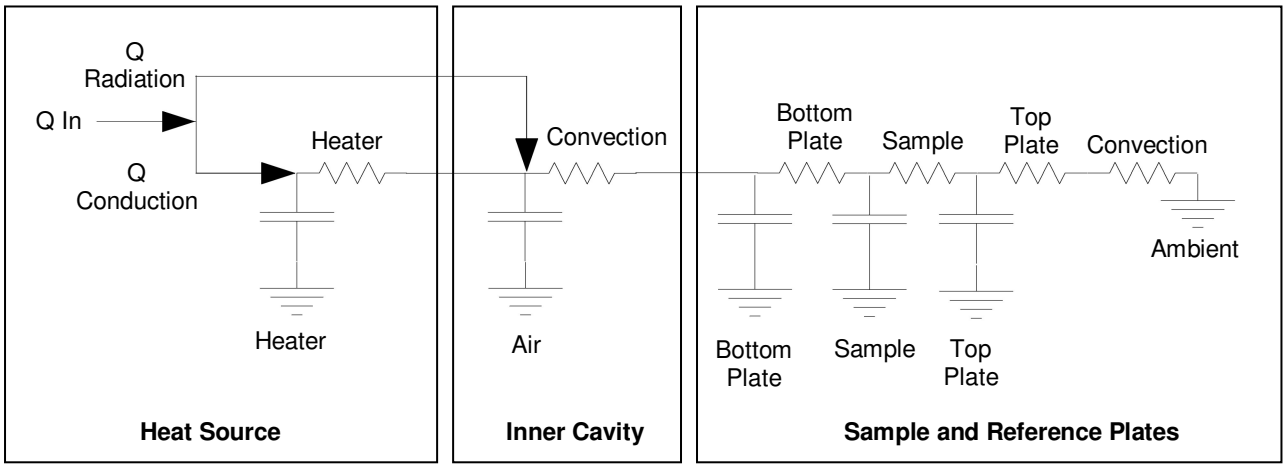

Figure 3.3 – Idealized R-C Thermal Network Model of the Flux Box

3.1.1.2.1. Heat Source

The heat source, comprised of a standard 15w incandescent lamp, produced heat by both radiation and conduction. The heat source comprised of a tungsten filament encased within a glass envelope containing an inert gas. Although radiation does transfer thermal energy between the filament and the glass envelope, for simplification purposes the model assumed that only conduction occurs within this component (Table 3.1). In other words, the filament and glass envelope are treated as one single component. Radiation is then assumed only to be present between the heat source and inner cavity components. A ratio was used to determine the conversion of energy input into the heat source component into conductive and irradiative thermal energy. The thermal capacitance and resistance is influenced by the properties of the filament, lamp gas, and glass envelope (Table 3.3). The cold start characteristics of the lamp were considered. Ben-Yaakov, Peretz and Hesterman (2005) show that the running temperature of the filament in most lamps reaches its running temperature within no more than two seconds. The thermal characteristics of the filament were thus not considered.

3.1.1.2.2. Inner Cavity

The inner cavity component comprises of an air filled cavity separated into two compartments by a perforated baffle. Radiation was assumed only to be

present within the lower compartment, where it was completely converted into conductive thermal energy before reaching the upper compartment (Table 3.1). Conductive heat was transported to the baffle by convection, where the convective heat flow was spread out evenly throughout the upper compartment. For simplification the model assumes that all heat transfer from the inner cavity to the bottom reference plate is by conduction alone. Therefore, all thermal energy generated by the heat source is converted into conductive thermal energy upon reaching the bottom reference plate. Thermal resistance is influenced by air convection, while the air and its moisture content influence the thermal capacitance (Table 3.3).

3.1.1.2.3. Sample and Reference Plates

Although convection processes are known to occur within and around the sample plate (Table 3.1), only conduction is assumed to occur within the bottom reference plate, the top reference plate and the sample. All of these components are thus lumped into a single node within the model. The constituency of the organic components, air pockets and moisture content influences thermal resistance and capacitance of the sample plate. Thermal resistance to ambient as influenced by convection is included within the plate thermal resistances lump. Figure 3.3 shows the ideal model including all components. Figure 3.4 shows the same model with the plate and ambient convection nodes lumped.

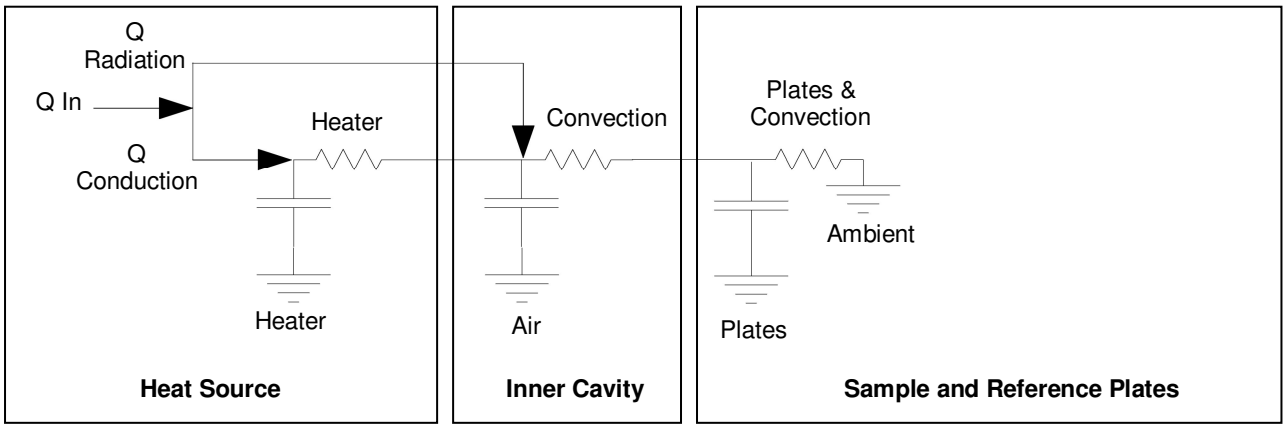

Figure 3.4 – Idealized R-C Lumped Thermal Network Model of the Flux Box

3.1.2. Assembly of the model in Matlab

The final flux box model comprised of three nodes, starting with an energy input (Q_{in}) and ending with heat flux to the ambient chamber environment of 20°C (Figure 3.5). In Matlab, the ODE113 differential equation solver was chosen to run the flux box model. Boundary values and model parameters as defined in Table 3.4 were calculated by fitting the model to the measured data.

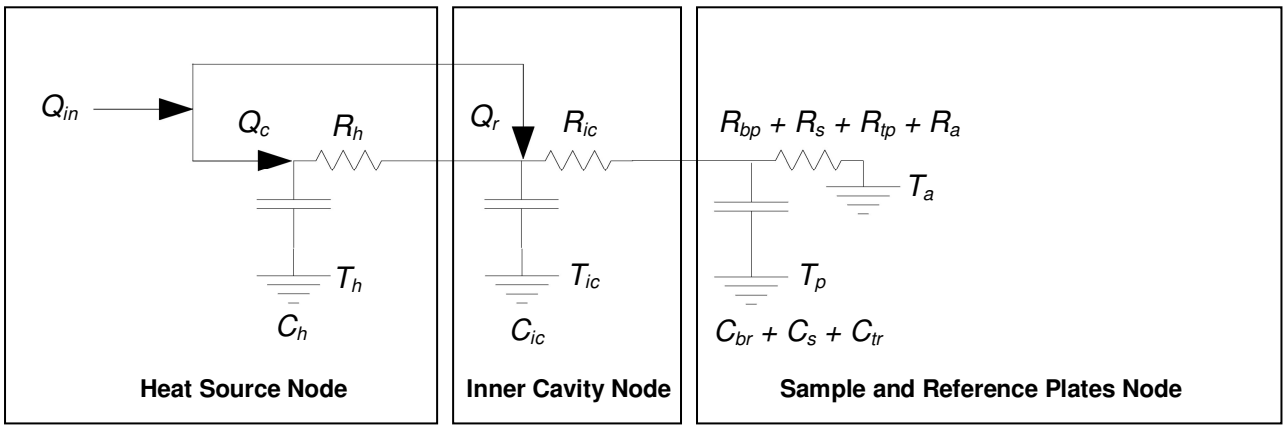

Figure 3.5 – R-C representation of the Final Matlab Flux Box Model

The final equations of the Matlab flux box model are presented:

$$q_h = \frac{T_h - T_{ic}}{R_h} \tag{3.4}$$

$$q_{ic} = \frac{T_{ic} - T_p}{R_{ic}} \tag{3.5}$$

$$q_p = \frac{T_p - T_a}{R_{bp} + R_s + R_{tp} + R_a} \tag{3.6}$$

$$\frac{d}{dt}T_h = \frac{Q_c - q_h}{C_h} \tag{3.7}$$

$$\frac{d}{dt}T_{ic} = \frac{Q_r + q_h - q_{ic}}{C_{ic}} \tag{3.8}$$

$$\frac{d}{dt}T_p = \frac{q_{ic} - q_p}{C_{bp} + C_s + C_{tp}} \tag{3.9}$$

The thermal fluxes between the heat source node, inner cavity node and plates node are represented by equations (3.4), (3.5) and (3.6) respectively. The temperature differential of the heat source node, inner cavity node and plates node are represented by equations (3.7), (3.8) and (3.9) respectively. The thermal resistance and capacitance lumping in the plates node is included in equations (3.6) and (3.9) respectively.

Table 3.4 – Final Matlab Flux Box Model Parameters

Parameter	Description	Units
Q_{in}	Energy input	J/s
Q_r	Energy conversion into radiation	J/s
Q_c	Energy conversion into conductive thermal energy	J/s
Q_{rr}	Energy to radiation ratio	Q_r / Q_{in}
R_h	Thermal resistance of heat source node	$K/J.s$
C_h	Thermal capacitance of heat source node	J/K
q_h	Thermal flux out of heat source node	J/s
T_h	Temperature of heat source node	^oC
R_{ic}	Thermal resistance of inner cavity node	$K/J.s$
C_{ic}	Thermal capacitance of inner cavity node	J/K
q_{ic}	Thermal flux out of inner cavity node	J/s
T_{ic}	Temperature of inner cavity node	^oC
R_{bp}	Thermal resistance of bottom reference plate	$K/J.s$
C_{bp}	Thermal capacitance of bottom reference plate	J/K
R_s	Thermal resistance of sample	$K/J.s$
C_s	Thermal capacitance of sample	J/K
R_{tp}	Thermal resistance of top reference plate	$K/J.s$
C_{tp}	Thermal capacitance of top reference plate	J/K
R_a	Thermal resistance of ambient air	$K/J.s$
q_p	Thermal flux out of plates node	J/s
T_p	Temperature of plates node	^oC
T_a	Temperature of the ambient environment	^oC

3.2. Fitting the Flux Box Model to the Measured Data

3.2.1. Model Parameters and Initial Estimates

Some thought was needed on which model parameters the optimisation routine was to adjust in order to fit the model to the measured data. In order for the optimisation routine to accurately determine the best fit for the model, a reasonable estimate was also needed on the initial values of the model parameters.

- **Energy input (Q_{in}):** The input energy may not be consistent due to inefficiencies within the heat source. Since the lamp is rated at 15 Watts, this was used as the initial value. $Q_{in} = 15$ (J.s).
- **Energy to radiation ratio (Q_{rr}: Q_r / Q_{in}):** The conversion ratio of thermal energy to thermal radiation was uncertain. The typical efficiency of a lamp is between 2% and 13% (Agrawel, Leff and Menon 1995), although this value usually applies to visible light. An initial ratio of 50% was used since a large portion of the energy dissipated by light bulbs is due to radiation (Clauss, Ralich and Ramsier 2001).
- **Capacity of the heat source (C_h):** The parameters of the heat source, such as gas content, were uncertain. Given the small size and the unknown properties of the heat source an initial value of $C_h = 1$ (kJ/K) was used.
- **Resistance of the heat source (R_h):** The composition of the materials that the heat source comprises of is uncertain. Given the small size and the unknown properties of the heat source an initial value of $R_h = 1$ (K/J.s) was used.
- **Capacity of inner cavity (C_{ic}):** The parameters of the inner cavity air, such as moisture content, were uncertain. Given the specific heat of air, $C_{ic} = 1.007(kJ / K)$.

- **Resistance of inner cavity (R_{ic}):** The effects of thermal convection and the separation caused by the baffle were uncertain. Considering the average heat transfer coefficient for convection of air is roughly h = 50 (W/m^2.K) for most situations (www.EngineeringToolBox.com), and the estimated area for the heat source is 0.01m^2:

  $$R = 1/[50(W/m^2.K) \times 0.01(m^2)]$$
  $$R = 2(K/J.s)$$

- **Capacity of sample plate (C_s):** While the two reference plates were well known, the sample plate was unknown. The same value as the inner cavity was used: C_s = 1.007 (kJ/K)
- **Resistance of sample plate and ambient convection (R_s & R_a):** While the resistance of the two reference plates were well known, the sample plate and ambient convection resistance was unknown. The same value as the inner cavity was used: $R_s + R_a = 1$ (kJ/K)

3.2.2. Model Regression

The flux box model was fitted to the measured data of the flux box experiments by the non-linear unconstrained optimisation function in Matlab, FminSearch. A function was passed to the optimisation routine that would return the squared residual error of the fitted curve, and the optimisation routine would then adjust the model parameters accordingly until the function tolerance of 0.02 was met. All of the measured values were checked for valid boundary conditions under the following criteria before the regression was performed:

- Initial temperature between 20°C and 22°C
- Final temperature of between 44.5°C and 45.5°C
- Between 5000 and 10000 measurements, at one measurement per second.

Any data set that did not meet the required criteria was rejected (Table 3.5). All data sets were processed automatically using a program loop. The validity check was run on each loop iteration. Models were validated based on sum of squares error and mean errors, as no accepted statistically valid test exists for models of this nature (Kleijnen 1999). A coefficient of determination approach

was explored, but due to the large sample size the total sum of squares (SST) averaged 281221, as opposed to the sum of squares error (SSE) average of 14.45, which resulted in an r^2 value average of 0.99994 with a minimum of 0.99958.

Table 3.5 – Sample boundary condition check results

Sample	**Passed**	**Rejected**
Bovine Manure 15mm	2	3
Bovine Manure 30mm	5	0
Bovine Manure 45mm	3	2
Bovine Manure 60mm	5	0
Thatch 15mm	5	0
Thatch 30mm	4	1
Thatch 45mm	4	1
Thatch 60mm	4	1
Cereal Straw 15mm	5	0
Cereal Straw 30mm	5	0
Cereal Straw 45mm	5	0
Cereal Straw 60mm	5	0
Typha Reeds 15mm	5	0
Typha Reeds 30mm	5	0
Typha Reeds 45mm	5	0
Typha Reeds 60mm	5	0

3.2.3. Regression Analysis

An example of the model regression output in comparison with the measured inner cavity temperature is presented in Figure 3.6. This plot, together with the residual sum of squares presented in Table 3.6, illustrates the very close fits that were attained for the regressions, with a maximum error of 0.013 °C.

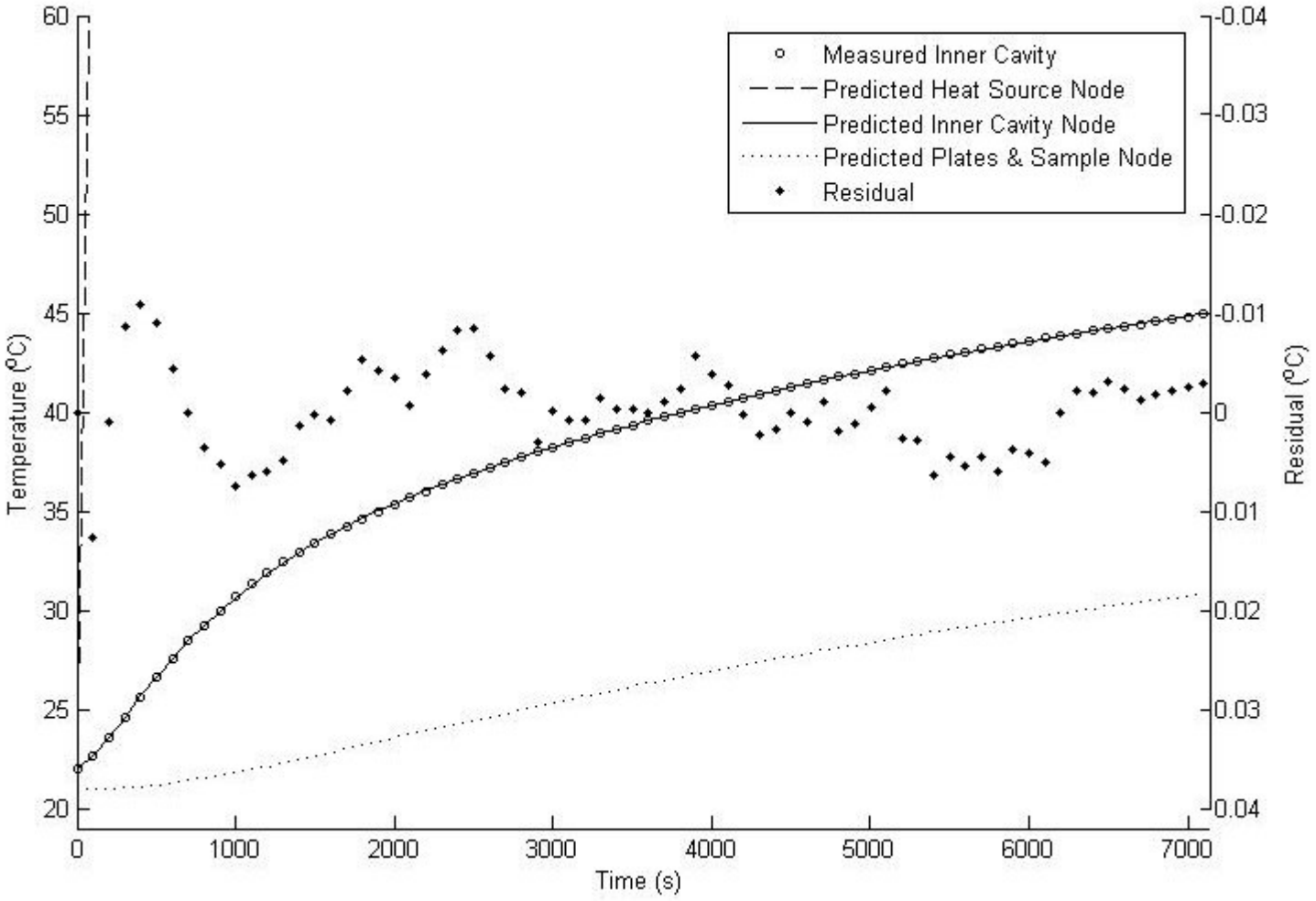

Figure 3.6 – Example of a flux box model regression output (60mm cereal straw sample)

Table 3.6 – Residual Sum of Squares Summary of Model Regression

	15mm			30mm			45mm			60mm		
	min	**mean**	**max**	**min**	**mean**	**Max**	**Min**	**mean**	**max**	**min**	**mean**	**Max**
Manure	3.2	5.7	8.2	2.3	4.4	9.1	3.7	9.8	17.9	4.2	12.8	37.3
Thatch	2.2	12.5	33.2	2.3	8.0	16.7	1.5	21.3	71.5	3.8	6.3	8.6
Straw	6.4	10.5	16.9	4.5	12.9	29.7	4.2	9.5	20.6	3.3	11.8	25.7
Reeds	5.8	13.7	21.2	10.3	16.0	28.7	9.8	19.1	34.6	3.7	11.3	18.0

The coefficient results of the regression were processed for mean values and standard deviations per material thickness. These results are presented in Figure 3.7, grouped by material thickness, and Figure 3.8, grouped by material, with standard deviation bars.

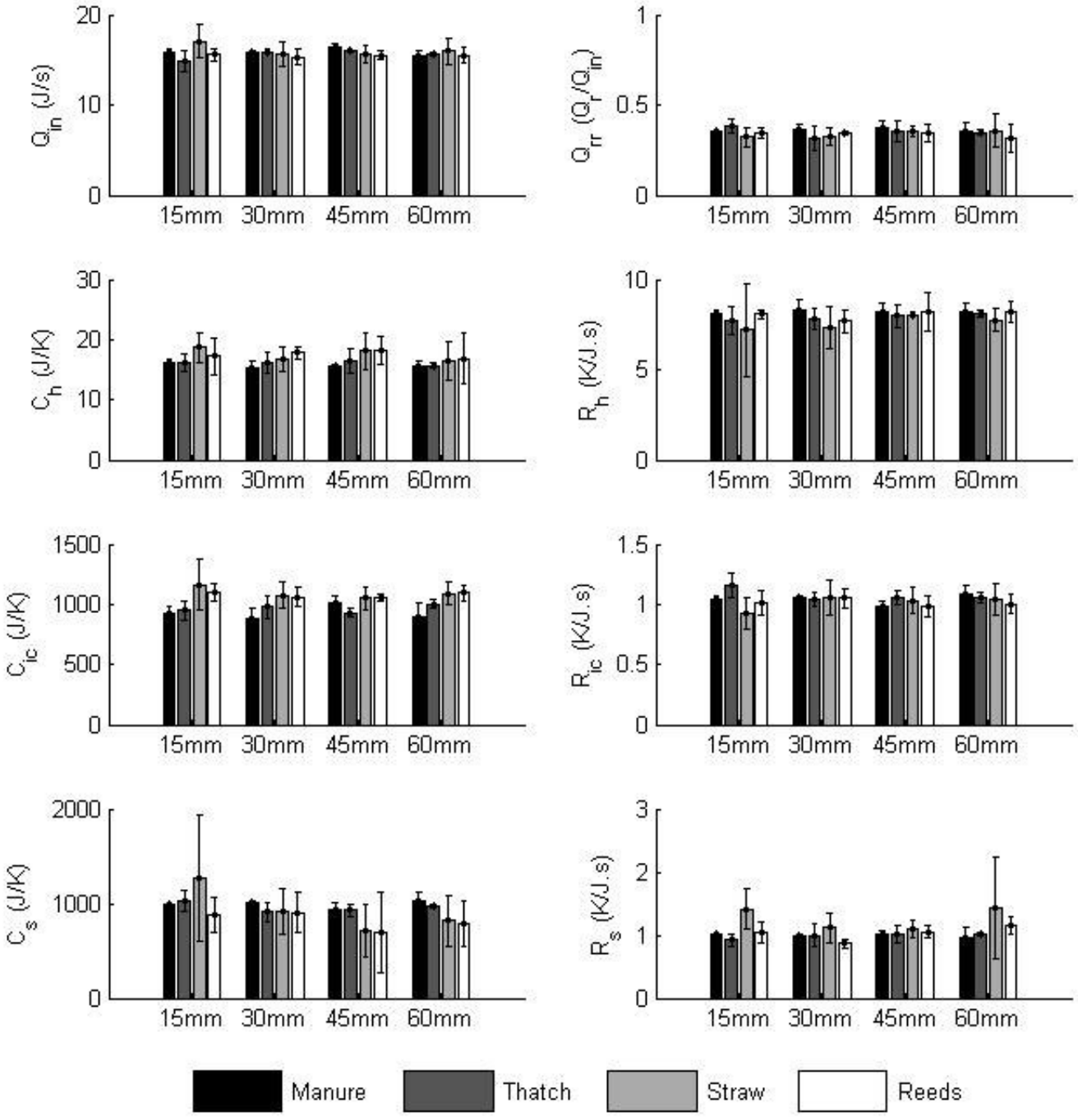

Figure 3.7 – Flux Box Model regression results, grouped by material thickness

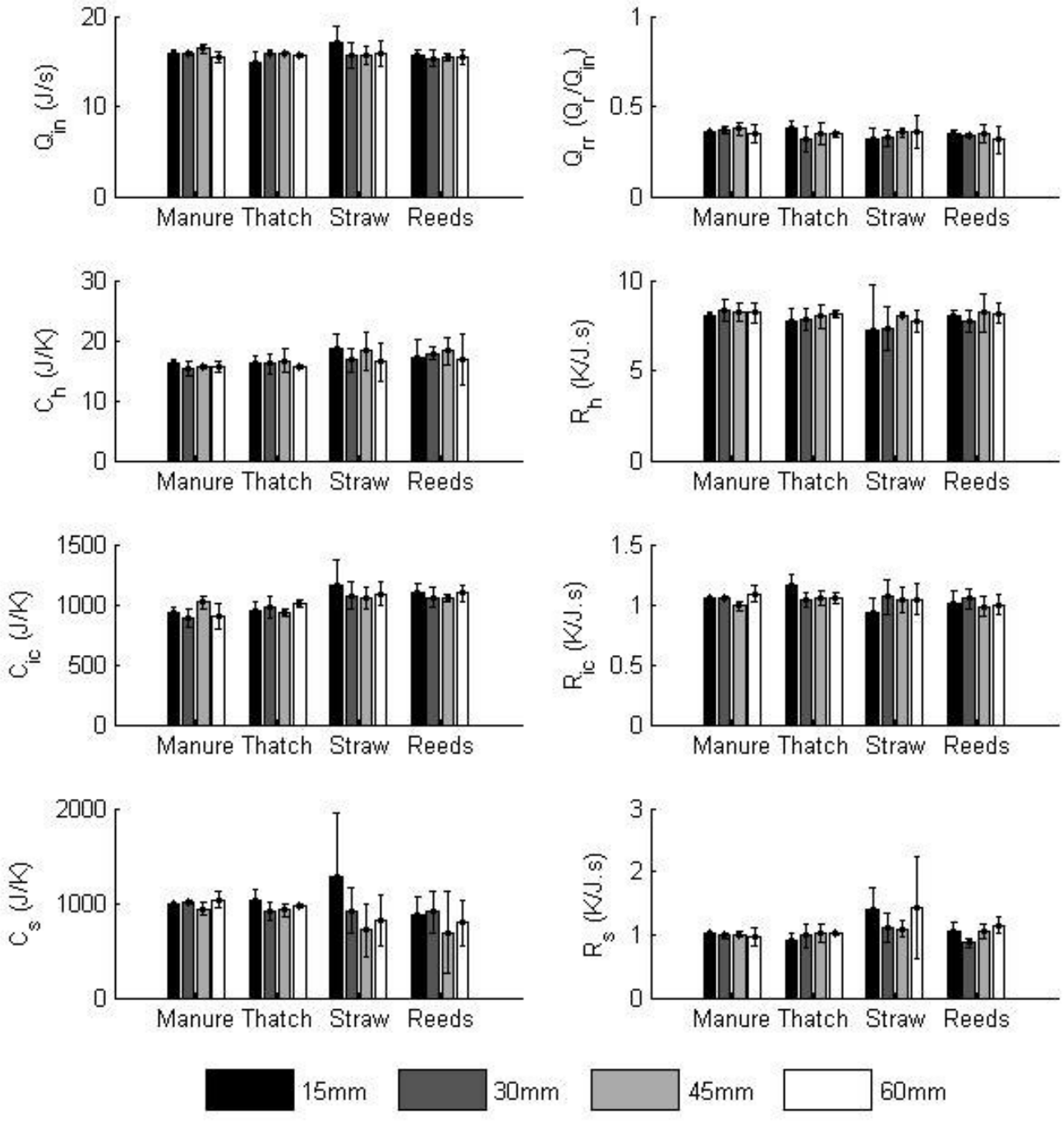

Figure 3.8 - Flux Box Model regression results, grouped by material

A Kruskal-Wallis analysis of variance by ranks was conducted on the model coefficients, grouped by material thickness, under the following conditions:

P > 0.05

H_o: Model coefficients per material thickness are the same for all materials

H_a: Model coefficients per material thickness are different for all materials

The ANOVA results are presented in Table 3.7.

Table 3.7 – P-values for Kruskal-Wallis ANOVA on Model Coefficients grouped by thickness

	15mm	**30mm**	**45mm**	**60mm**
Q_{in}	*0.367*	*0.449*	*0.308*	*0.612*
Q_{rr}	*0.493*	*0.229*	*0.738*	*0.732*
C_h	*0.379*	*0.081*	*0.057*	*0.832*
R_h	*0.829*	*0.576*	*0.951*	*0.687*
C_{ic}	*0.063*	*0.043*	*0.045*	*0.014*
R_{ic}	*0.06*	*0.507*	*0.384*	*0.34*
C_s	*0.44*	*0.172*	*0.352*	*0.111*
R_s	*0.052*	*0.07*	*0.716*	*0.086*

Apart from the 30mm, 45mm and 60mm C_{ic} coefficients, no statistically significant difference could be found between the coefficient values from materials of the same thickness (Table 3.7).

A linear regression to determine parameter dependence on material thickness was performed on the model coefficients under the following conditions:

P < 0.05

H_o: No significant difference between model parameters from materials of different thicknesses

H_a: Significant difference between model parameters from materials of different thicknesses

The results of the regression are presented in Table 3.8.

Table 3.8 – Linear regression to determine parameter dependence on material thickness

		C_h	R_h	C_{ic}	R_{ic}	C_s	R_s
Manure	**r^2**	0.00688	1.79E-05	0.00215	0.0426	0.0181	0.0308
	P	*0.769*	*0.988*	*0.87*	*0.461*	*0.633*	*0.531*
Thatch	**r^2**	0.00175	0.0946	0.0457	0.198	0.0522	0.0918
	P	*0.873*	*0.23*	*0.41*	*0.073*	*0.378*	*0.237*
Straw	**r^2**	0.037	0.0499	0.0308	0.0482	0.162	0.00494
	P	*0.445*	*0.373*	*0.486*	*0.382*	*0.098*	*0.782*
Reeds	**r^2**	0.00149	0.0208	0.000513	0.015	0.0331	0.146
	P	*0.872*	*0.544*	*0.924*	*0.607*	*0.456*	*0.097*

The regression of coefficients from materials of increasing thickness yielded no discernable dependence of coefficient values on material thickness (Table 3.8).

3.2.4. Calibration Regression and Result Comparison

Five calibration runs were conducted with no materials loaded. The top reference plate was placed directly on top of the bottom reference plate, seperated by a layer of scattered polystyrene beads. The beads prevented direct contact between the two plates. An example of the output from the regression of the calibration data is presented in Figure 3.9.

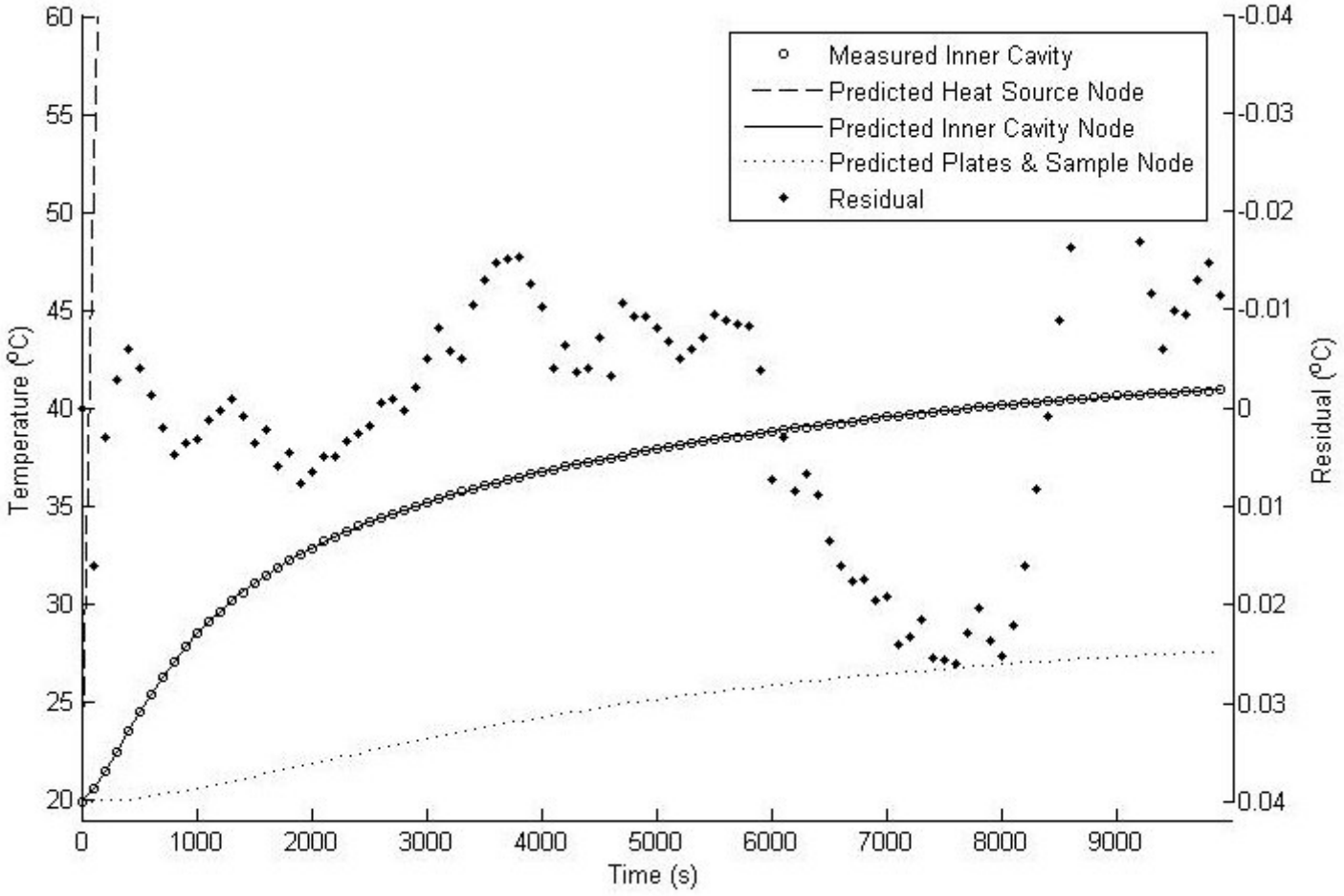

Figure 3.9 – Example of flux box calibration curve regression output

The material thermal capacity coefficient was zeroed before the calibration. All other values were left as predicted for the sample runs. The coefficient mean results of the regression are presented in Table 3.9, with a maximum error of 0.0085 °C.

Table 3.9 – Mean and standard deviation of calibration regression results

RSS	30.21	+/- 20.26	$^oC^2$
$\mathbf{Q_{in}}$	12.00	+/- 1.83	J.s
$\mathbf{Q_{rr}}$	0.38	+/- 0.11	Q_r / Q_{in}
$\mathbf{C_h}$	18.60	+/- 3.87	J/K
$\mathbf{R_h}$	11.44	+/- 3.49	K/J.s
$\mathbf{C_{ic}}$	789.41	+/- 136.16	J/K
$\mathbf{R_{ic}}$	1.14	+/- 0.21	K/J.s
$\mathbf{C_s}$	0.07	+/- 0.12	J/K
$\mathbf{R_s}$	0.74	+/- 0.12	K/J.s

The results of the flux box sample regressions were compared with that of the calibration regression. Relative outputs were generated and are presented in Figure 3.10. The results in this graph are presented as the differences between the mean values of the calibration and material results. Therefore, since the standard deviation can vary significantly, they may not be a true reflection of the actual difference between the material and calibration coefficients.

Each data set, consisting of five samples for each thickness of each material, were compared to the calibration data set one at a time using a two-tailed students t-test. This was performed to determine if there were any significant differences between the calibration coefficients and the material coefficients.

P > 0.05

H_o: Material coefficients are the same as calibration coefficients.

H_a: Material coefficients are not the same as calibration coefficients.

The results are presented in Table 3.10

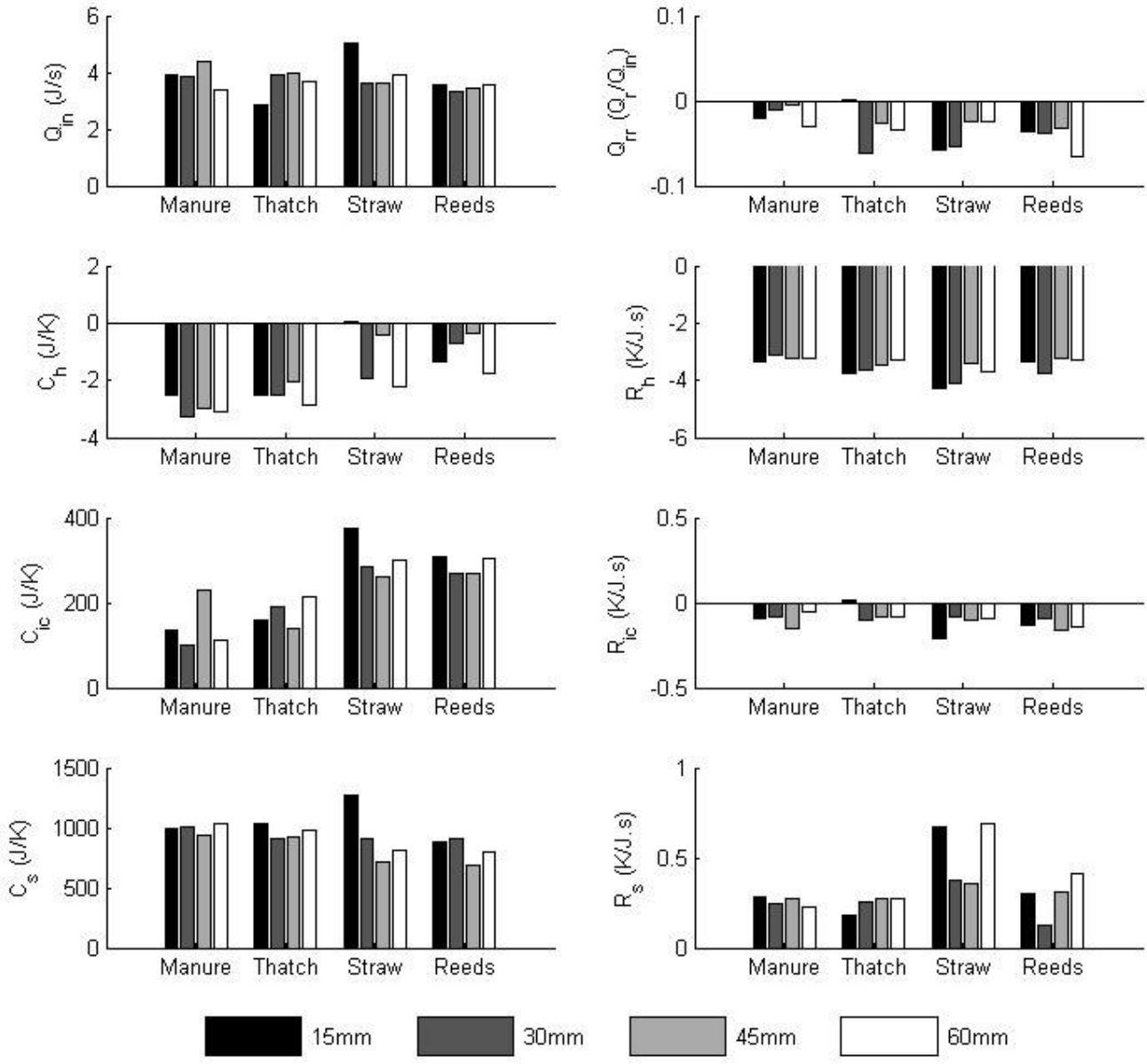

Figure 3.10 – Relative mean values of material regression results to calibration results, grouped by material

.

Table 3.10 – P-values of two-tailed students t-test between the calibration coefficients and material coefficients

	15mm	30mm	45mm	60mm
		Manure		
Q_{in}	*0.085*	0.005	0.027	0.012
Q_{rr}	*0.607*	*0.756*	*0.735*	*0.676*
C_h	*0.400*	*0.213*	*0.350*	*0.233*
R_h	*0.271*	*0.173*	*0.275*	*0.157*
C_{ic}	*0.269*	*0.324*	*0.082*	*0.301*
R_{ic}	*0.505*	*0.556*	*0.381*	*0.684*
C_s	0.001>	0.001>	0.001>	0.001>
R_s	*0.073*	0.008	0.039	*0.068*
		Thatch		
Q_{in}	0.041	0.014	0.013	0.017
Q_{rr}	*0.770*	*0.493*	*0.697*	*0.648*
C_h	*0.348*	*0.401*	*0.502*	*0.313*
R_h	*0.107*	*0.165*	*0.186*	*0.201*
C_{ic}	*0.121*	*0.107*	*0.176*	0.049
R_{ic}	*0.760*	*0.515*	*0.582*	*0.569*
C_s	0.001>	0.001>	0.001>	0.001>
R_s	*0.064*	*0.081*	0.037	0.012
		Straw		
Q_{in}	0.029	0.018	0.012	0.013
Q_{rr}	*0.530*	*0.492*	*0.697*	*0.721*
C_h	*0.735*	*0.497*	*0.757*	*0.488*
R_h	*0.200*	*0.086*	*0.136*	*0.111*
C_{ic}	*0.050*	0.015	0.019	0.009
R_{ic}	*0.263*	*0.618*	*0.488*	*0.552*
C_s	0.013	0.001>	0.001	0.001>
R_s	0.015	0.024	0.005	*0.146*
		Reeds		
Q_{in}	0.010	0.018	0.010	0.012
Q_{rr}	*0.622*	*0.600*	*0.658*	*0.451*
C_h	*0.642*	*0.716*	*0.756*	*0.609*
R_h	*0.140*	*0.106*	*0.171*	*0.157*
C_{ic}	0.006	0.014	0.008	0.006
R_{ic}	*0.381*	*0.547*	*0.283*	*0.340*
C_s	0.001>	0.001>	0.012	0.001>
R_s	0.027	*0.152*	0.006	0.003

3.2.5. Model Discussion

3.2.5.1. Regression

The regressions yielded very good fits of the models to that of the data, as shown with the residual sum of squares presented in Table 3.6. The 45mm thatch sample run yielded both the worst and best residual sum of squares, 71.5°C^2 and 1.4°C^2 respectively.

3.2.5.2. Energy Input (Q_{in})

A 15-Watt incandescent lamp powered directly from mains electricity was used as a heat source. During the calibration runs it became apparent that the power supplied to the lamp was not constant and varied with the time of day. As a result, the measurements of the experiments exhibited strange anomalies caused by the changes in heat input. This anomaly was not evident until one of the calibrations accidentally ran over several days.

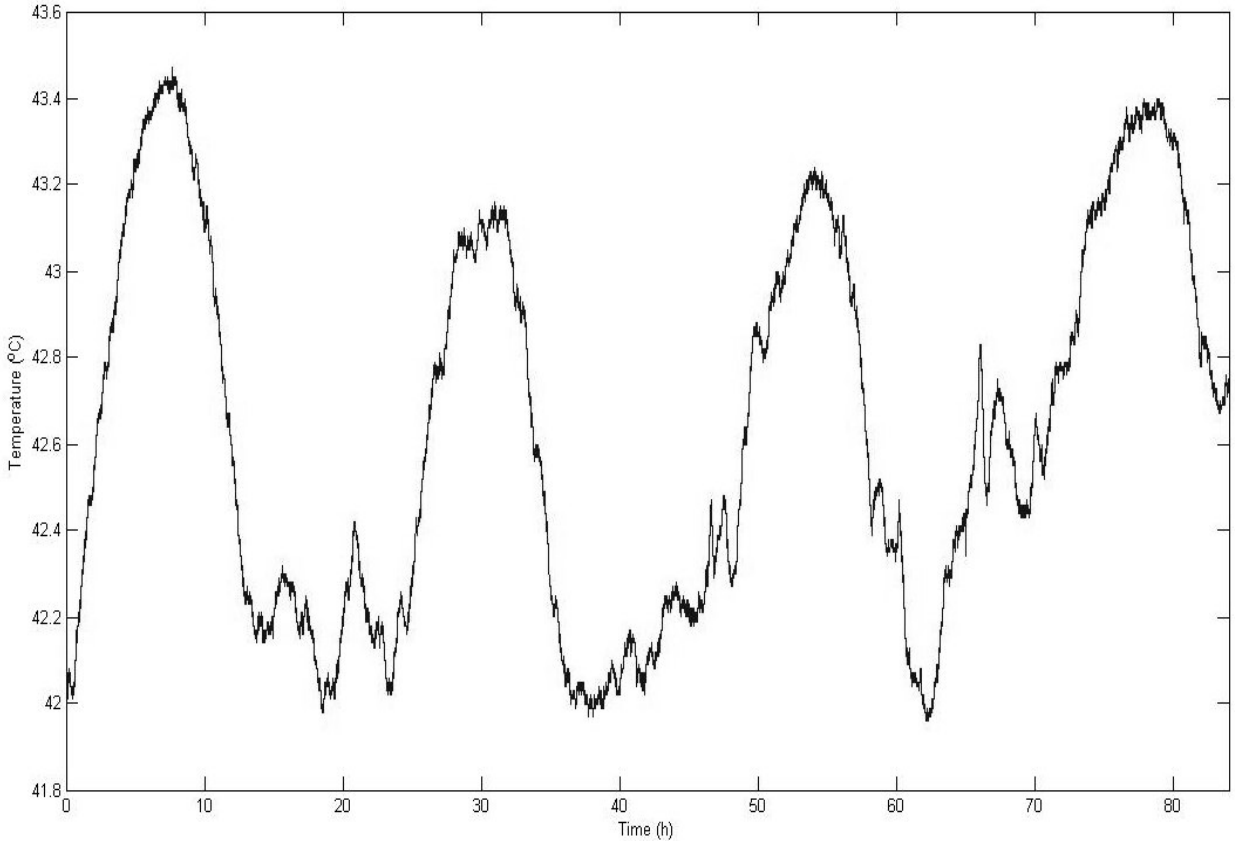

Figure 3.11 – Steady state error from heat source power variance

The variance in the power input of the mains supply appeared to vary with the time of day. Figure 3.11 illustrates the temperature variation within the Flux

Box during the calibration run over several days. It was clear that the variance within the mains supply was caused by changes in electricity supply demand over the course of the day. A surplus of power was available in the evenings while a deficit was evident during normal working hours. The variation in filament colour temperature with voltage as shown by Zanetti (1984) is presented in Table 3.11.

Table 3.11 – Comparison of lamp colour temperatures at different voltages (after Zanetti (1984)

Lamp Rating	**Voltage (V)**	**Temperature (K)**
100 W, 220 V	140	2320
	220	2760
60 W, 220 V	140	2295
	220	2730
40W, 220 V	140	2190
	220	2620

The maximum deviation measured over the 85-hour interval as per Figure 3.11 was approximately 1.5^{o}C, which in the 25^{o}C temperature range that the flux box experiments were conducted, constitutes a 6% error. Unfortunately, due to the lack of supply voltage data, the fluctuation in the heat source could not be quantified sufficiently to compensate the model regressions. However, the models exhibited sufficient robustness that resulted in only small residual errors during regression. The total global mean power input for the flux box model for sampling runs was 15.69 +/-0.89 J/s.

Given the variance in the incoming supply voltage and subsequent lamp temperature, the energy input shown by the model regression was taken as the global average for the entire sampling run. The Kruskal-Wallis test on variance showed that the energy input for all sampling runs was not significantly different (Table 3.7). Comparison of the sampling run results with that of the calibration results shows that the differences were significant, as shown in the results of the t-test represented in Table 3.10. Only the 15mm manure sample was shown not to be significantly different, but as this

sampling run consisted of only two repititions (Table 3.5) this result is contestable and not considered. It is highly probable that the apparent difference that was observed may have been caused by the lack of thermal "damping" caused by the sample plates. The high rate of energy leaving the flux box resulted in greatly varying temperatures as the incoming voltage fluctuated. Clauss, Ralich and Ramsier (2001) show the effects of thermal damping, regarded in their case as hysterisis, of a light bulb filament to power inputs of varying frequencies (Figure 3.12).

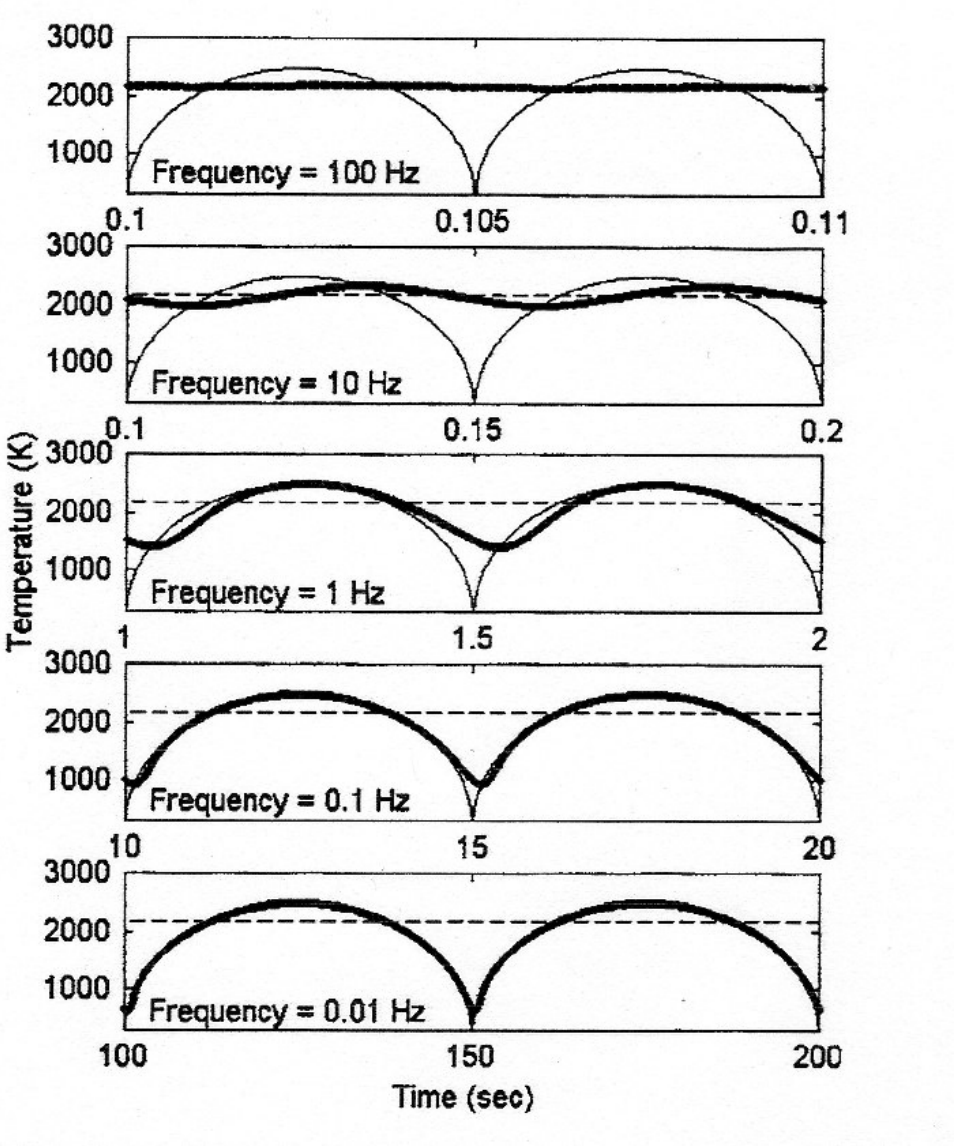

Figure 3.12 – Variation of lamp filament temperature with varying power frequencies (from Clauss *et. al.* (2001))

3.2.5.3. Energy to radiation ratio (Q_{rr})

Clauss *et. al.* (2001) show an emissivity value of around 0.35 for their light bulb hysterisis experiment. This emissivity value is considerably close to the global mean model energy to radiation ratio prediction of 0.35 +/-0.05 . This is illustrated in figures 3.7 and 3.8, and the results of the calibration shown in Table 3.9. This emissivity value is also shown by Agrawel *et al.* (1995).

The null hypothesis that the radiation ratio was the same between sampling runs and the calibration run stands for all samples and thicknesses (Table 3.10). The global mean difference in the variance was less than 0.1, as shown in Figure 3.10.

3.2.5.4. Heat Source Thermal Capacity (C_h)

The thermal capacity of the heater did not vary significantly between materials for all cases, shown in Table 3.7, and was not significantly different between the calibration and the materials (Table 3.10). The variance of thermal capacitance in the calibration sample shown in the standard deviation in Table 3.9 illustrates that the relative measures represented by Figure 3.10 are not true reflections of the relation between the calibration and material coefficients. As the heater was running at different temperatures due to the fluctuation in input power, this would have most likely affected the models prediction of its thermal capacity. The total mean capacity for manure, thatch, straw and reeds was 15.54 +/-0.9 J/K, 16.1 +/-1.5 J/K, 17.3 +/-2.8 J/K and 17.84 +/-2.4 J/K respectively. The global mean thermal capacity was 16.71 +/-2.3 J/K for all materials. No significant relation was found between the heat source thermal capacity and material thickness (Table 3.8).

3.2.5.5. Heat Source Thermal Resistance (R_h)

No significant difference was found between materials (Table 3.7) or between the calibration and any of the materials (Table 3.10). The thermal resistance of the heater is thus considered constant through all experiments. The total mean thermal resistance for manure, thatch, straw and reeds was 8.22 +/- 0.47 K/J.s, 7.86 +/-0.61 K/J.s, 7.62 +/-1.24 K/J.s and 7.98 +/-0.50 K/J.s respectively, with a global mean of 7.93 +/-0.78 K/J.s for all materials. No significant relation was found between the heat source thermal resistance and material thickness (Table 3.8).

3.2.5.6. Inner Cavity Thermal Capacity (C_{ic})

A significant difference was evident between the calibration and the 60mm thatch; 30mm, 45mm, and 60mm straw and all reed thicknesses (Table 3.10). The Kruskal-Wallis ANOVA indicated a significant difference between the thermal capacities of materials of thicknesses of 30mm, 45mm, and 60mm (Table 3.7). The total mean capacity for manure, thatch, straw and reeds was 923.45 +/-88.93 J/K, 762.28 +/-71.90 J/K, 1104.2 +/-120.85 J/K and 1081.30 +/-63.55 J/K respectively. The global mean thermal capacity was 1018.78 +/-109.73 J/K for all materials. No significant relation was found between the inner cavity thermal capacity and material thickness (Table 3.8).

3.2.5.7. Inner Cavity Thermal Resistance (R_{ic})

There were no significant differences between different materials of the same thickness (Table 3.7), or when compared to the calibration coefficients as represented in Table 3.10. The total mean thermal resistance for manure, thatch, straw and reeds was 1.05 +/-0.05 K/J.s, 1.09 +/-0.09 K/J.s, 1.02 +/-0.13 K/J.s and 1.01 +/-0.08 K/J.s respectively, with a global mean of 1.01 +/-0.08 K/J.s for materials. No significant relation was found between the inner cavity thermal resistance and material thickness (Table 3.8).

3.2.5.8. Material Thermal Capacity (C_s)

Although there was no significant difference between materials of the same thickness (Table 3.7), there was a significant difference between the calibration and material coefficients for all samples (Table 3.10). The average thermal capacity of the calibration coefficients was 0.07 +/-0.12 J/K, compared with the total mean capacity for manure, thatch, straw and reeds at 1001.77 +/-67.28 J/K, 964.82 +/-97.11 J/K, 891.38 +/-410.15 J/K and 844.37 +/-199.45 J/K respectively. The global mean thermal capacity was 911.53 +/-250.91 J/K for all materials. No significant relation was found between the material thermal capacity and material thickness (Table 3.8).

3.2.5.9. Material Thermal Resistance (R_s)

All material coefficients were not significantly different for different materials of the same thickness (Table 3.7). There were six scattered cases where calibration coefficients were not significantly different to that of material coefficients (Table 3.10). The average thermal resistance of the calibration coefficients was 0.74 +/-0.12 K/J.s, compared with the total mean resistance for manure, thatch, straw and reeds at 0.99 +/-0.09 K/J.s, 0.98 +/-0.13 K/J.s, 1.26 +/-0.49 K/J.s and 1.00 +/- 0.14 K/J.s respectively. The global mean thermal resistance was 1.07 +/-0.27 K/J.s for all materials. No significant relation was found between the material thermal resistance and material thickness (Table 3.8).

4. Dynamic Pond System Model for Rural Aquaculture

4.1. Background

Various pond system models have been proposed and tested against a variety of commercial aquaculture systems. Fairly simple computer based models of heat balances between pond systems and the environment were put forward by authors such as Singh and Marsh (1995) and Klemetson and Rogers (1985). Their models comprised of simple numeric heat balance equations based on monthly averages of climatic data. While these models are useful for deriving the basic operating conditions of the ponds, and can be used for determining monthly heat load requirements and identifying heat loss components, they lack the resolution often required for finer control and prediction of pond states. As this may be, these system models have still laid the basic foundations for further model development in the field of aquaculture.

Cathcart and Wheaton (1987) put forward a model for predicting the temperature distribution in freshwater ponds. The model, based on a set of differential heat balance equations, could predict hourly temperature variations through stratified layers of pond water. Models such as this were a significant step in model development, as previous models often did not account for stratification in pond systems. Zhu, Deltour and Wang (1999), well known names in the field of aquaculture modelling, presented a series of aquaculture models based on differential heat balances. Their greenhouse pond system model (GPS), based primarily on the Gembloux Greenhouse Dynamic Model by de Halleux, Nijskens and Deltour (1985), illustrated the important dynamic processes taking place in greenhouse pond systems and the small, somewhat subtle effects of small heat balances often left out by other authors. Zhu *et al.* (2000) also described a model for predicting thermal stratification in aquaculture ponds. Their model predicted the effect of sunlight on varying depths of the pond, and was tested extensively at various pond locations.

4.2. A model proposal for rural aquaculture

Although extensive work has been done on aquaculture models, these have all been aimed at improving large commercial aquaculture systems. They often employ the use of commercially available skills, materials and equipment, often not accessible to the average rural farmer. Proposed here, based on the extensive tests conducted on common materials used for traditional rural construction, is a set of models based on the rural situation. A total of six scenarios will be explored:

- Open earthen aquaculture ponds
- Earthen aquaculture ponds enclosed in a kraal fence
- Aquaculture ponds enclosed in well-ventilated traditional Xhosa structures.
- Aquaculture ponds enclosed in sealed or poorly ventilated traditional Xhosa structures.
- Aquaculture ponds enclosed in sealed or poorly ventilated traditional Xhosa structures, with temperature controlled basic thermosiphon driven solar heating.
- Aquaculture ponds enclosed in sealed or poorly ventilated traditional Xhosa structures, with basic thermosiphon driven solar heating with no temperature control.

These models will be used to explore the potential opportunities available to rural farmers in the subsistence aquaculture field. This may even improve the potential for migration to commercial aquaculture schemes. The models will illustrate their importance in planning such rural aquaculture developments, as a variety of situations and scenarios can be explored before time, resources and money is wasted on a set-up that is doomed to fail. It was envisaged that the theoretical scenarios put forward in this study be tested physically using existing structures, but time and resources put this beyond the scope of this project.

4.3. Overview of weather variables and available data

Data kindly sponsored by the South African Weather Service was obtained for the Port Elizabeth and Mthatha regions. The variables required for the models included:

- Temperature
- Humidity
- Wind speed
- Global solar radiation

Although it was originally intended to use Mthatha weather data for the project, it became apparent that the conditions at the Mthatha weather office, which is located at: Lat:-31.53, Long:28.67, Height: 747m, were not reflective of the conditions of the coastal regions, where it was anticipated the models would be based. Furthermore, the Mthatha weather station did not record global solar radiation, and had erroneous pressure and humidity data. It was also uncertain as to the accuracy of the temperature and wind data. Given these circumstances, the models were based on Port Elizabeth weather office data located at: Lat:-33.984, Long:25.61, Height: 63m. This was the data used for setting up and calibrating the initial model, which was based on a system only five kilometres from the weather office. Five-minute weather data for the year 2005 was processed and summarised per hour. Monthly 24-hour averages along with their standard deviations are presented in Figure 4.1.

The overall average temperature for the year of 2005 was 17.4 +/-3.6 ^{o}C. Mean averages for summer, autumn, winter and spring are 20.4 +/-2.8 ^{o}C, 18.0 +/-3.7 ^{o}C, 14.0 +/-4.3^{o}C and 17.21 +/-3.7^{o}C respectively.

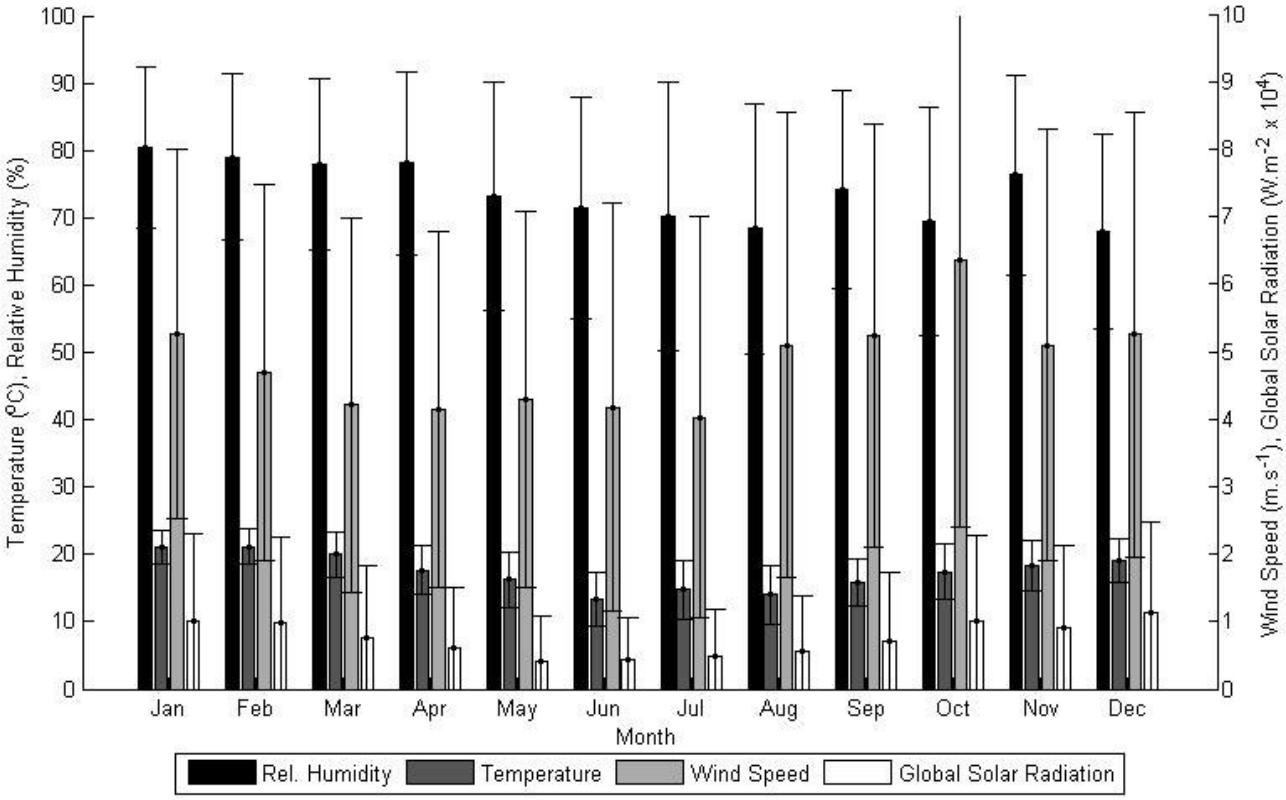

Figure 4.1 – Average climatic data with standard deviations for Port Elizabeth in 2005

4.4. Open Pond System Model

The first part of the model development required the set up of a basic set of heat balance equations depicting the thermal flux transfers between an open pond and the surrounding ambient environment. A real physical system was required that could be used to calibrate and validate the model to. The dolphin pool at Bayworld, Port Elizabeth was chosen for a number of reasons including:

- Proximity to the coastline and weather office
- Large open system with large surface area
- Well mixed with continuous turnover
- No active thermal or physical environmental control measures in place
- Continuous hourly pool temperature data available from the past five years

The pool provided an excellent opportunity to develop the models and put them to the test. The architectural drawings were studied to extract basic dimensional measures of the system. From the air, the pool is in the shape of

a glove, and was thus broken down into three blocks of varying size for practical reasons (Table 4.1).

Table 4.1 – Dimensional measures of the dolphin pool at Bayworld, Port Elizabeth

Block	Length (m)	Breadth (m)	Height (m)	Area (m^2)	Volume (m^3)
1	24	24	2.79	576	1607.1
2	22	26	4.57	572	2614.1
3	20	15	2.1	300	630
Total				1448	4851.1

4.4.1. Model Development

A basic set of heat balance equations was needed to determine the change in pool temperature under the given climatic conditions. Based on the models presented by Zhu *et al.* (1999, 2000), Cathcart and Wheaton (1987), Singh and Marsh (1995) and Klemetson and Rogers (1985), the following components were to be included:

- Radiation gain from sun: S_{rg}
- Radiation gain from sky: Sk_{rg}
- Radiation loss to sky: Sk_{rl}
- Convective heat balance with air: qC_{air}
- Heat loss to evaporation: qE_{air}
- Heat loss from water replacement: qW_r

The basic heat balance equation was thus derived:

$$C_w \frac{dT_w}{dt} = S_{rg} + Sk_{rg} - Sk_{rl} - qC_{air} - qE_{air} - qW_r \qquad (4.1)$$

where:

C_w is the thermal capacity of the pool in *J/K*
T_w is the temperature of the pool in ^oC

Each component was investigated and developed separately before the final model was assembled. Radiation fluxes were calculated based on surface emissivities (ε), while convection and evaporation were calculated from Nusselt (Nu_k) and Meyer evaporation determinations (E_{air}) respectively.

The R-C thermal network representation of the pool model is presented in Figure 4.2.

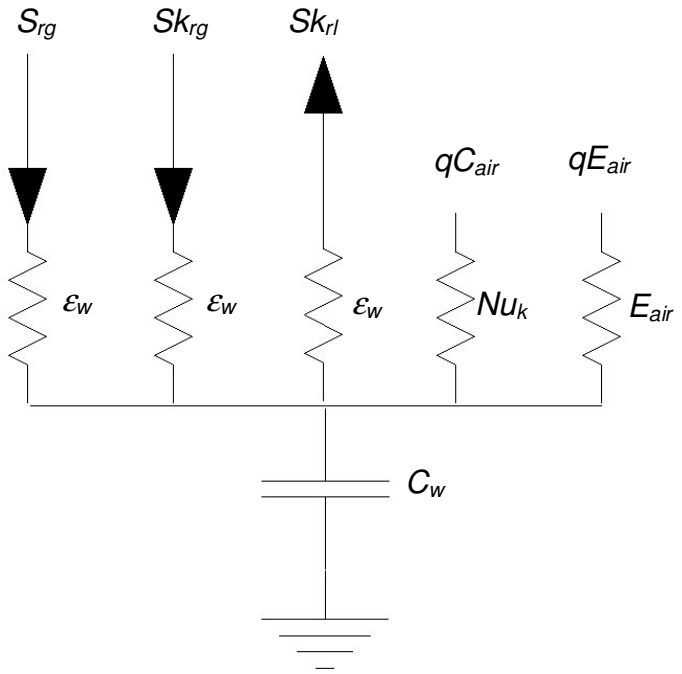

Figure 4.2 – R-C Thermal Network Model of Open Pool Thermal System

4.4.1.1. Radiation fluxes

Zhu *et al.* (1999) presented an equation that could determine heat gain from solar radiation input. This equation could calculate nett energy input into a pond system, as well as the amount of energy absorbed within a particular layer of a stratified pond with compensation for reflectance off the water surface from the angle of the sun. This level of detail, however, was not required for this model, and a simpler approach as used by Klemetson and Rogers (1985) was adopted.

The basic equation employed calculated the total energy absorbed by multiplying the incoming global solar radiation (*S, in W.m*$^{-2}$) by the emmisivity factor of the water (ε_w, typically 0.97 for water). The equation was thus derived:

$$S_{rg} = S \times \varepsilon_w \tag{4.2}$$

Zhu *et al.* (1999) pointed out that the background radiation from the temperature of the sky should be taken into account. The sky is usually treated as an equivalent black body in this case, with the equation:

$$T_{sky} = 0.0552(T_a + 273)^{1.5} \quad (4.3)$$

where

T_{sky} is the ambient sky temperature in *K*
T_a is the ambient air temperature in ^oC

The thermal radiation from bodies such as the sky and water are determined using the Stefan-Boltzmann law:

$$q_r = \varepsilon \times \sigma \times T_k^{\ 4} \quad (4.4)$$

where

q_r is the thermal radiation in $W.m^{-2}$
ε is the emmisivity
σ is the Stefan-Boltzmann constant $5.67 \times 10^{-8}\ W.m^{-2}.K^{-4}$
T_k is the temperature of the radiating body in *K*

The absorption of radiation energy Sk_{rg} from T_{sky} is modelled the same as solar absorption from the sun. The radiation energy loss to the sky from the pool Sk_{rl} is modelled using the Stefan-Boltzmann law as described.

4.4.1.2. Convective heat flux

Convective heat flux problems have been addressed by different authors in varying manners. Klemetson and Rogers (1985) used a basic equation using a set of basic constants derived from Velz (1970). Zhu *et al.* (1999, 2000) made extensive use of Nusselt determinations based on a set of limits defined by Montieth and Unsworth (1990).

The heat transfer equation for convection based on the nusselt determination is thus derived:

$$qC_{air} = Nu \times k \times \left(\frac{T_i - T_a}{d} \right) \quad (4.5)$$

where

qC_{air} is the nett thermal flux due to convection in $W.m^{-2}$
Nu is the dimensionless nusselt number
k is the thermal conductivity of air in $W.m^{-1}.K^{-1}$
T_i is the surface temperature in ^oC
T_a is the air temperature in ^oC
d is the characteristic length in m

Table 4.2 – Nusselt determinations for various flows (from Zhu *et al.*,1999)

	Laminar Flow	**Turbulent Flow**
$Gr/Re^2 >= 16$,	**$Gr <= 10^8$**	**$Gr > 10^8$**
Natural Convection	$Nu = 0.54 \times Ra^{1/4}$	$Nu = 0.15 \times Ra^{1/3}$
$Gr/Re^2 <= 0.1$,	**$Re <= 5 \times 10^4$**	**$Re > 5 \times 10^4$**
Forced Convection	$Nu = 0.66 \times Re^{1/2} \times Pr^{1/3}$	$Nu = 0.036 \times Re^{4/5} \times Pr^{1/3}$

Table 4.3 – Definitions and values for dimensionless numbers for air at 20°C (from Zhu *et al.*, 1999)

Name	**Symbol**	**Definition**	**Value**
Grashof	Gr	$g\beta_{air}d^3(T_i-T_a)v^{-2}$	$1.576 \times 10^8\ d^3\ (T_i-T_a)$
Prandtl	Pr	v/D_a	0.7020
Reynolds	Re	Wd/v	6.623×10^4 W d
Rayleigh	Ra	Gr Pr	

Table 4.2 outlines the basic set of equations, based on the dimensionless numbers described in Table 4.3, for determining the Nusselt number *Nu* for various states of the air above the convecting surface. The movement of the air is taken into account by the Reynolds number, which accounts for thermal energy lost to wind. Calculations for natural convection often involve complicated fluid dynamics, and accurate modelling can be very difficult. The methods employed between authors are not always agreed upon, hence the variation in modelling approaches (Tieszen, Ooi, Durbin and Behnia 1998). Each model has its application that has been tested to a certain degree. The approach presented by Zhu *et al.* (1999, 2000) appears to fit well with the intended application and is thus employed for this model.

Table 4.4 – Basic parameters and descriptions

Parameter	Description	Units
g	Gravitational acceleration	$m.s^{-2}$
β_{air}	Expansion coefficient for air	K^{-1}
d	Characteristic length	m
v	Kinematic viscosity	$m^2.s^{-1}$
D_a	Thermal diffusivity of air	$m^2.s^{-1}$
W	Wind speed	$m.s^{-1}$

4.4.1.3. Evaporation

There are currently several evaporation equations in use. Singh and Xu (1997) evaluated the performance of several equations against measured data and reported on optimal parameter settings. Meyers formula, as used by Klemetson and Rogers (1985), produced the most favourable results, as confirmed by Singh and Xu (1997).

This equation was used to determine the rate of evaporation for the pool model:

$$E = a_1 \cdot (1 + a_2 \cdot W) \cdot (e_o - e_a) \tag{4.6}$$

where

E is the evaporation in *mm/h*
a_1, a_2 are dimensionless constants
W is the wind speed in $m.s^{-1}$
e_o is the saturation vapour pressure in *millibars*
e_a is the vapour pressure in *millibars*

For hourly data required in the model, the constants determined for daily evaporation from Singh and Xu (1997) were modified as presented:

- a_1 = 0.362 / 24
- a_2 = 0.214

Saturation vapour pressure was determined based on the standard psychrometric formula:

$$e_o = \frac{2.718^{(77.345 + 0.0057 \times Tk - \frac{7235}{Tk})}}{Tk^{8.2}} \tag{4.7}$$

Vapour pressure was thus calculated as a proportion of the saturation vapour pressure based on the relative humidity:

$$e_a = \frac{RH}{100} \times e_o \tag{4.8}$$

where

Tk is the air temperature in *K*
RH is the relative humidity in *%*

Calculation for heat loss was determined by the product of evaporation and the latent heat of vaporization:

$$qE_{air} = E \times L_v \times 0.00027778 \tag{4.9}$$

where

qE_{air} is the heat lost to evaporation in $W.m^{-2}$
E is the rate of evaporation in *mm/h*
L_v is the latent heat of vaporization for water: 2260872 *J/kg*

4.4.1.4. Water Replacement

Energy lost by water replacement was calculated based on the difference in energy lost per unit volume per unit time and energy gained per unit volume per unit time:

$$qW_r = (T_w + 273) \times C_w \times V_{in} - (T_{in} + 273) \times C_w \times V_{in} \quad (4.10)$$

where

qW_r is the energy lost by water replacement in *W*
T_w is the pool temperature in ^oC
T_{in} is the temperature of the incoming water in ^oC
C_w is the thermal capacity of the pool in *J/K*
V_{in} is the water replacement volume in m^3/h

4.4.1.5. Model validation

The model was compiled under MatLab and run with the hourly data extracted from the weather office data for 2005. Water replacement rates and temperatures were not available, but based on normal operating parameters and average sea intake temperatures were assumed to be 25 m^3/h and 20 ^oC respectively throughout the year.

The simulation was run in time steps of one hour, and then compared with the measured data from the dolphin pool. Apart from some data formatting issues, no calibration was required. The model exhibited a very satisfactory fit with the measured data, with a residual sum of squares of 5538.1$^oC^2$, a r^2 value of 0.998 and a mean error of 0.795 ^oC. Figure 4.3 illustrates the extremely good fit of the model prediction with that of the actual temperature.

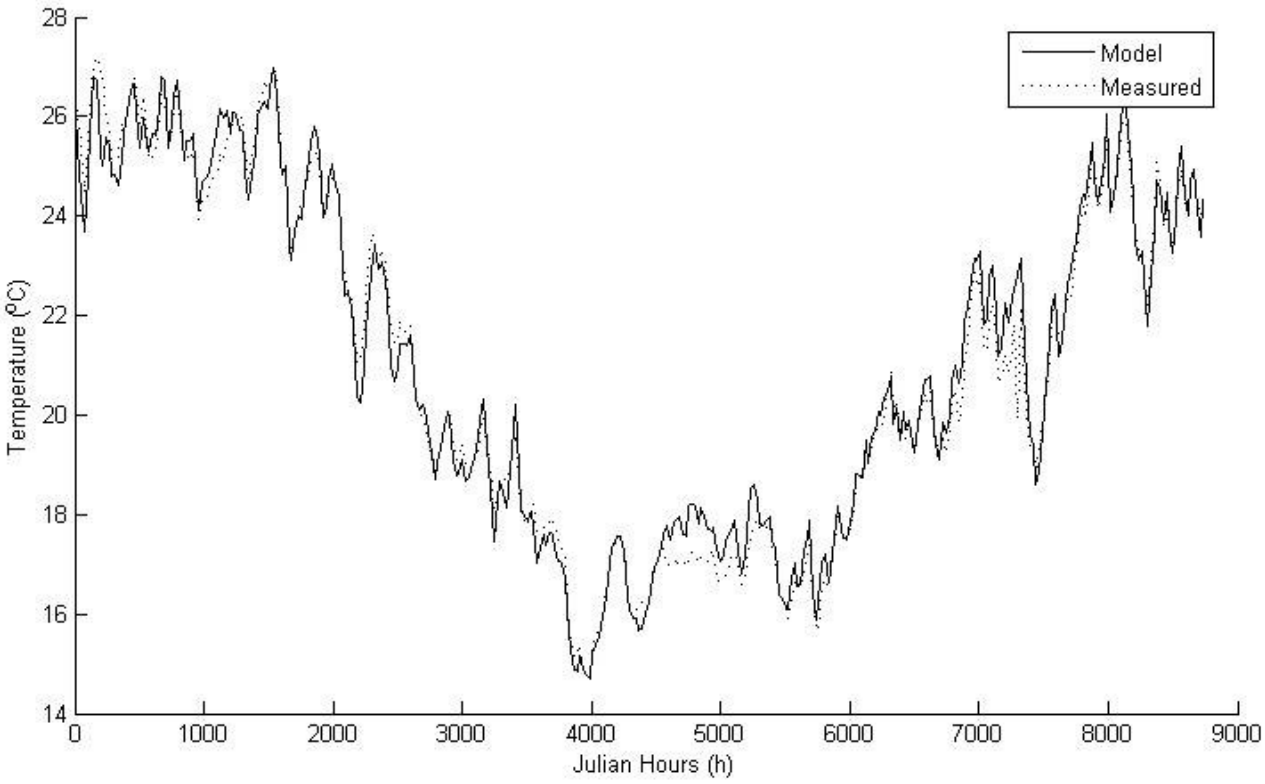

Figure 4.3 – One-year temperature simulation for the dolphin pool at Bayworld, Port Elizabeth

4.5. Model application to rural environments

Once the model was validated, it was modified appropriately for each rural scenario. The open and kraal enclosure scenario used the existing model unmodified, except for a modification of the wind strength for the latter. The vented Xhosa traditional hut scenario, referred to as the vented hut model, included heat balance equations for the roof and wall structures. The closed Xhosa traditional hut scenarios, referred to as the sealed hut model, included heat balance equations for the roof and wall structures, as well as the internal air temperature. The last two solar control scenarios included a simple equation for calculating solar heat input via a solar heater. No water exchange was included in the models. Results are presented as yearly and seasonal averages, with summer ranging from December to February, autumn from March to May, winter from June to August and spring from September to November.

4.5.1. Open Pond Scenario

The existing model was run with a smaller pool size. For the scenario, a round pool with a surface area of 200 m^2, a depth of 3m and a resulting volume of 600m^3 was run. A two-week output for the month of January is presented in Figure 4.4 for illustrative purposes, demonstrating the typical output from the model.

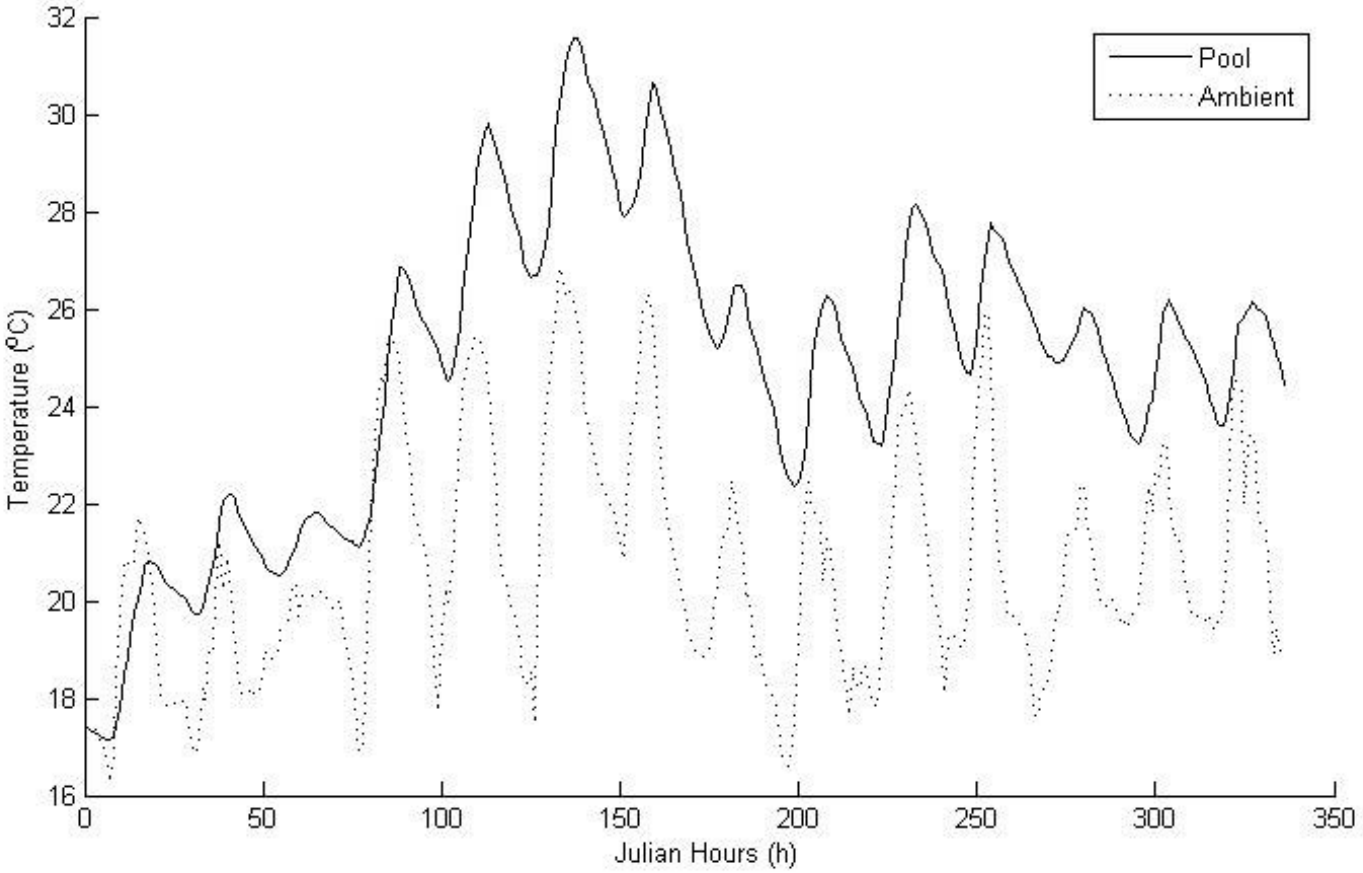

Figure 4.4 – Two week model output for rural open pond model

The calculated averages for each month of the year is presented in Figure 4.5. The overall average temperature for the year of 2005 was 21.2 +/-3.74 °C. Mean values for summer, autumn, winter and spring are 25.6 +/-2.3 °C, 21.3 +/-2.3 °C, 16.5 +/-1.5°C and 21.4 +/-2.4°C respectively.

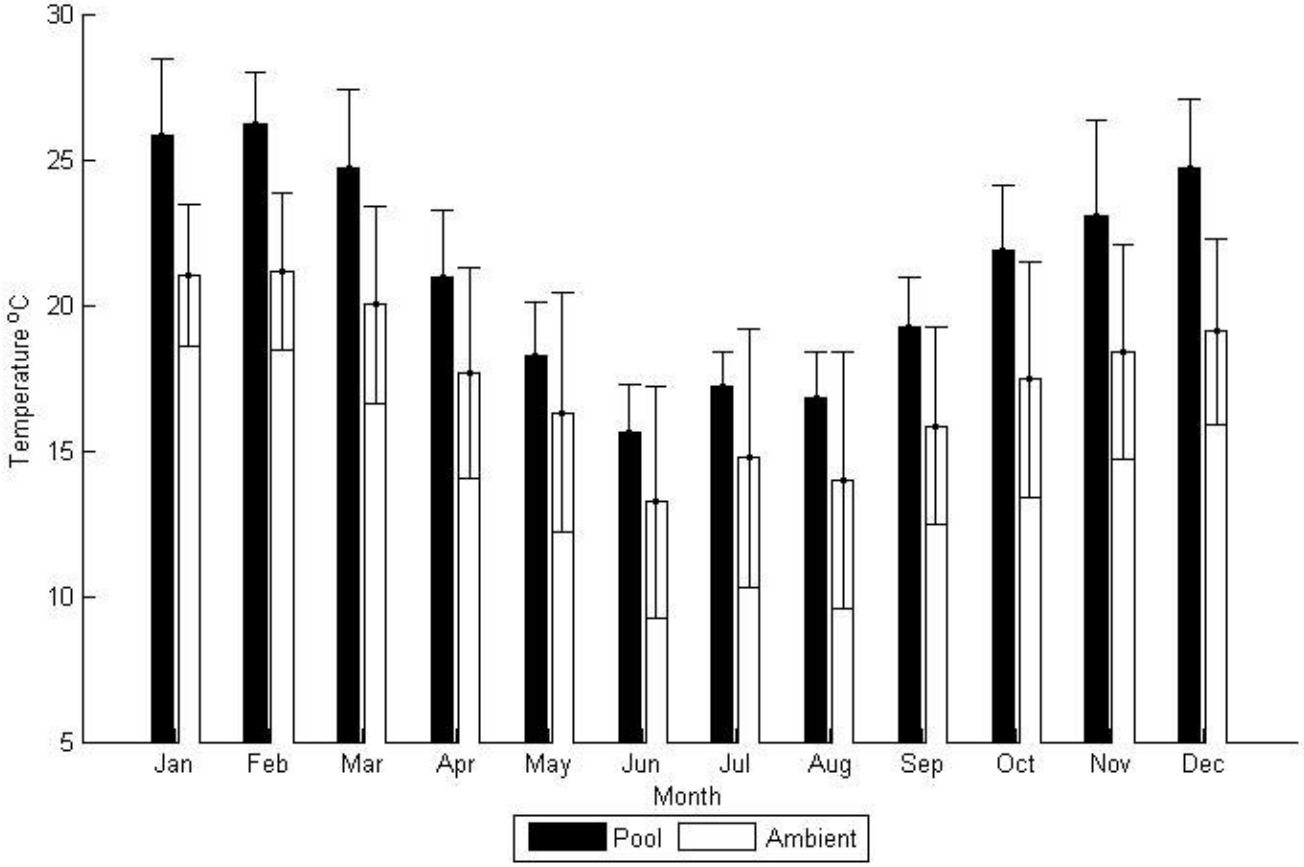

Figure 4.5 – Monthly averages of model output with air temperature

4.5.2. Kraal enclosed pond scenario

For the scenario, the open pond model described above was placed in a theoretical proposed kraal 20m by 20m by 1.25m. These dimensions were derived from the wind-break experiments of Wilson and Flesch (2003). The wind variable was then damped by a factor of 0.4 as determined in their experiments.

A two-week output for the month of January is presented in Figure 4.6 for illustrative purposes, demonstrating the typical output from the model. The calculated averages for each month of the year is presented in Figure 4.7. The overall average temperature for the year of 2005 was 23.4 +/-4.5 ^{o}C. Mean values for summer, autumn, winter and spring are 28.6 +/-2.5 ^{o}C, 23.3 +/-2.3 ^{o}C, 17.9 +/-1.4^{o}C and 23.8 +/-2.5^{o}C respectively.

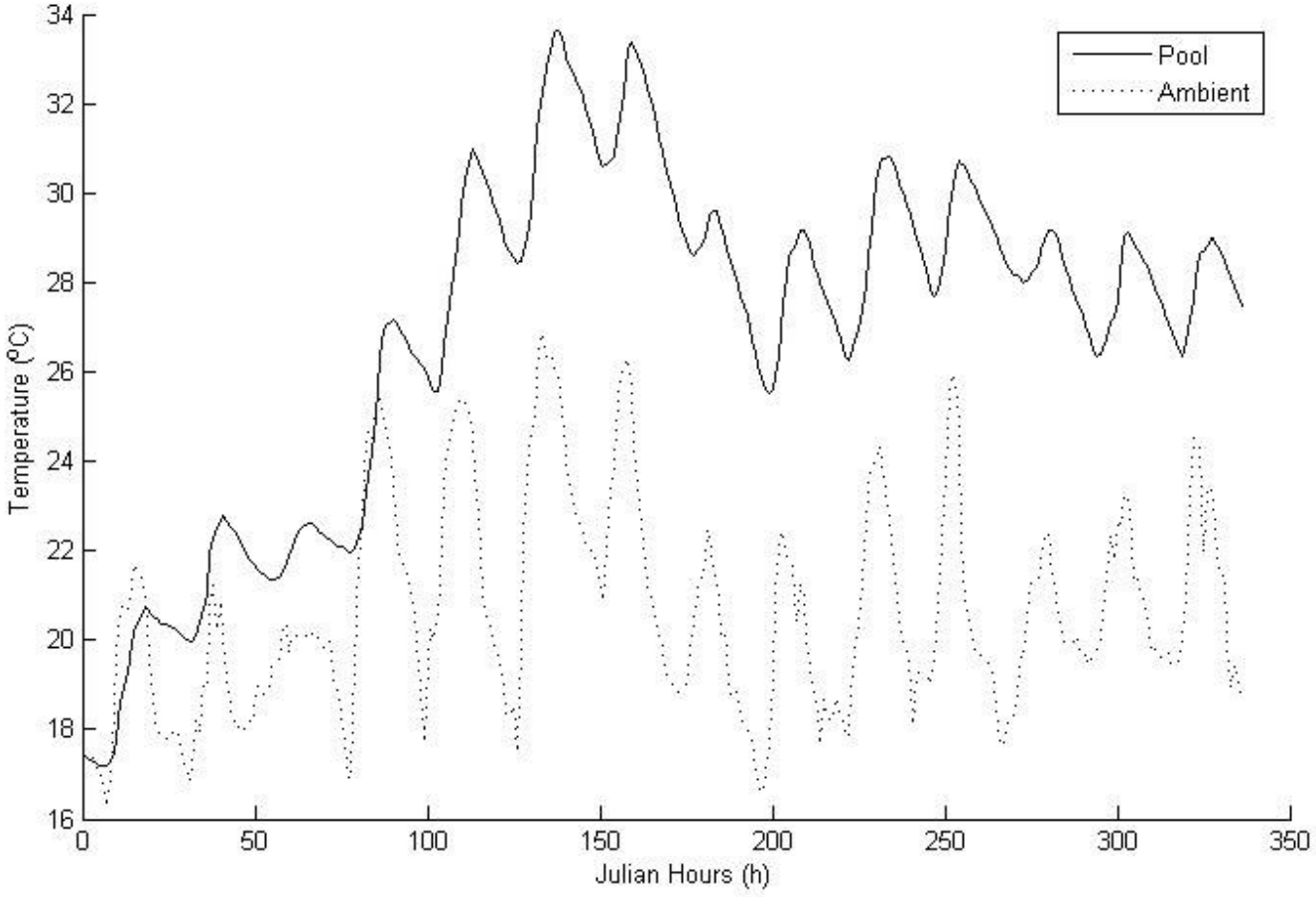

Figure 4.6 - Two week model output for rural kraal enclosed pond model

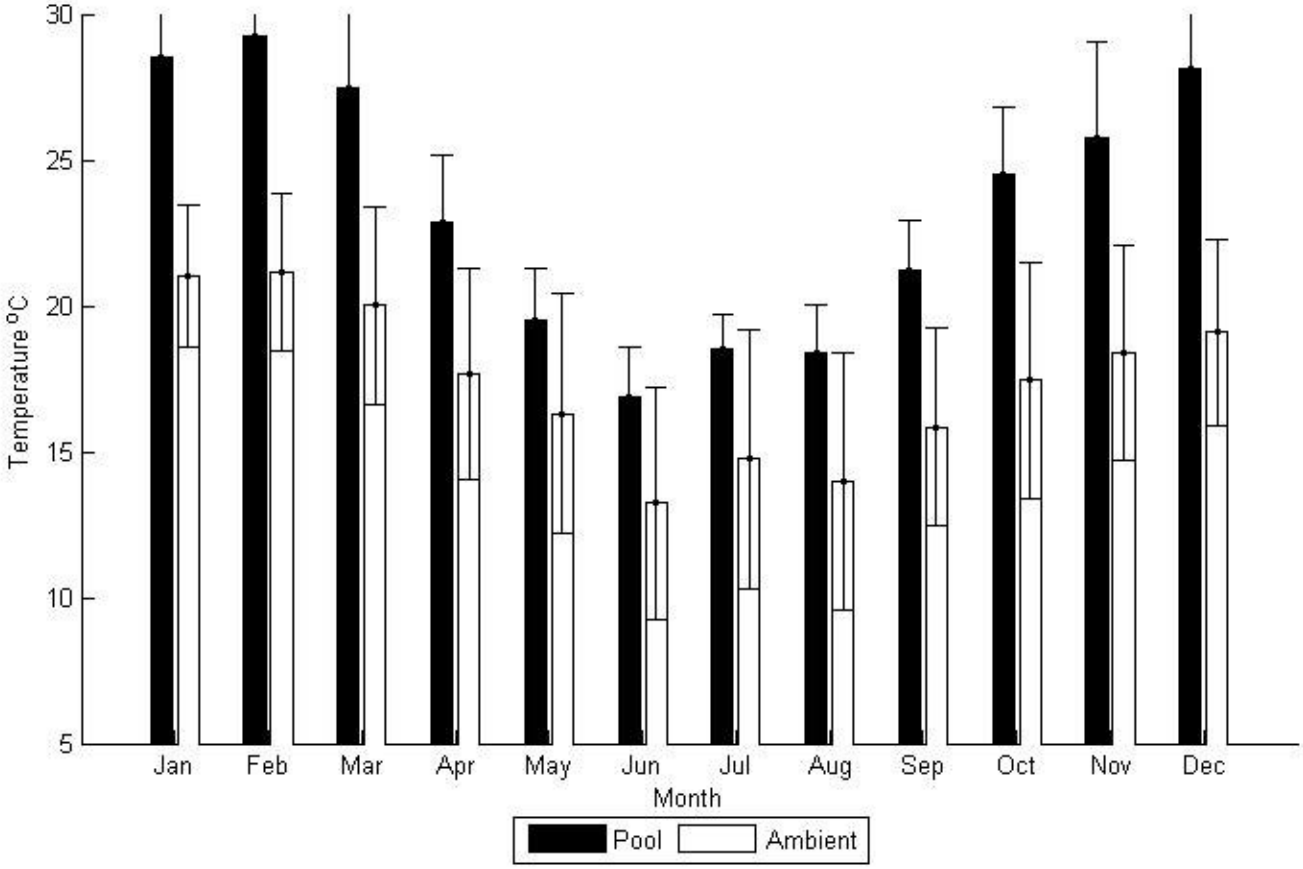

Figure 4.7 – Monthly averages of model output with air temperature

4.5.3. Ventilated Hut Scenario

For this scenario, the pond was placed into a theoretical hut with low walls to allow for good ventilation (Figure 4.8). The internal air temperature and humidity would thus follow the ambient conditions. Wind was damped with a factor of 0.1. Sunlight would be excluded, instead replaced by a radiation balance between the walls, roof and pond. A smaller more practical sized pond was used for this scenario, with a pond surface area 12.57 m^2 and a depth of 1m giving a volume of 12.57 m^3.

In the model, only radiation would exchange between the wall and roof nodes and the pond node. The wall and roof node comprised of two nodes representing the inner and outer surfaces. The global mean thermal resistance and capacitance values for the materials tested in the Flux Box experiments were put to use for the wall and roof nodes. Since the analysis

showed no significant difference between the materials tested, the roof, comprising of thatch or reeds, and walls, comprising of a dung/straw/reed mixture, would have the same values and be treated the same. The dimensions of the hut were determined from Makaka and Meyer (2006). A slightly larger hut was envisaged to accommodate the pond. The hut had a floor radius of 2.5m and a height of 2.2m, with a roof and wall thickness 0.3m. The RC thermal network model is presented in Figure 4.9.

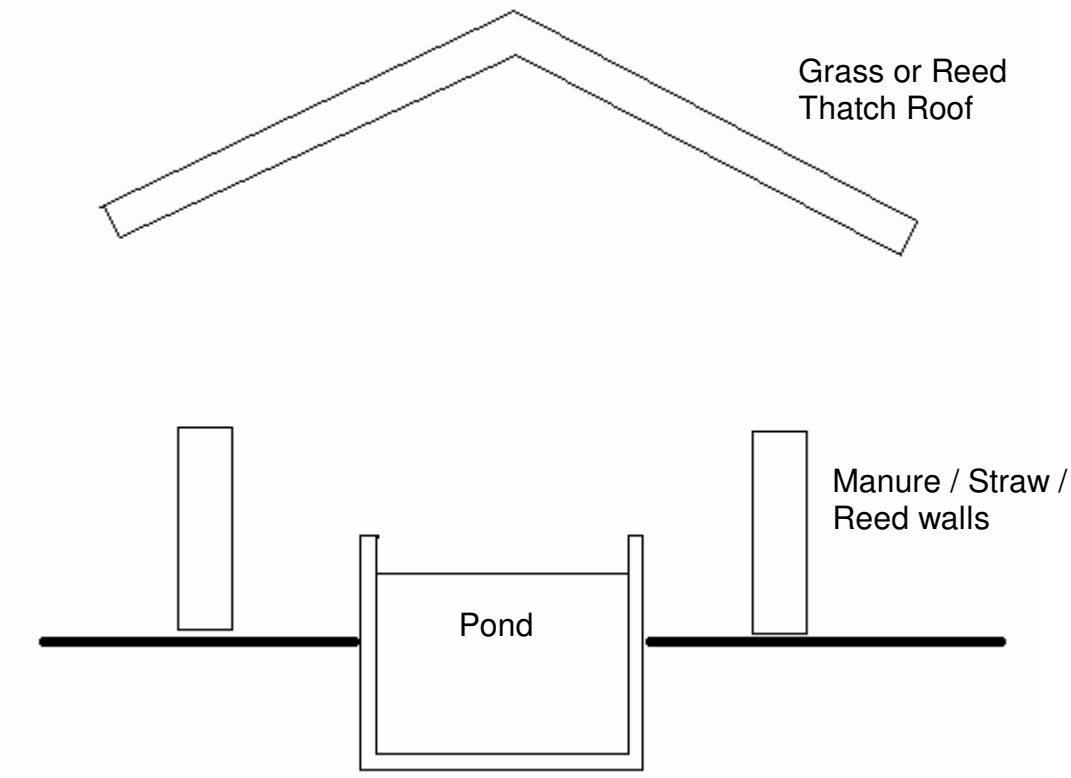

Figure 4.8 – Illustration of the ventilated hut model

The global mean thermal capacity was 911.53 +/-250.91 J/K for all flux box measured materials. The global mean thermal resistance was 1.07 +/-0.27 K/J.s for all flux box measured materials. Given the average mass and volume for all materials, the average density is 97.807 kg/m^3, with a mean depth of 0.0375m. The resultant thermal resistance and capacitance values, compensated with calibration data, were thus 26.6 m.K/W and 1430 J/kg/^{o}C respectively.

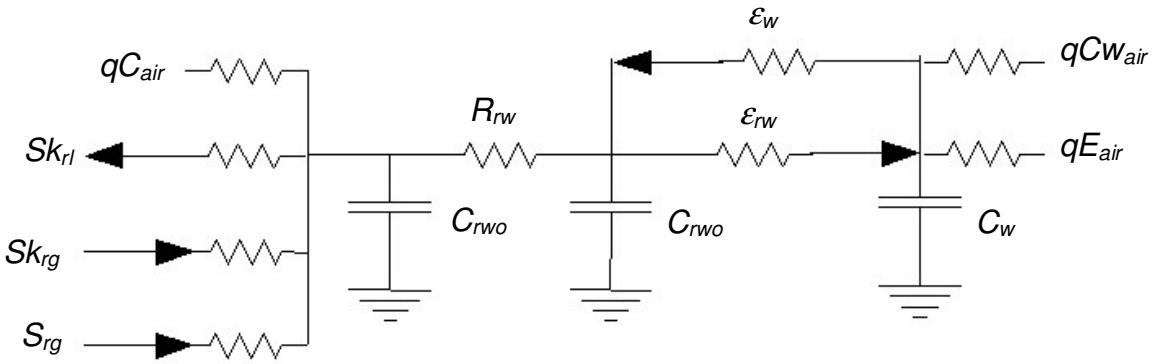

Figure 4.9 – RC Thermal Network model of ventilated hut scenario

The heat balance equations for the vented hut model are thus presented:

$$q_{rw} = \frac{T_{rwo} - T_{rwi}}{R_{rw}} \tag{4.11}$$

$$C_{rwo}\frac{dT_{rwo}}{dt} = S_{rg} + Sk_{rg} - Sk_{rl} - qC_{air} - q_{rw} \tag{4.12}$$

$$C_{rwi}\frac{dT_{rwi}}{dt} = q_{rw} + r_w - r_{rw} \tag{4.13}$$

$$C_w\frac{dT_w}{dt} = r_{rw} - r_w - qCw_{air} - qEw_{air} \tag{4.14}$$

where

S_{rg} is radiation gain from sun in $W.m^{-2}$
Sk_{rg} is radiation gain from sky in $W.m^{-2}$
Sk_{rl} is radiation loss to sky in $W.m^{-2}$
qC_{air} is convective heat balance between roof/wall and air in $W.m^{-2}$
qCw_{air} is convective heat balance between pond and air in $W.m^{-2}$
qEw_{air} is heat loss to evaporation in $W.m^{-2}$
q_{rw} is heat transfer through the wall and roof in $W.m^{-2}$
r_{rw} is radiation heat transfer from roof/wall in $W.m^{-2}$
r_w is radiation heat transfer from pond in $W.m^{-2}$
R_{rw} is the thermal resistance of the wall/roof in $J/K.s$
T_{rwo} is the outer wall/roof temperature in K
T_{rwi} is the inner wall/roof temperature in K
C_{rwo} is the outer wall/roof thermal capacity in J/K
C_{rwi} is the inner wall/roof thermal capacity in J/K

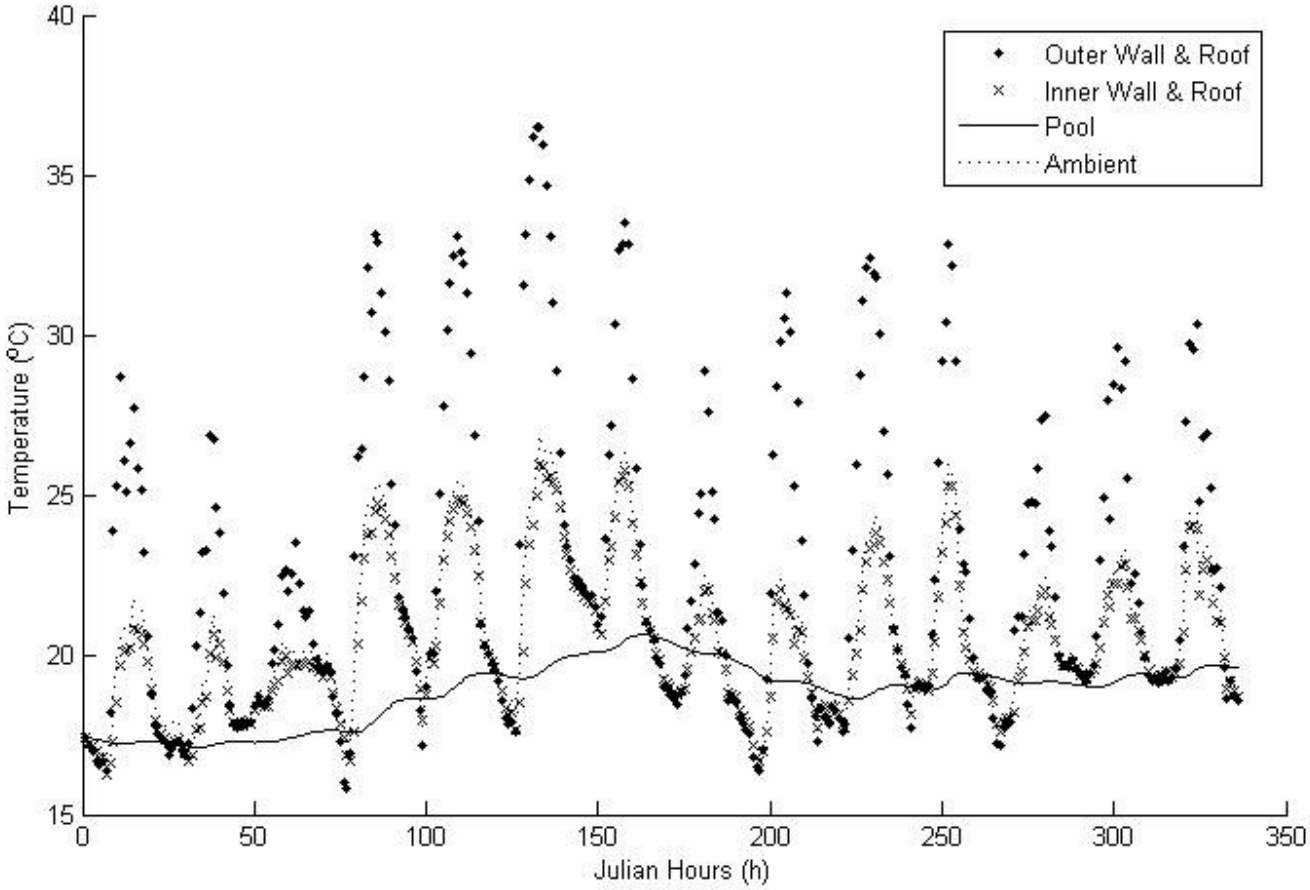

Figure 4.10 - Two week model output for rural ventilated hut pond model

A two-week output for the month of January is presented in Figure 4.10 for illustrative purposes, demonstrating the typical output from the model. The calculated averages for each month of the year is presented in Figure 4.11. The overall average temperature for the year of 2005 was 15.9 +/-2.6 ^{o}C. Mean values for summer, autumn, winter and spring are 18.8 +/-0.7 ^{o}C, 16.5 +/-1.0 ^{o}C, 12.6 +/-0.9^{o}C and 15.6 +/-1.3^{o}C respectively.

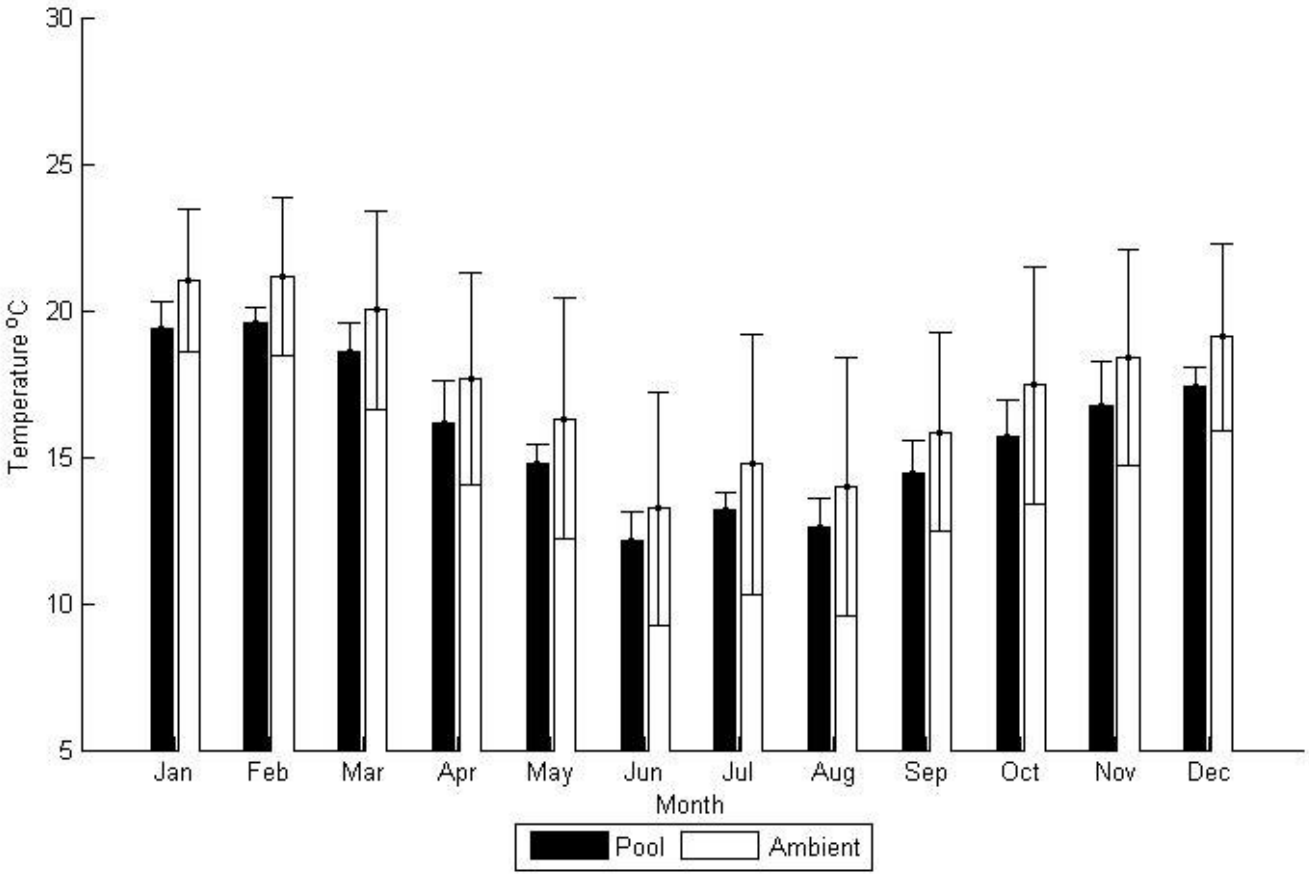

Figure 4.11 - Monthly averages of model output with air temperature

4.5.4. Sealed Hut Scenario

The sealed hut scenario comprised of the same hut design as in the ventilated hut scenario, but this time sealed from the outside environment (Figure 4.12). Thus, ambient sunlight, temperature, wind and humidity would be excluded. The inner humidity was assumed to be 95% throughout the year. Inner air movement, or air replacement with outside through cracks and the door was predicted using a damping factor of 0.001 on the wind variable. Internal temperature was predicted using heat balance equations. No windows were anticipated for this scenario. The RC thermal network model is presented in Figure 4.13.

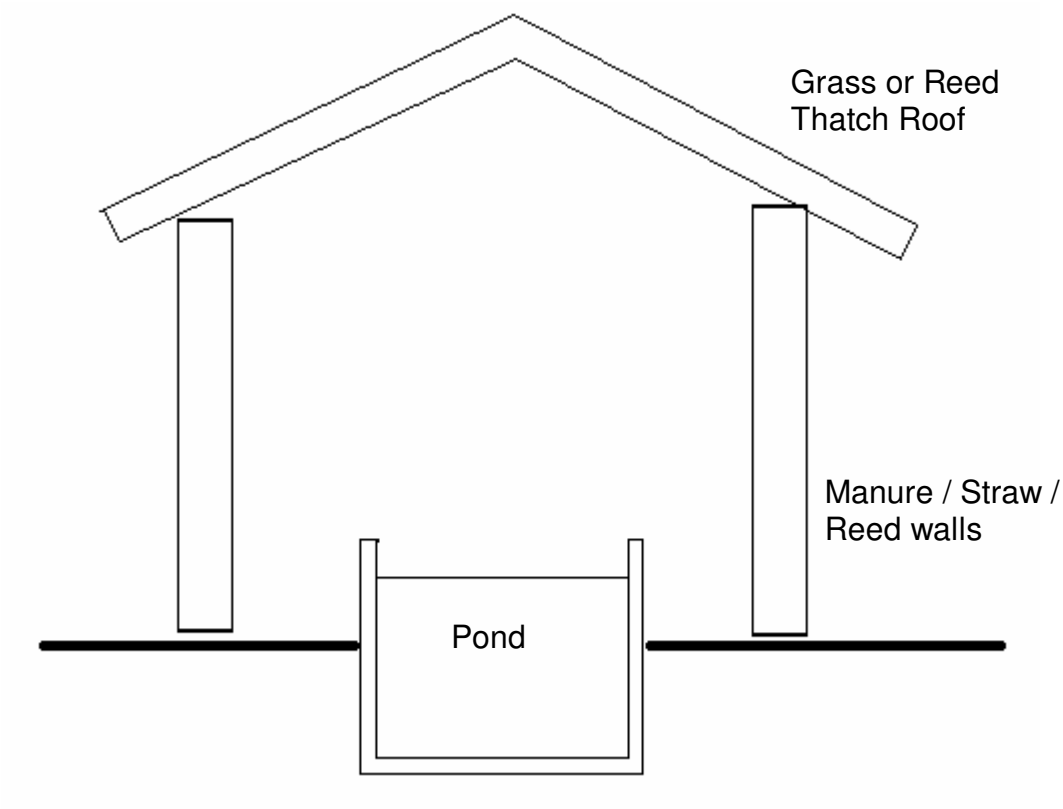

Figure 4.12 – Illustration of the sealed hut model

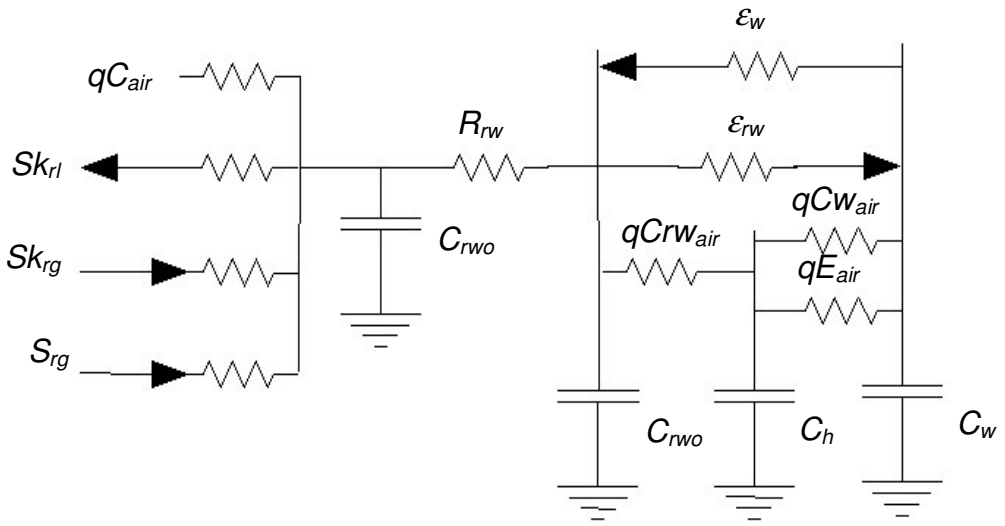

Figure 4.13 – RC Thermal Network Model of the Sealed Hut scenario

The heat balance equations for the sealed hut model are thus presented:

$$q_{rw} = \frac{T_{rwo} - T_{rwi}}{R_{rw}} \tag{4.15}$$

$$C_{rwo} \frac{dT_{rwo}}{dt} = S_{rg} + Sk_{rg} - Sk_{rl} - qC_{air} - q_{rw} \tag{4.16}$$

$$C_{rwi} \frac{dT_{rwi}}{dt} = q_{rw} + r_w - r_{rw} - qCrw_{air} \tag{4.17}$$

$$C_h \frac{dT_h}{dt} = qCrw_{air} + qCw_{air} \tag{4.18}$$

$$C_w \frac{dT_w}{dt} = r_{rw} - r_w - qCw_{air} - qEw_{air} \tag{4.19}$$

where

S_{rg} is radiation gain from sun in $W.m^{-2}$
Sk_{rg} is radiation gain from sky in $W.m^{-2}$
Sk_{rl} is radiation loss to sky in $W.m^{-2}$
qC_{air} is convective heat balance between roof/wall and air in $W.m^{-2}$
qCw_{air} is convective heat balance between pond and air in $W.m^{-2}$
qEw_{air} is heat loss to evaporation in $W.m^{-2}$
q_{rw} is heat transfer through the wall and roof in $W.m^{-2}$
r_{rw} is radiation heat transfer from roof/wall in $W.m^{-2}$
r_w is radiation heat transfer from pond in $W.m^{-2}$
R_{rw} is the thermal resistance of the wall/roof in $J/K.s$
T_{rwo} is the outer wall/roof temperature in K
T_{rwi} is the inner wall/roof temperature in K
C_{rwo} is the outer wall/roof thermal capacity in J/K
C_{rwi} is the inner wall/roof thermal capacity in J/K
C_h is the inner hut thermal capacity in J/K
$qCrw_{air}$ is the convective heat balance between the inner wall/roof and inner hut air in $W.m^{-2}$

A two-week output for the month of January is presented in Figure 4.14 for illustrative purposes, demonstrating the typical output from the model. The calculated averages for each month of the year are presented in Figure 4.15. The overall average temperature for the year of 2005 was 11.8 +/-2.6 ^{o}C. Mean values for summer, autumn, winter and spring are 14.9 +/-0.3 ^{o}C, 12.3 +/-0.4 ^{o}C, 8.6 +/-0.4 ^{o}C and 11.3 +/-0.6 ^{o}C respectively.

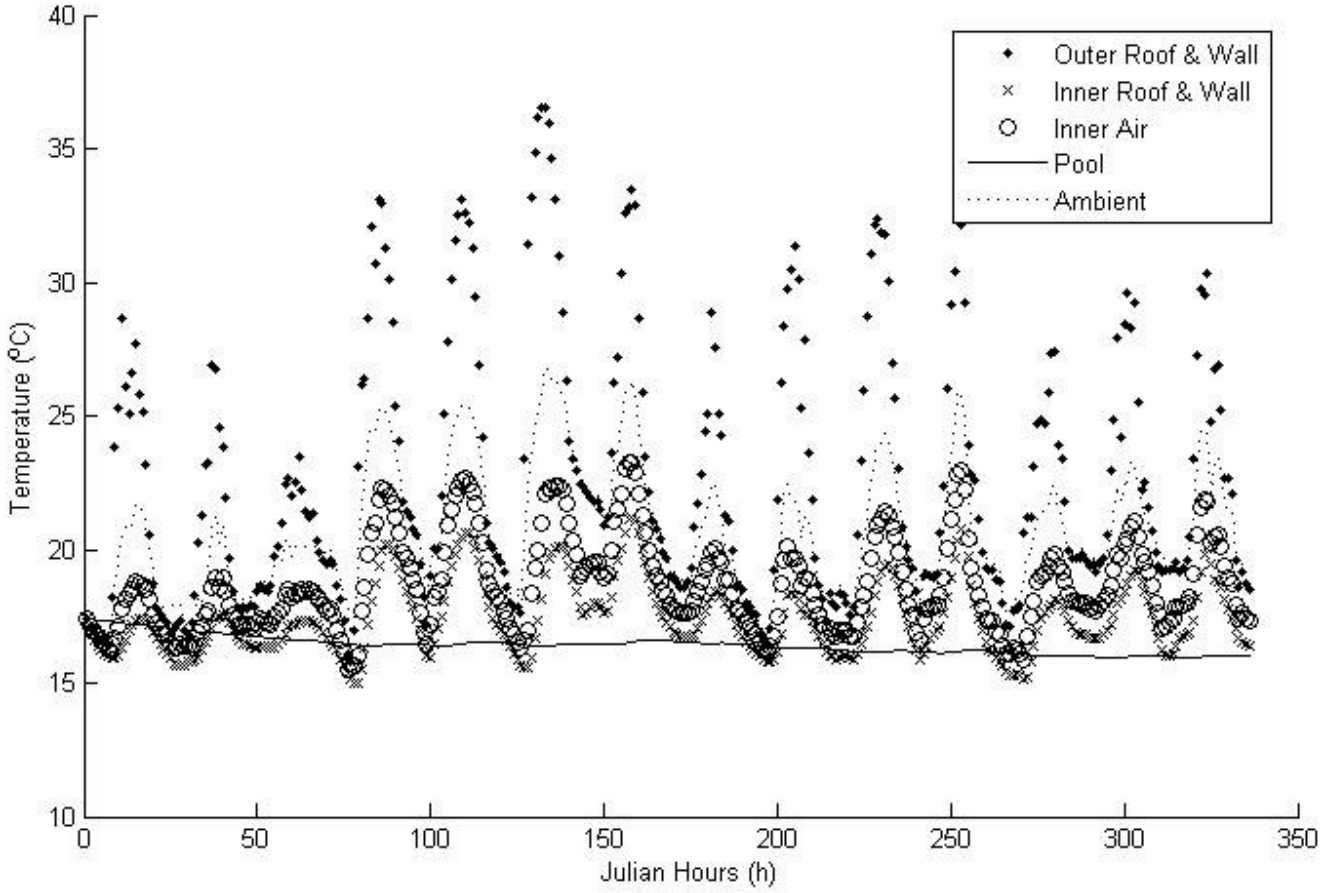

Figure 4.14 - Two-week model output for rural sealed hut pond model

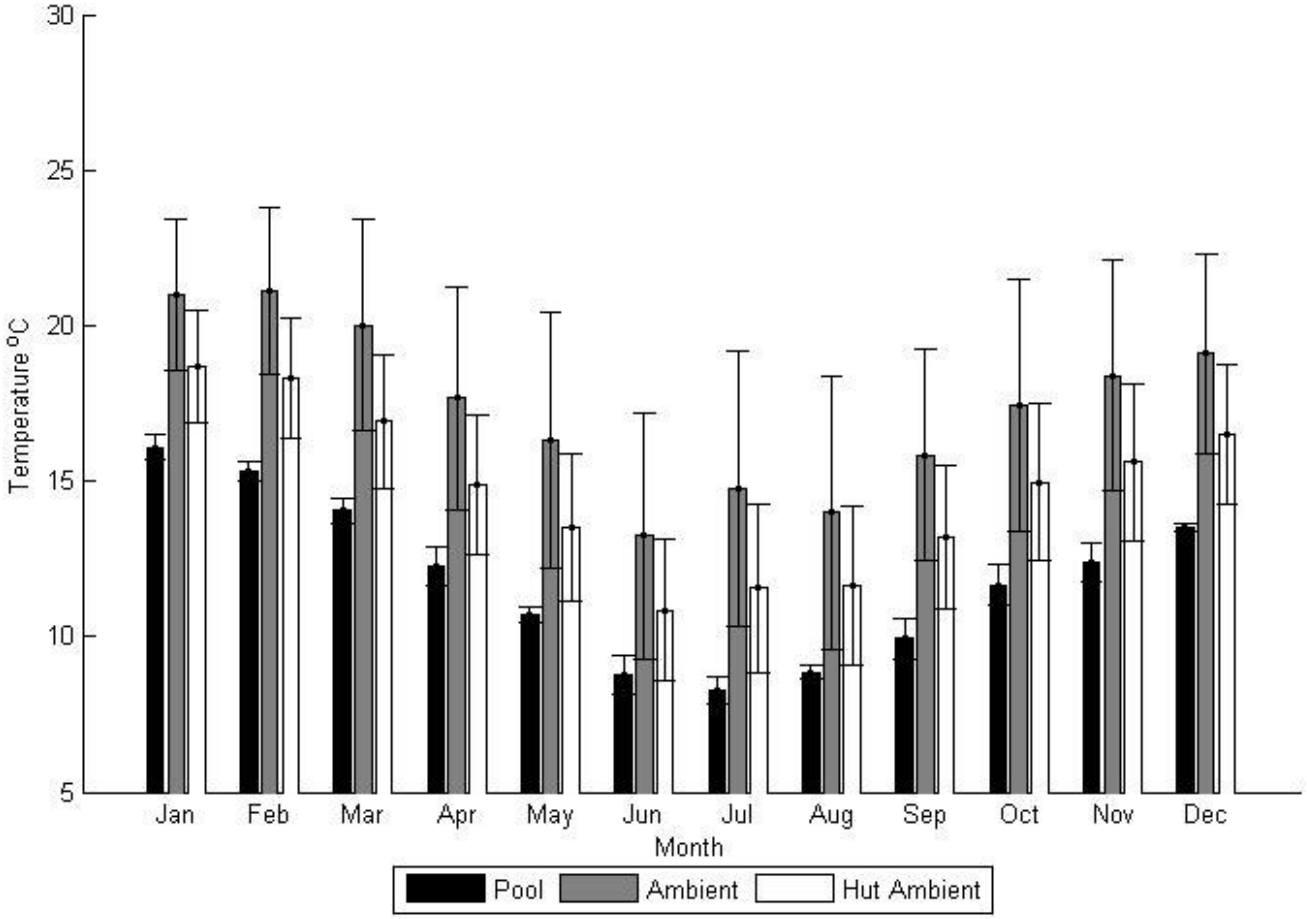

Figure 4.15 - Monthly averages of model output with air temperature

4.5.5. Sealed Hut with Passive Solar Heating Scenario

A simplified passive thermosiphon operated solar heater was developed in MatLab based on the unglazed passive solar water heaters tested by Burch, Shoukas, Brandemuhl and Krarti (2006). The model was based on a $3m^2$ unglazed solar collector. A solar collector of this type could be easily manufactured from low cost low-density polyethylene (LDPE) plumbing as used in irrigation.

Water circulation by thermosiphon was based on a simple ratio of global solar radiation to flow rate. The thermosiphon would only operate once a certain global solar radiation threshold was met. The amount of heat the solar collector would absorb was determined by the product of the emmisivity and the global solar radiation. The transfer of this heat to the pond was

determined based on the thermosiphon flow rate and the efficiency of the collector, as determined by Burch *et al.* (2006) and presented in Table 4.5.

Table 4.5 – Parameters of the solar heating model

Property	Description	Value
SH_e	Solar heating efficiency	0.35
TS_{thresh}	Solar radiation threshold for thermosiphon flow	833 $W.m^{-2}$
TS_{rate}	Ratio of thermosiphon flow to solar radiation	0.070 / 3333
SH_{sa}	Solar collector surface area	3 m^2
SH_{wv}	Water volume in solar collector	0.006 m^3

The output from the solar heating model was added to the heat balance equation of the pond. For this scenario the solar heating system was run continuously to ascertain theoretical maximum achievable temperatures.

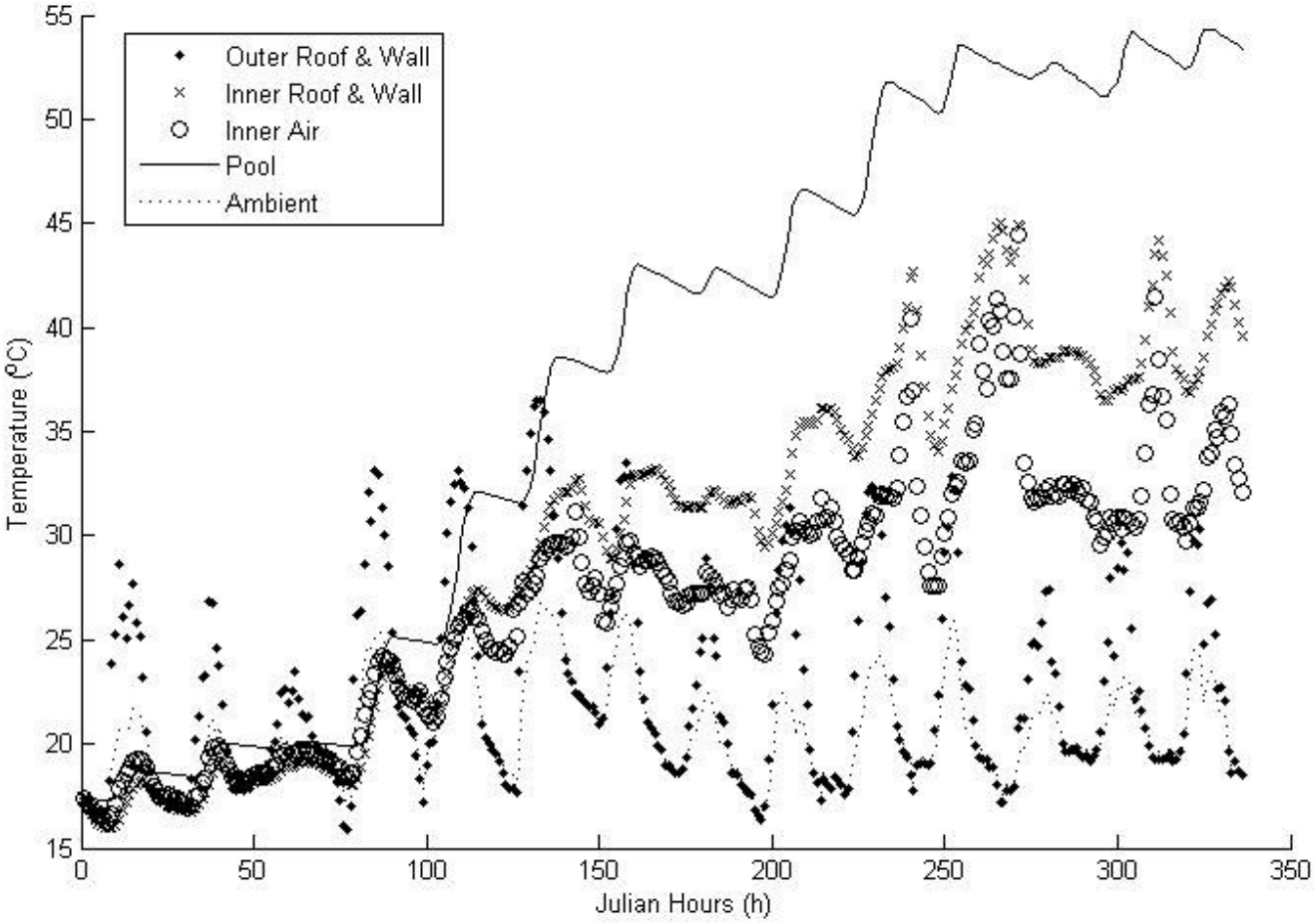

Figure 4.16 - Two-week model output for rural sealed hut solar pond model

A two-week output for the month of January is presented in Figure 4.16 for illustrative purposes, demonstrating the typical output from the model. The calculated averages for each month of the year is presented in Figure 4.17. The overall average temperature for the year of 2005 was 52.2 +/-19.3 ^{o}C. Mean values for summer, autumn, winter and spring are 71.2 +/-7.7 ^{o}C, 51.2 +/-4.3 ^{o}C, 29.4 +/-1.6 ^{o}C and 56.8 +/-6.2 ^{o}C respectively.

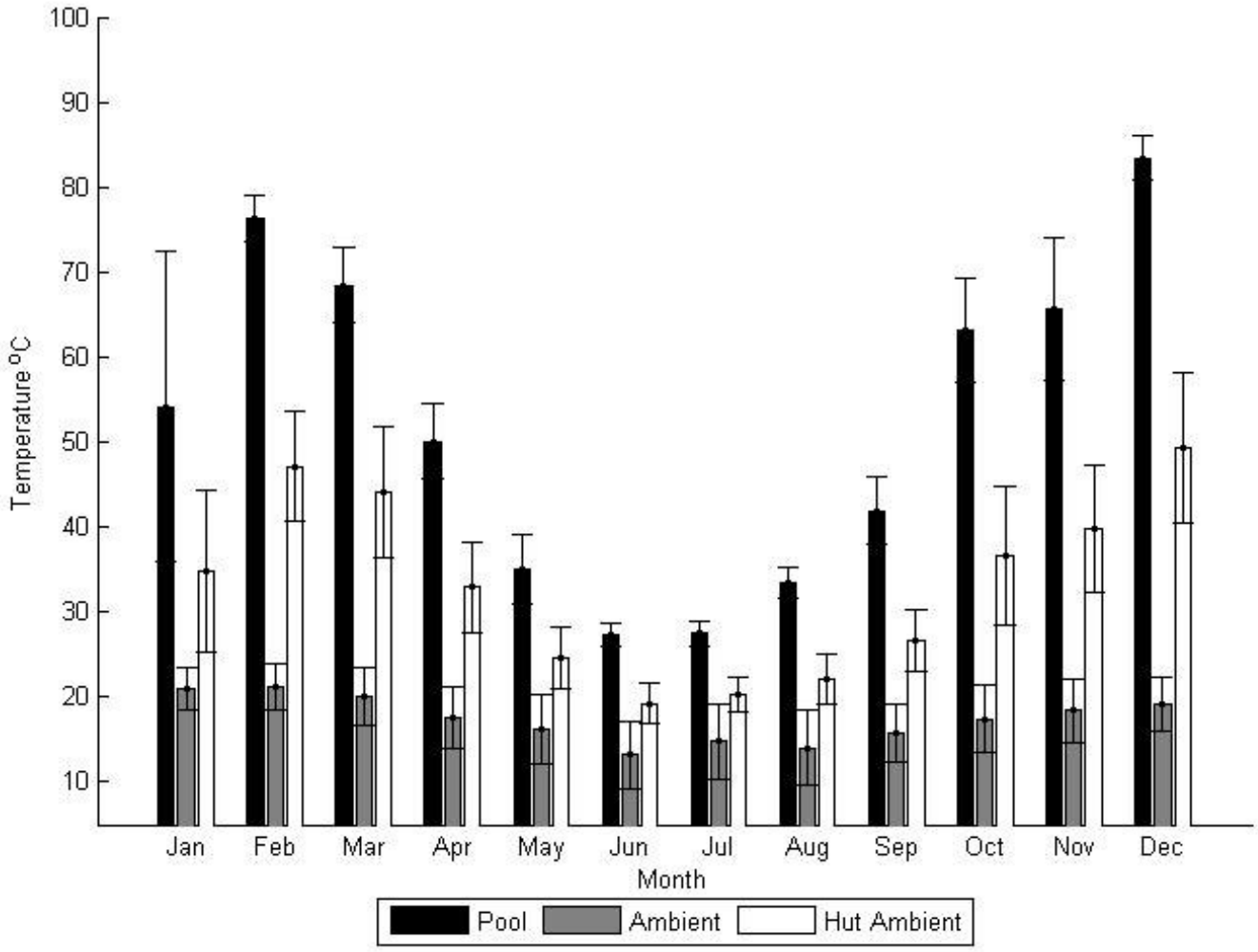

Figure 4.17 - Monthly averages of model output with air temperature

4.5.6. Sealed Hut with Controlled Passive Solar Heating Scenario

The solar heating scenario described above was run again with a temperature limitation on the solar heating. The energy input from the solar heater would be shut off when the pond temperature exceeds 25 °C.

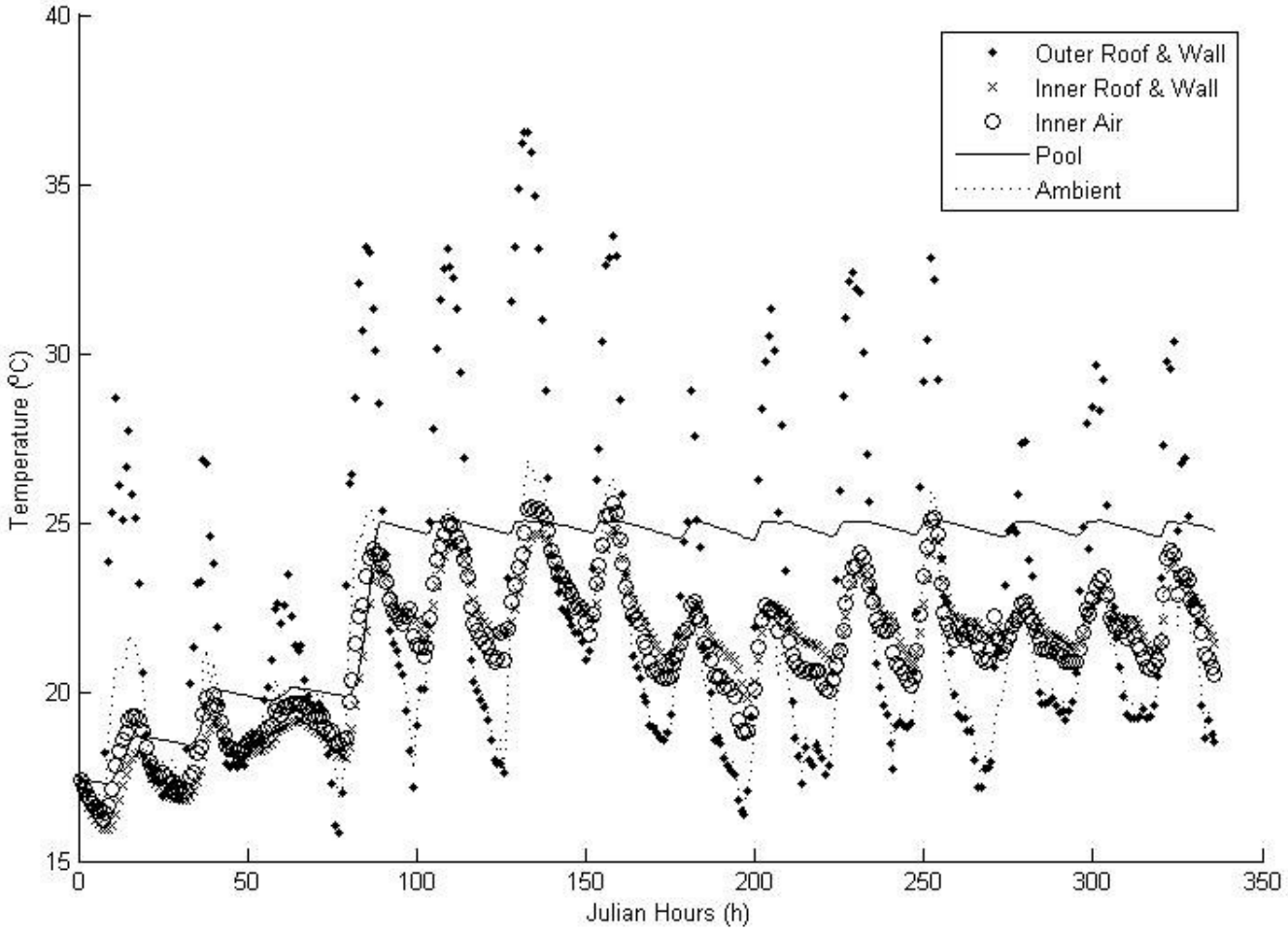

Figure 4.18 - Two-week model output for rural sealed hut controlled solar pond model

A two-week output for the month of January is presented in Figure 4.18 for illustrative purposes, demonstrating the typical output from the model. The calculated averages for each month of the year is presented in Figure 4.19. The overall average temperature for the year of 2005 was 24.6 +/-0.3 °C. Mean values for summer, autumn, winter and spring are 24.6 +/-0.7 °C, 24.5 +/-0.4 °C, 24.5 +/-0.4 °C and 24.7 +/-0.3 °C respectively.

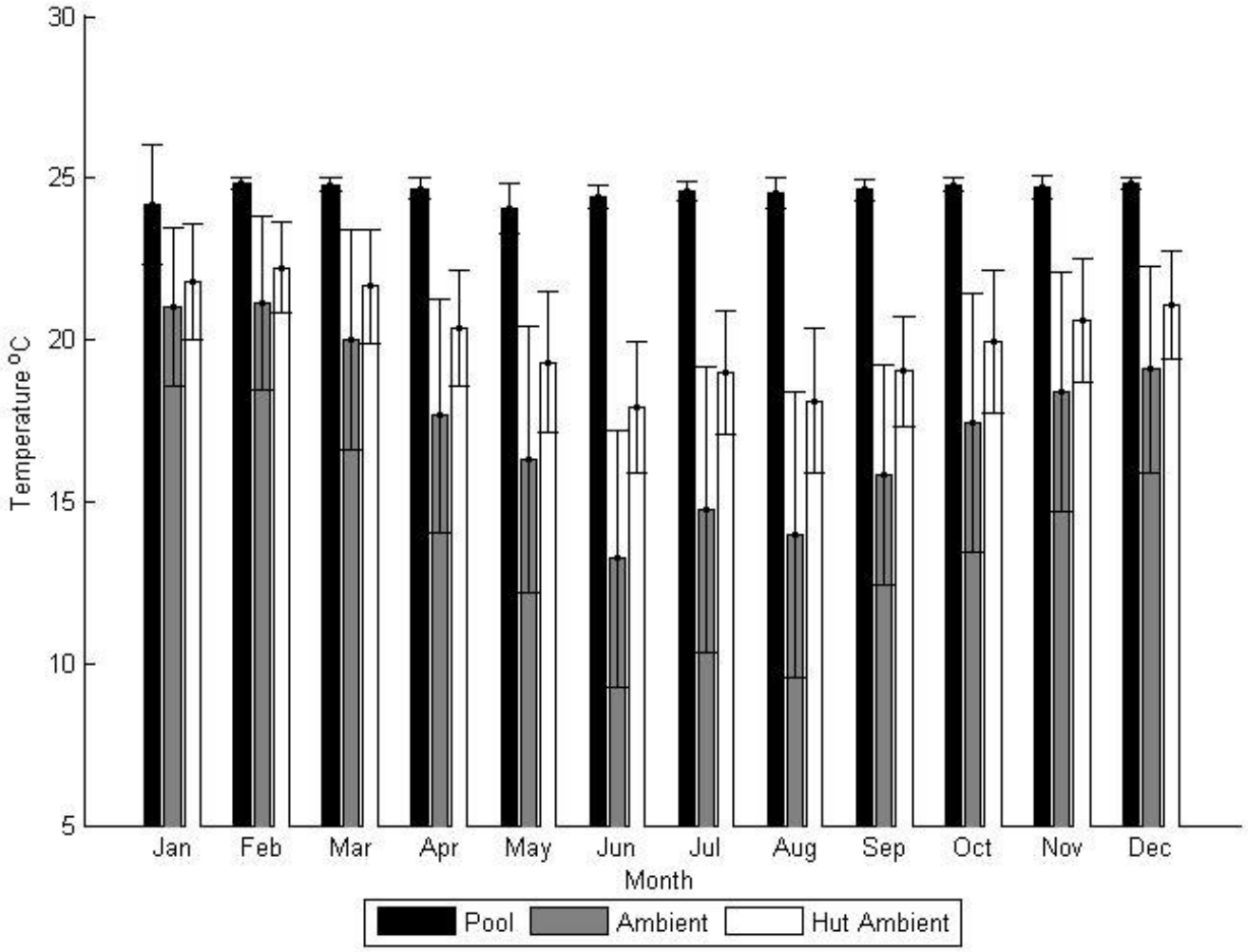

Figure 4.19 - Monthly averages of model output with air temperature

5. Discussion

5.1. Flux Box model output and material thermal performance

The final output from the Flux Box models indicated that the thermal properties of organic materials used for insulation or construction should be used very loosely. No significant relationship could be established between the thickness of the materials and any of the Flux Box model parameters, including the thermal resistance and capacity of the materials tested (Table 3.8). It is a strong possibility that the differences in thickness were too small to yield a detectable difference with the method used in this project. When the same thickness was compared between materials, no statistically significant difference could be found (Table 3.7). These results show that for most organic materials used in rural situations, the thermal performance does not vary significantly.

The thermal performance of such materials is highly dependent on their structure. Materials of natural organic origin will vary tremendously in their composition based on their life and environmental history. All materials tested in this project were ultimately from floral origin, with the manure sample undergoing a form of "natural processing" before use. Manure is particularly interesting in that its composition will vary according to the material the originating cow has fed on. Furthermore, the manner in which these materials are collected and prepared, such as thatch harvesting or manure application, will affect their thermal performance.

There does not appear to be any formal agreement between authorities on the thermal performance of certain organic insulation materials. Straw and straw thatching are the best examples. The project identified a global thermal resistance (R) of 26.6 (m.K)/W for all materials tested, resulting in a conductivity value (k) of 0.038 W/m.K. The Food and Agricultural publication "Farm Structures in Tropical Climates" by Bengtsson and Whitaker (1986) reports a thermal conductivity of 0.042 W/m.K for straw, while Beck, Heinemann, Reidinger and Fricke (2004) report the thermal conductivity of straw at 0.041 W/m.K. Commins and Stone (1998) of the Oak Ridge National

Laboratory (ORNL) indicate that values for straw bale insulation are as low as 0.018 W/m.K. In their study, they also demonstrate the problems with reporting insulative measures for organic materials such as straw (Table 5.1).

Table 5.1 - Various insulation measures of straw bales (From Commins and Stone 1998)

	Joe McCabe	**Sandia Lab**	**ORNL**	**CEC**	**CEC**	**ORNL**
Test procedure	Hot plate, single bale	Thermal probe, single bale	Hot box, full wall	Approved values	Hot box, full wall	Hot box, full wall
Test date	1993	1994	1996	1996	1997	1998
Type of straw	Wheat	Not listed	Wheat	Any	Rice	Wheat
Type of bale	3-string, 584mm	2-string, 457mm	2-string, 457mm	3-string, 584mm	3-string, 584mm	2-string, 482mm
Moisture content	8.40%	Not listed	Not listed	20%	11%	13%
Density kg/m3	132.9	83.3	Not listed	112.1	107.3	128.1
Conductivity W/m.K	0.011	0.010	0.027	0.045 to 0.028	0.022	0.018

As pointed out, one aspect of the differences of reported values, which applies to any organic insulation material, centres on the method used to apply the insulation. The way in which the materials are packed will determine the density, and subsequent thermal performance of that application. The measure of thermal resistance only takes into account the thickness, not the density of the material. It would therefore be a logical assumption to conclude that current units used in reporting the thermal resistance or conductivity of organic insulators are not valid, unless a universally accepted method of application is adopted. Thatch, being the most widely used organic substance in the building industry, has been standardized, so the use of thermal resistance measurements in this case is warranted as its method of application has been standardized. Thermal properties of other less used organic materials, however, should not be treated or reported in the same manner. Considering this, using strict protocols and measuring techniques to quantify the thermal properties of such materials, coupled with stringent

modelling approaches would therefore most likely not yield any plausibly improved result accuracy for rural situations.

5.2. Thermal performance of rural aquaculture models

The thermal performance of the ponds would determine the variety of potential aquaculture species available for farming. It would also depict the productivity of the venture. The primary aim in any aquaculture venture from a thermal perspective is to narrow the temperature variation to within the optimal production range for the selected species. Therefore, the mean temperature and deviation are the most critical factors to consider.

5.2.1. Open and Kraal enclosed pond models

The open pond model yielded an average of 21.2^{o}C for the year (Figure 4.5). The kraal enclosed pond model achieved a 2.2^{o}C average gain on the open pond model per year (Figure 4.7), although both the open and kraal enclosed pond models yielded high standard deviations in temperature, up to 2.4^{o}C and 2.52^{o}C respectively for spring. The temperature of the open and kraal enclosed pond models ranged over 10.6^{o}C and 12.4^{o}C respectively for the year. Despite the improvement in summer temperatures gained by reducing wind speeds over the kraal enclosed pond, the variation in water temperature exceeded that of the open pond. This can be explained by the reduction in the boundary layer of air over the water, since the open pond model had higher wind speeds allowing thermal energy to enter and leave the water at a faster rate. This allowed the water to follow the ambient air temperature more closely to that of the kraal enclosed pond model.

An effective thermal management solution for this case were to erect the kraal enclosure for the winter months to retain thermal energy gained from the sun, and to take down the enclosure for the summer months, to allow the pond to cool down. This will promote a tighter temperature range for the ponds, 9.4 ^{o}C in the case of the ponds used in these models.

5.2.2. Ventilated hut model

The ventilated hut model provided an opportunity to observe the pond temperature in a case where sunlight was excluded and the wind speed was considerably reduced. Radiation fluxes were taken into account between the water, walls and roof. Using the values obtained from the flux box experiments, the temperature of the pond was determined for the year from the model.

The output of the ventilated hut model yielded an average yearly pond temperature of 15.9^{o}C, with a temperature range of 7.5^{o}C. The maximum and minimum monthly pond temperature was 19.6^{o}C and 12.1^{o}C in February and June respectively (Figure 4.11). This result poses a possibility for temperate or cold-water aquaculture. The elimination of sunlight allowed the pond temperature to remain relatively low to that of the open pond models, while the reduction of wind promoted its thermal stability throughout the year.

5.2.3. Sealed hut scenario

The work of Makaka and Meyer (2006) illustrates the thermal stability of traditional Xhosa structures. The insulative properties of the organic components used in these structures are also apparent in the results of the flux box experiments (Figure 3.8). In the sealed hut model, the average indoor air temperature for the year was 14.7^{o}C, with a temperature range of 7.9^{o}C. The maximum and minimum monthly indoor air temperature was 18.7^{o}C and 10.8^{o}C in January and June respectively (Figure 4.15).

Pond water temperatures in these conditions were cooler than all the previous model outputs. The average pool temperature for the year was 11.8^{o}C, with a temperature range of 7.8^{o}C. The maximum and minimum monthly indoor pond temperature was 16.1^{o}C and 8.3^{o}C in January and July respectively (Figure 4.15). Despite the further reduction in pond temperatures to that of the ventilated hut model, the temperature range was not improved. This is once again due to the further reduction in wind movement over the pond.

5.2.4. Sealed hut with passive solar heating model

Since the hut enclosure offered shelter from outside variables such as wind, sunlight and temperature, thermal energy loss from the pond would be reduced considerably. This raised the question of using active heating inputs to maintain higher water temperatures and higher stability. In a rural situation, a natural form of active heating would be needed, and solar heating provided the answer. The results of tests conducted by Burch *et al.* (2006) were put into the model and run for the year to observe the gain in pond and hut temperatures. The solar heater ran passively, that is, relied on natural thermosiphon phenomena for water circulation. The results were quite considerable.

The pond temperature had an annual average of 52.2^{o}C and a range of 56.1^{o}C. The maximum and minimum monthly pond temperature was 76.2^{o}C and 27.2^{o}C in February and June respectively (Figure 4.17). Indoor air temperatures averaged at 33.12^{o}C for the year with a range of 30^{o}C. The maximum and minimum monthly air temperature was 47.2^{o}C and 19.2^{o}C in February and June respectively (Figure 4.17).

If employed, the solar heater would operate optimally if installed at an inclination of around 45^{o}, with the top in line with the bottom of the pond. A cheap solar water heater can be easily manufactured from low-density polyethelyne irrigation plumbing.

5.2.5. Sealed hut with controlled passive solar heating model

As shown above, it is obvious that runaway temperatures will occur if a solar heater is left to run continuously. The scenario does, however, give a good indication of the achievable energy inputs from using passive solar heating. Should a simple device capable of shutting off the flow to the solar heater be installed, the pond would be capable of maintaining very stable water temperatures.

With a 25^{o}C temperature control installed, the pond maintained an average of 24.6^{o}C with a range of 0.7^{o}C for the year. The maximum and minimum

monthly pond temperature was 24.8°C and 24.1°C in December and May respectively (Figure 4.18). Indoor air temperatures averaged at 20.1°C for the year with a range of 4.3°C. The maximum and minimum monthly air temperature was 22.2°C and 17.9 °C in February and June respectively (Figure 4.18).

As a further thought, it may be possibly to use the solar water heater as a water sterilizer. Burch *et al.* (2006) indicate that water temperatures within the solar heating panel can exceed 90°C. This can help control pathogens and parasites in the pond.

5.3. Potential species for aquaculture

Rouhani and Britz (2004) indicate that the potential for fresh water aquaculture in South Africa is significantly constrained by the natural environment. Scarcity of water and extreme temperatures over most of the interior of the country make successful aquaculture ventures challenging. Managing an aquaculture system under such conditions requires a specialized approach. This is the primary problem in rural aquaculture, as skilled expertise, capital and efficient extension services are required to make the venture successful. The open pond model presented in this project is a good example, with a minimum and maximum monthly mean temperature of 15.6°C and 26.2°C respectively.

These factors severely restrict the choice of species available for aquaculture. Species that can survive in such conditions are few and far between, and often require specialized culture techniques. The results of the scenarios presented in this project indicate that thermal modelling can indeed be used to optimise rural aquaculture ventures to allow access to a wider variety of species without significant capital and skill input.

Current freshwater and brackish species of considerable economic interest farmed in South Africa include:

- *Ctenopharyngodon idella*
- *Hypophthalmichtys molitrix*
- *Cyprinus carpio*
- *Micropterus salmoides*
- *Oreochromis* spp.
- *Oreochromis mossambicus*
- *Tilapia rendalli*
- *Oncorhynchus mykiss*
- *Salmo trutta*
- *Cherax tenuimanus*
- *Penaeus indicus*
- *Penaeus japonicas*
- *Aponogeton distachyos*
- *Carassius auratus*
- *Clarias gariepinus*
- *Labeo* spp.
- *Mugilidae*

(From Hoffman, Swart and Brink (1998) and Hecht (2005))

5.3.1. Cold temperate water aquaculture

The sealed hut scenario yielded a pleasant and unexpected surprise. The potential for cold-water aquaculture was not considered at the onset of this project, but has presented itself based on the model outcomes. With the average pool temperature for the year at 11.8^{o}C, and a maximum and minimum monthly indoor air temperature of 16.1^{o}C and 8.3^{o}C respectively (Figure 4.15), a range of cold water species becomes available. Of primary interest are rainbow trout (*Oncorhynchus mykiss*) and other salmonids. Large drives by government and other organizations are promoting the expansion of trout farming to small-scale farmers (Rouhani and Britz, 2004), providing much needed access to essential skills, materials and expert guidance. The

typical temperature tolerance range of the rainbow trout is 8°C to 24°C, with its preferred natural habitat ranging between 10°C and 15°C (Povlsen 1993; Vondracek and Longanecker 1993; Berman and Quinn 1991). Highest production of rainbow trout occurs when winter temperatures do not drop below 7-8°C, with a winter mean of 10°C or more (Povlsen 1993).

5.3.2. Warm water aquaculture

The solar heated hut scenario showed that very stable temperatures in the tropical range could be maintained throughout the year (Figure 4.19). This provides opportunities for a number of warm water species including Carp (*Cyprinus* spp., *Ctenopharyngodon* spp., *Hypophthalmichthys* spp., *Aristichthys* spp.), Tilapia (*Tilapia* spp.), Barbell (*Clarius* spp.) and ornamental fish (Rouhani and Britz, 2004). The opportunity also exists for warm water prawn (*Machrobrachium rosenbergii*) and shrimp cultures, as well as other species of invertebrates such as mud crabs (*Scylla serrata*) (Safriel and Bruton, 1984).

5.3.3. Mixed water aquaculture

The low temperatures that can be achieved inside the sealed hut, together with controlled solar heating inputs, provides a controllable temperature range from 16°C (Figure 4.15) to 27°C (Figure 4.19). This extends the range of available species tremendously. Locally occurring species, such as Cape Stumpnose (*Rhabdosargus holubi*), Blacktail (*Diplodus sargus*) and Mullet (*Mugil cephalus*) can be harvested from the wild as juveniles and then grown out within the ponds. The temperature control range allows this flexibility in selecting species for culturing. By controlling the solar heating output, species could be triggered to spawn at certain times of the year based on their thermal requirements or triggers for reproduction.

5.4. Site selection, thermal management and future prospects

The report to the FAO on aquaculture potential in Latin America by Kapetsky and Nath (1997) is a good example of the application of thermal models to suitable site selection. Many site selection criteria used by current projects in South Africa are based on yearly ambient temperatures, and few take global

radiation, wind speed and humidity into account (Rouhani and Britz, 2004; Safriel and Bruton 1984; Hecht and Britz 1990). As shown in the models presented in this project, these factors play a very large role in determining the temperature profile of the pond throughout the year. It would thus be premature to assume pond temperatures follow that of the ambient environment.

Another important factor, which was not investigated in this project, is thermal stratification. The modelling of thermal stratification in ponds has been applied successfully by authors such as Zhu *et al.* (1999) and will have application to future aquaculture related projects in South Africa. Microclimate and microhabitat availability is an important consideration in aquaculture. Salmonids will often retire to the cooler microclimates of deeper parts of dams, rivers and lakes during the summer months to escape the heat (Vondracek and Longanecker 1993; Berman and Quinn 1991). By understanding the characteristics and conditions of thermoclines a dam can be designed to accommodate bottom water temperatures that will ensure the health and survival of the fish therein.

The knowledge gained from models such as that used in this project can be used to effectively manage ponds both small and large alike. As demonstrated, open ponds can be thermally managed by the erection and removal of suitable windbreaks through certain seasons of the year. The control of solar radiation by the erection and removal of roofs or covers provides a further means of controlling water temperature. Complete enclosure in a thermally insulated structure such as in the sealed hut scenario can provide excellent water temperature control, especially when coupled with a controlled passive solar heating system. Knowledge of the effects that such activities will have on water temperature, together with the critical seasons in terms of temperature, aquaculture pond temperatures can be managed effectively without the use of specialized technology and with little financial implication.

6. Conclusion

Despite the error encountered in the power input of the Flux Box model, the results of the experiments indicate that the thermal properties of organic materials can be fairly consistent. This makes modelling approaches using organic-based insulation much simpler. The Flux Box approach provided a convenient platform for developing, experimenting and validating the thermal network models. When applied to the various scenarios, the outcomes indicate that thermal modelling can indeed be used to improve subsistence rural aquaculture by providing essential information on potential aquaculture approaches.

The results of the project show that with careful planning and implementation, opportunities available to rural subsistence aquaculture farmers can be significantly improved upon through the effective use of tools such as thermal modelling. When one enables a larger variety of species to become available to a rural aquaculture development, it is more likely that a suitable candidate species that is manageable in a rural aspect will be selected. Where traditionally, low cost aquaculture ventures were implemented with a species that could only be farmed for that particular area, increasing the range of temperatures available to rural farmers allows them to choose a suitable species according to current circumstances. Another positive outcome is that any exotic species can be cultured at a much higher temperature than the local climate and natural waters permit, decreasing the risk of alien invasion into natural waters considerably.

The future holds many prospects for the application of thermal modelling to rural aquaculture situations. Further expansion of such models to include greenhouse pond systems and thermocline models can be used to investigate new methods and technologies for aquaculture ventures. Solar heating systems provide a low cost energy efficient approach to heating aquaculture ponds, and may provide a means of regulating water borne pathogens by way of high temperature sterilization.

Effective thermal management practices are a key ingredient to the success of many aquaculture ventures. Practical demonstration to rural farmers along with simple guidelines will equip them with the basic knowledge required for managing the temperatures of a pond system. By using traditional rural structures the costs and skill levels required can be kept to a minimum. Expert intervention can be cut down, although will always be essential in any aquaculture venture (Hecht 2005). If a passive, low-cost thermally controllable solar water heater were feasible and available, coupled with the thermal stability offered by traditional architecture, the range of opportunities available to the rural farmer can be increased considerably.

With the ever increasing demand for low cost protein sources, coupled with increasing pressures on natural resources, the expansion of farming practices for both commercial and subsistence use alike will be essential in maintaining an ever growing population of people. Dwindling natural stocks increase market prices, which put increasing pressure on consumers, especially those relying on self-subsistence farming practices with little or no income. By employing the correct approaches through the use of tools such as thermal modelling, projects aimed at improving subsistence farming, particularly in aquaculture, can be improved upon significantly.

7. Acknowledgements

I would like to extend a much-deserved warm thank-you to everyone who helped with this project. Without the generous help from these people this project would never have achieved what it was set out to do.

- Japie Strydom
- Anelle Strydom
- Matthew Skelton
- Les Kemsley
- My parents, Pat and Felicity Bailey
- Garth Sampson of the Port Elizabeth Weather Office
- Jenny Robertson, Steve Warren and Robyn Greyling of Bayworld
- Master Thatchers
- Rocklands Poultry
- Prof. Gonsalves, Pieter du Toit, Brian Seale, Anton Cloete and Michelle Harrison of NMMU
- My supervisor, Deo Winter

8. References

Agrawel, D.C., Leff, H.S., and Menon, V.J., 1995 – Efficiency and efficacy of incandescent lamps. American Journal of Physics, Vol 64, No. 5, pp 649-654.

Beck, A., Heinemann, U., Reidinger, M., and Fricke, J., 2004 - Thermal transport in Straw Insulation. Journal of Thermal Envelope and Building Science, Vol. 27, No. 3, pp 227-234.

Bengtsson, L.P., and Whitaker, J.H., 1986 - Farm structures in tropical climates. FAO/SIDA Cooperative Programme, Rural Structures In East And South-East Africa. Food And Agriculture Organization Of The United Nations, Rome, 1988.

Ben-Yaakov, S., Perets, M.M., and Hesterman, B., 2005 – A Spice compatible Behavioural Electrical Model of a Heated Tungsten Filament. Proceedings of the Twentieth Annual IEEE Applied Power Electronics Conference and Exposition, 2005. APEC 2005.

Berman, C.H., and Quinn, T.P., 1991 - Behavioural thermoregulation and homing by spring Chinook salmon, *Onchorhynchus tshawytscha* (Walbaum), in the Yakima River. Journal of fish biology, Vol. 39, Iss. 3, pp 301-312.

Brown, A.I. and Marco, S.M., 1958 – Introduction to heat transfer. McGraw-Hill Book Company, Inc, New York.

Burch, J., Shoukas, G., Brandemuhl,M., and Krarti, W., 2006 – Modelling and test-and-rate methods for innovative thermosiphon solar water heaters. National Renewable Energy Laboratory Conference Paper. Presented at Solar 2006 Conference, Denver, Colorado.

Cathcart, T.P., and Wheaton, F.W., 1987 - Modeling Temperature Distribution in Freshwater Ponds. Aquacultural Engineering, Vol. 6, pp 237-257.

Cengel, Y.A., 2002 – Heat transfer, a practical approach. McGraw-Hill Book Company, Inc, New York.

Clauss, D.A., Ralich, R.M., and Ramsier, R.D., 2001 – Hysterisis in a light bulb: Connecting Electricity and Thermodynamics with Simple Experiments and Simulations. European Journal of Physics, Vol. 22, pp 385-394.

Commins, T.R., and Stone, N.I., 1998 - Tested R-value for Straw Bale Walls and Performance Modeling for Straw Bale Homes. 1998 ACEEE Summer Study on Energy Efficiency in Buildings Proceedings.

de Halleux, D., Nijskens, J., Deltour, J., 1985 – Dynamic simulation of heat fluxes and temperatures in horticultural and low emissivity glass covered greenhouses. Acta Horticulturae, Vol 170, pp 91-96.

Hecht, T. and Britz, P.J., 1990 – Aquaculture in South Africa: History, status and prospects. Aquaculture Association of southern Africa. Lynnwood Ridge, Pretoria.

Hecht, T., 1995 – Misconceptions in African Aquaculture. Seminar, Zoology Department, University of Port Elizabeth, 1995.

Hecht, T., 2005 - Regional Review On Aquaculture Development
4. Sub-Saharan Africa. FAO Fisheries Circular No. 1017/4. Food And Agriculture Organisation Of The United Nations, Rome, 2004.

Hoffman, L.C., Swart, J.J., and Brink, A., 1998 - The 1998 production and status of aquaculture in South Africa. Water SA, Vol. 26,No. 1, pp133 - 135.

Incropera, F.P. and DeWitt, D.P., 2002 – Fundamentals of Heat and Mass Transfer. Fifth Edition. John Wiley and Sons, Inc, New York.

Jakob, M. and Hawkins, G.A., 1957 – Elements of Heat Transfer. John Wiley and Sons, Inc, New York.

Kapetsky, J.M., and Nath, S.S., 1997 - A strategic assessment of the potential for freshwater fish farming in Latin America. COPESCAL Technical Paper. No. 10. Food And Agriculture Organisation Of The United Nations, Rome, 1997.

Kleijnen, J.P., 1999 - Validation of models: Statistical techniques and data availability. Proceedings of the 1999 Winter Simulation Conference.

Klemetson, S.L. and Rogers, G.L., 1985 – Aquaculture pond temperature modeling. Aquacultural Engineering, Vol. 4, Iss. 3, pp 191 – 208.

Koenigsberger, O.H., Ingersoll, T.G., Mayhew, A., and Szolozay, S.V., 1974 – Manual of Tropical Housing and Building, Climatic Design, Part 1. Longman, New York.

Makaka, G., and Meyer, E., 2006 - Temperature Stability of Traditional and Low-cost Modern Housing in the Eastern Cape, South Africa. Journal of Building Physics. Vol 30, pp 71-86.

Monteith, J.L., and Unsworth, M.H., 1990 – Principles of environmental physics. Hodder and Stoughton Limited, Great Britain.

Povlsen, A.F., 1993 - Observations on the biology and ecology of rainbow trout, *Oncorhynchus mykiss*, and its implications for fisheries in the highlands of Papua New Guinea. A report prepared for the Sepik River Fish Stock Enhancement Project, PNG/85/001. Food And Agriculture Organisation Of The United Nations, Rome, 1993.

Rohsenow, W.M. and Choi, H, 1961 – Heat, Mass, and Momentum Transfer. Prentice-Hall, Inc, New Jersey.

Rose, J. and Svendsen, S., 2004 – Validating numerical calculations against guarded hot box measurements. Nordic Journal of Building Physics, Vol. 4, http://www.byv.kth.se/avd/byte/bphys.

Rouhani, Q.A., and Britz, P.J., 2004 - Contribution of Aquaculture to Rural Livelihoods in South Africa: A Baseline Study. Report to the Water Research Commission, WRC Report No. TT 235/04.

Safriel, O., and Bruton, M.N., 1984 - Aquaculture in South Africa: A Cooperative Research Program. South African Scientific Programmes Report No. 89, Foundation for Research Development, Council for Scientific and Industrial Research.

Schechter, E., 2006 – The Cubic Formula. Solve any 3rd degree equation. www.math.vanderbilt.edu/~schectex/courses/cubic

Singh, S., and Marsh, L.S., 1995 - Modelling thermal environment of a recirculating aquaculture facility. Aquaculture Vol. 139, pp 11-18.

Singh, V.P., and Xu, C.Y., 1997 - Sensitivity of Mass Transfer-Based Evaporation Equations to Errors in Daily and Monthly Input Data. Hydrological Processes, Vol. 11, pp 1465-1473.

Spence, R.J.S. and Cook, D.J., 1983 - Building materials in developing countries. John Wiley and Sons, New York.

Tieszen, S., Ooi, A., Durbin, P., and Behnia, M., 1998 – Modelling of natural convection heat transfer. Center for Turbulence Research. Proceedings for the Summer Program 1998.

van Soest, P. J., 1982 – Nutritional ecology of the ruminant. Ruminant metabolism, nutritional strategies, the cellulolytic fermentation and the chemistry of forages and plant fibers. Comstock Publishing Associates, Cornell University Press, London.

Velz, C.T., 1970 – Applied Stream Sanitation. John Wiley and Sons, New York.

Vondracek, B., and Longanecker, D.R., 1993 - Habitat selection by rainbow trout *Onchorynchus mykiss* in a California stream: implications for the Instream Flow Incremental Methodology. Ecology of freshwater fish, Vol. 2, Iss. 4, pp 173 - 186.

Walton, J., 1956 – African Village. J.L. van Schaik Ltd., Pretoria.

Wangaard, D.B, McDonell, J.P., Burger, C.V. and Wilmot, R.L., 1991 – Apparatus for Precise Regulation and Chilling of Water Temperatures in Laboratory Studies. The Progressive Fish-Culturist, Vol. 53, pp 251-255.

West, R. C., 1987 – Thatch. David & Charles, London.

Wilson, J.D., and Flesch, T.K., 2003 - Wind Measurements In A Square Plot Enclosed By A Shelter Fence. Boundary-Layer Meteorology, Vol. 109, pp 191–224.

Zanetti, V., 1985 – Temperature of Incandescent Lamps. American Journal of Physics, Vol. 53, No. 6, pp 546-548.

Zhu, S., Deltour, J., and Wang, S., 1999 - Modeling the Thermal Characteristics of Greenhouse Pond Systems. Proceedings of 99 International Conference on Agricultural Engineering, pp 85-93.

Zhu, S., Wang, S. and Deltour, J., 2000 – Modeling thermal stratification in aquaculture ponds. Asian Fisheries Society, Vol. 13, pp 169 – 182.

9. Appendix

9.1. MatLab Flux Box Model and Curve Regression Code

9.1.1. Main Code

```
%Thermal node models fitted by unconstrained nonlinear optimization.
%Dylan Bailey
%198443750
%NMMU Zoo M.Sc. 2006

clc;
Curve = 83; %22,24: bad boundary data :21 start tests
Limits = 10000; %Max t Limit
fit = 1; %0 = Preview Data , 1 = Fit Data
Batch = 1; %Process all curves in one batch
Rules = 1; %Check boundary conditions
Cal = 0;
clear runn;

if Cal
    Batch = 0;
    Curve = 1;
end

DataOffset=3; %Offset to eliminate bad boundary data
MatrixData=load('MatrixData'); %Load Data Set
MatrixStart=load('MatrixStartTimes'); %Load Data Set Times
CalData=load('ConBoxCalReference2');

[MaxDataLength DataSets]=size(MatrixData.MatrixData);

BatchStart=Curve;
BatchEnd=Curve;

if Batch
    BatchStart=Curve;
    BatchEnd=DataSets-1;
    BatchCount=1;
    if exist('CoeffMatrix','var')
     %   clear CoeffMatrix
    end
end

Area = (0.422-0.03)^2; %Suface area
%Calibration Values
CBox = 1000; %Box Cavity Capacity
RBox = 1.0; %Box Cavity Resistance
CTest = 1000; %Sample Capacity
RTest = 1.0; %Sample Resistance
if Cal
    CTest = 0.1;
    RTest = 0.5;
end
QiRadRatio = 0.35; %Energy to Radiation Efficiency
CHeater = 16; % Capacitance of Heater
RHeater = 8; % Resistance of Heater
Q = 15;

BoxCap=CBox/(0.345^2*0.185*1.2);
BoxCond=(RBox*0.185)*0.345^2;
```

```
for Curve=BatchStart:BatchEnd

if Curve == 40
    continue
end

Data=MatrixData.MatrixData(DataOffset:Limits,Curve); %Pull out curve
if Cal
    %Data=CalData.SelectedCurve(DataOffset:Limits);
    Data=SelectedCurve(DataOffset:Limits);
end
T1=Data(1); %Boundary conditions

WN = find(isnan(Data))-1;
if isempty(WN)
    WhereNaN=Limits-DataOffset;
else
    WhereNaN = WN(1);
     if (WhereNaN > (Limits-DataOffset))
         WhereNaN = (Limits-DataOffset);
     end
end

% Check for boundary condition violations
if Rules
if (WhereNaN < 5000) | (T1 < 19) | (T1 > 23) | (Data(WhereNaN) <
40.0)
   if Batch
       continue
   else
       errordlg('Data does not conform to boundary condition rules')
       return
   end
end
end

if exist('runn','var') %If the solver has run, start from last
estimates
    params = estimates;
else
    params = [Q QiRadRatio CHeater RHeater CBox RBox CTest RTest];
end

TInt=1:100:WhereNaN;
Error(TInt)=0;
YY(TInt,1:3)=0;
h =
plot(TInt,Data(TInt),'x',TInt,YY(TInt,:),TInt,20+(Error(TInt).^2*1000
),'.');
axis([0 WhereNaN(1) 19 60])
set(h,'EraseMode','xor','MarkerSize',8)

%%
%Fit using Least Squares
[estimates, model] =
fitcurve(h,TInt,fit,T1,params,1:WhereNaN,Data(1:WhereNaN));
runn = 1;
%%

%ShowCurve
```

```
[sse, Error, y] = model(estimates);

BoxCap=estimates(4)/(0.345^2*0.185*1.2);
BoxCond=(estimates(5)*0.185)*0.345^2;
TestCond=(estimates(5)*0.185)*0.345^2;

if Batch
    CoeffMatrix(:,BatchCount)=[Curve sse estimates];
    BatchCount=BatchCount+1
end
Sizes(:,BatchCount)=[Curve WhereNaN-DataOffset];
meanies(BatchCount)=mean(Data(1:WhereNaN));
meadies(BatchCount)=median(Data(1:WhereNaN));
end
```

9.1.2. fitcurve Function Code

```
%Curve fitting using nonlinear least squares optimization
%Dylan Bailey
%198443750
%NMMU Zoo M.Sc. 2006

function [estimates, model] =
fitcurve(h,TInt,fit,T1,SParams,xdata,ydata)
model = @expfun;
estimates = SParams;
if fit
estimates = fminsearch(model, SParams,optimset('TolX',1e-
1,'TolFun',1e-2,'Display','iter'));
end
    function [sse, ErrorVector, ModelY] = expfun(params)
        [t ModelY] = ThermalNodeModel(T1,params,xdata);
        drawnow
        ErrorVector = ModelY(:,2) - ydata;
        sse = sum(ErrorVector .^ 2);

set(h,{'YData'},{ydata(TInt);ModelY(TInt,1);ModelY(TInt,2);ModelY(TIn
t,3);20+ErrorVector(TInt).^2*1000});
    end
end
```

9.1.3. ThermalNodeModel Function Code

```
%Flux Box Thermal Node Model
%Dylan Bailey
%19443750
%NMMU Zoo M.Sc. 2006

function [t, y] = ThermalNodeModel(T1,params,tstep)
RTest=params(8);
QiRadRatio=params(2);
CBox=params(5);
RBox=params(6);
CHeater=params(3);
RHeater=params(4);
Q=params(1);
CTest=params(7);

Area = (0.422-0.03)^2;
RConv = 1 / (Area * 4.5);
```

```
PlateL = 0.006;
CPlates = Area * PlateL * 2700 * 896;
RPlates = PlateL / (220 * Area);

To = 20; %Ambient temperature
if T1<To
    To=T1;
end
Tm = To + (T1 - To)/2;
Ti = [T1 T1 Tm]; %Initial node temperatures
Qi = [Q*(1-QiRadRatio) Q*QiRadRatio 0]; %Node heat inputs
C = [CHeater CBox CPlates+CTest+CPlates]; %Node thermal capacities
R = [RHeater RBox RPlates+RTest+RPlates]; %Node thermal Resistances
[t,y] = ode113(@RCThermalSystem, tstep, [Ti], [], To, R, C, Qi);
end
```

9.1.4. RCThermalSystem Function Code

```
%1-D Thermal system solved with a system of linear differential
equations.
%Solved using the RC Method (Resistance Capacitance Model) with node
flux determinations
%Will calculate for conduction, and eventually radiation and latent
heat fluxes
%Dylan Bailey
%198443750
%NMMU Zoo M.Sc. 2006

%RCSystem ODE
function System = RCSystem(t,T,Ti,R,C,Qi)
%Set up initial states
[Nodes nn] = size(T); %Number of system nodes
T(Nodes+1) = Ti; %Initial Temperature (C)
q(1)=0;

%Calculate Nodes on System from Left to Right
for n=1:Nodes
    q(n+1) = ( T(n) - T(n+1) ) / R(n); %Node Conduction Flux
    System(n,1) = ( (q(n) - q(n+1)) + Qi(n) ) / C(n); %Differential,
nett flux into system resulting in delta T
end;
end
```

9.2. MatLab Open Pool Model Code

9.2.1. Main Code

```
%Dynamic Pond Thermal Model
%Dylan Bailey
%NMMU 2006 MSc 198443750

clc
PoolVol=sum(prod(PoolDimensions));
PoolArea=sum(prod(PoolDimensions(1:2,1:3)));
WOData=WODataImport('PEData 2005.txt',1);

Humidity=WOData{7};
Wind=WOData{2};
Temperature=WOData{6};
GlobalRadiation=WOData{11};
DiffuseRadiation=WOData{12};
```

```
PEHumidity=StepMeans(Humidity,12,1);
PEWind=StepMeans(Wind,12,1);
PETemperature=StepMeans(Temperature,12,1);
PERadiation=StepMeans(GlobalRadiation,12,1);
PEDiffuseRadiation=StepMeans(DiffuseRadiation,12,1);

%if sim==1 PERadiation=IdealRadiation; end;
%IdealRadiation=ModelForecast(PERadiation);



Twi=0;
Tw=0;
Cw=4181; %Water specific heat J/kg.K
Cwm=Cw*1000; %One cubic meter water thermal capacity J/K
hold off;
%Model Simulation
global tsT;
[nsn n]=size(PETemperature);
tsT=0;
sn=1;
n=8758;
tstep=sn:1:n;
Tin(tstep)=20;
Vin(tstep)=25;
h=odeset('MaxStep',1);
Tdp=DPTemperature(tstep);
Ti = DPTemperature(sn); %Initial temperature
[t,y] = ode113(@CThermalSystem, tstep, [Ti], h,
Cwm,PoolVol,PETemperature,PEWind,PEHumidity,PERadiation.*4000,PEDiffu
seRadiation,PoolArea,Tin,Vin);
tstep=sn:24:n;
plot(tstep,y(tstep),'r',tstep,Tdp(tstep),'b')
RSS=sum((y.^2)); %Model Sum of Squares
TSS=sum((Tdp.^2)); %Total Sum of Squares
ReSS=abs(TSS-RSS);
r2=1-ReSS/TSS %r Squared value
ME=sqrt(ReSS/8760)
DF=n-2;
ReMS=ReSS/DF
RMS=RSS/DF
F=RMS/ReMS
[t P]=ttest(y(sn:n)',Tdp(sn:n)')
```

9.2.2. CthermalSystem Function Code

```
%1-D Thermal system solved with a system of linear differential
equations.
%Calculates heat fluxes between pool and ambient environment
%Dylan Bailey
%NMMU MSc 2006
%198443750

%RCSystem ODE
function dT = CThermalSystem(x,y,C,Vol,Ta,W,H,GSR,DR,A,Tin,Vin)
global tsT;
if x==tsT %t already evaluated?
    Q=0;
else %Calculate heat flux between pool and environment
```

```
    t=int16(x);

    qawi=AirWaterInterfaceModel(Ta(t),y,W(t),H(t),GSR(t),DR(t));
    qwr=WaterReplacement(Vin(t),Tin(t),y,C);
    Q=qwr + qawi*A*3600; %W/m2 to J.h
end;
tsT=x;
dT = Q / (C*Vol); %Differential, nett flux into system resulting in
delta T
end
```

9.2.3. AirWaterInterfaceModel Function Code

```
%Dynamic Air Water Interface Thermal Model
%Dylan Bailey
%NMMU MSc 2006
%198443750
function qawi=AirWaterInterfaceModel(Ta,Tw,W,H,GSR,DR)
TaK=Ta+273;
TwK=Tw+273;

%Psychrometrics
SVP=2.718.^(77.3450 + 0.0057.*TaK - 7235./TaK) ./ TaK.^8.2;
%Saturation vapour pressure Pa
PropH=H./100;
VP=SVP.*PropH; %Vapour Pressure Pa
B = (log((VP./100) ./ 6.108)) ./ 17.27;
Td = (237.3 .* B) ./ (1 - B); %Dewpoint Temperature

%Evaporation
eM=0; %Evaporation Model: (0)Meyer or (1)Singh and Xu
if eM==1
a1=0.402/24; %Hourly=(Daily/24)
a2=0.249;
a3=0.018;
else
a1=0.362/24;
a2=0.214;
end;
I=a1.*(1+a2.*W).*(SVP./100-VP./100);%Meyers Formula
if eM==1 I=I.*(1-a3.*(Ta-Td)); end;%Sing and Xu optimisation
Lhvw=2260872; %Latent heat of vaporization for water J/kg
hec=0.00027778; %Scale from hours to seconds
qEair=hec.*Lhvw.*I; %Heat loss due to evaporation W/m2

%Convection
Wk=0.024; %Conductivity air W/m.K
d=1/400;%0.0025; %Characteristic Length A/P m
Nu=Nusselt(d,Tw,Ta,W); %Nusselt determination
qCair = Nu*Wk*((Tw-Ta)/d); %Heat loss due to convection J

%Radiation
SBc=5.67*10^-8; %Stefan-Boltzman Constant
Tsky=0.0552.*TaK.^1.5; %Absolute radiation temperature of sky. Zhu,
wang and deltour
qSky=SBc.*Tsky.^4;
qRwsky=0.97.*SBc.*TwK.^4; %Radiation energy loss to sky. Zhu,wang and
deltour
ew=0.97; %Emissivity of water
psw=0; %Proportion reflectance with sun angle
```

```
qS=GSR.*(1-psw).*ew; %Solar energy gain. Zhu, wang and deltour;
Cathcart and wheaton; Klemetson & Rogers

%Nett Heat Gain
qawi=qS-(qRwsky-qSky)-qCair-qEair;

end
```

9.2.4. WaterReplacement Function Code

```
%Dynamic Water Replacement Thermal Model
%Dylan Bailey
%NMMU MSc 2006
%198443750
function qwr=WaterReplacement(Vin,Tin,Twater,Cwater)
qwr=((Tin+273)*Cwater*Vin)-((Twater+273)*Cwater*Vin);%Heat flux from
water replacement
end
```

9.3. MatLab Vented Hut Pond Model Code

9.3.1. Main Code

```
%Dynamic Pond Thermal Model
%Dylan Bailey
%NMMU 2006 MSc 198443750

clc
%PoolVol=sum(prod(PoolDimensions));
%PoolArea=sum(prod(PoolDimensions(1:2,1:3)));

PEData=WODataImport('PEData 2005.txt',1);
%WOData=WODataImport('UMTATAData 2005.txt',0);

Humidity=PEData{7};
Wind=PEData{2};
Temperature=PEData{6};
GlobalRadiation=PEData{11};
DiffuseRadiation=PEData{12};

uDamping=1; %Wind damping
SolarDamping=1; %Solar Damping

%Humidity=WOData{9};
%Wind=WOData{6};
%Temperature=WOData{5};


PEHumidity=StepMeans(Humidity,12,1);
PEWind=StepMeans(Wind,12,1);
PETemperature=StepMeans(Temperature,12,1);
PERadiation=StepMeans(GlobalRadiation,12,1);
PEDiffuseRadiation=StepMeans(DiffuseRadiation,12,1);

%if sim==1 PERadiation=IdealRadiation; end;
%IdealRadiation=ModelForecast(PERadiation);

PEWind=PEWind.*uDamping;
PERadiation=PERadiation.*SolarDamping;
```

```
Twi=0;
Tw=0;

hold off;
%Model Simulation
global tsT;
[nsn n]=size(PETemperature);
tsT=0;
sn=1;
n=8758;

Tin(1:n)=20;
Vin(1:n)=0;

tstep=sn:1:n;
h=odeset('MaxStep',1);
%Tdp=DPTemperature(tstep);
Ti = [PETemperature(sn) PETemperature(sn) PETemperature(sn)];
%Initial temperature
[t,y] = ode113(@HutThermalSystem, tstep, [Ti], h
,PETemperature,PEWind,PEHumidity,PERadiation.*4000,PEDiffuseRadiation
,Tin,Vin);
%%
hold off
tstep=1:1:336;%729.84 hrs per month
%plot(PETemperature(tstep),'c');
%hold on
plot(y(tstep,:))
Stats=0;
for month=1:12
    hrmnth=floor(n/12);
    step=((hrmnth*(month-1))+1):1:(hrmnth*month);
Stats(1,month)=max(y(step,3));
Stats(2,month)=min(y(step,3));
Stats(3,month)=mean(y(step,3));
Stats(4,month)=std(y(step,3));

Stats(5,month)=max(PETemperature(step));
Stats(6,month)=min(PETemperature(step));
Stats(7,month)=mean(PETemperature(step));
Stats(8,month)=std(PETemperature(step));

end;
```

9.3.2. HutThermalSystem Function Code

```
%1-D Thermal system solved with a system of linear differential
equations.
%Calculates heat fluxes between pool and ambient environment
%Dylan Bailey
%NMMU MSc 2006
%198443750

%Well-ventilated organic material hut model. Assumes inside
temperature and
%humidity same as outside.

%RCSystem ODE
function dy = HutThermalSystem(x,y,Ta,W,H,GSR,DR,Tin,Vin)
global tsT;
```

```
% Constants
HutR=26.6;
He=0.9;

HutRadius=2.5;
HutHeight=2.2;
RoofRadius=HutRadius+0.4;
HutWallOutside = 2 * pi * HutRadius;
HutThickness=0.300;
HutWallInside = 2 * pi * (HutRadius-HutThickness/2);

HutWallOutsideArea=HutWallOutside*HutHeight;
HutWallInsideArea=HutWallInside*HutHeight;

RoofOutsideArea = (pi * RoofRadius) * sqrt(RoofRadius^2 +
RoofRadius^2);
RoofRadius=RoofRadius-HutThickness;
RoofInsideArea = (pi * RoofRadius) * sqrt(RoofRadius^2 +
RoofRadius^2);

RoofVol=RoofInsideArea*HutThickness;
WallVol=HutWallInsideArea*HutThickness;

Density=0.64699/(0.0375*0.42*0.42); %mean mass/mean volume kg/m3,
from experiments
Capacity=(925.21/0.64699); %J/kg.`C, capacity from experiments

if 0
He=0.5;
HutR=1/70;
Capacity=230;%
Density=7300;
RoofVol=RoofOutsideArea*0.002;
WallVol=HutWallOutsideArea*0.002;
end;

HutMass=(RoofVol+WallVol)*Density;
TotalHutCapacity=Capacity*HutMass;
TotalHutInnerArea=RoofInsideArea+HutWallInsideArea;
TotalHutOuterArea=RoofOutsideArea+HutWallOutsideArea;

Cw=4181; %Water specific heat J/kg.K
C=Cw*1000; %One cubic meter water thermal capacity J/K
A=pi*2^2;
Vol=A*1;
SBc=5.67*10^-8; %Stefan-Boltzman Constant
Wk=0.024; %Conductivity air W/m.K
d=1/400; %Characteristic Length A/P m
a1=0.362/24;
a2=0.214;
Lhvw=2260872; %Latent heat of vaporization for water J/kg
hec=0.00027778; %Scale from hours to seconds
uDamp=0.1; %Air movement damping inside hut

if x==tsT %t already evaluated?
    Q1=0;
    Q2=0;
    Q3=0;
else %Calculate heat flux between pool and environment
    t=int16(x);
```

```
ThutOut=y(1);
ThutIn=y(2);
Tw=y(3);
TaK=Ta(t)+273;
TwK=Tw+273;
ThutOutK=ThutOut+273;
ThutInK=ThutIn+273;

%******POND NODE*******

%Psychrometrics
SVP=2.718.^(77.3450 + 0.0057.*TaK - 7235./TaK) / TaK.^8.2;
%Saturation vapour pressure Pa
PropH=H(t)./100;
VP=SVP.*PropH; %Vapour Pressure Pa
B = (log((VP./100) ./ 6.108)) ./ 17.27;
Td = (237.3 .* B) ./ (1 - B); %Dewpoint Temperature

%Evaporation
I=a1.*(1+a2.*W(t).*uDamp).*(SVP./100-VP./100);%Meyers Formula
qEair=hec.*Lhvw.*I; %Heat loss due to evaporation W./m2

%Convection
Nu=Nusselt(d,Tw,Ta(t),W(t).*uDamp); %Nusselt determination
qCair = Nu.*Wk.*((Tw-Ta(t))./d); %Heat loss due to convection J

%Water replacement
qWr=WaterReplacement(Vin(t),Tin(t),Tw,C);

%.*.*.*.*.*.*.*.*.*.*.*Hut Node.*.*.*.*.*.*.*.*.*.*.*.*.*.*.*.*.*.*.*
%Convection outside
Nu=Nusselt(d,ThutOut,Ta(t),W(t)); %Nusselt determination
qCairOut = Nu.*Wk.*((ThutOut-Ta(t))./d); %Heat loss due to convection
J

%Radiation with sky
Tsky=0.0552.*TaK.^1.5; %Absolute radiation temperature of sky. Zhu,
wang and deltour
qhutSky=SBc.*Tsky.^4; %Radiation energy gain from sky
qhutRwsky=He.*SBc.*ThutOutK.^4; %Radiation energy loss to sky.
Zhu,wang and deltour
qS=GSR(t).*He; %Solar energy gain. Zhu, wang and deltour; Cathcart
and wheaton; Klemetson & Rogers

%Convection Inside
Nu=Nusselt(d,ThutIn,Ta(t),W(t).*uDamp); %Nusselt determination
qCairIn = Nu.*Wk.*((ThutIn-Ta(t))./d); %Heat loss due to convection J

%.*.*.*.*.*.*.*.*.*.*Radiation balance between pool and hut
nodes.*.*.*.*.*.*.*.*.*.*.*.*.*
qhutRloss=He.*SBc.*ThutInK.^4;
qWRgain=qhutRloss.*0.97; %Radiation Energy gain from hut

qWRloss=0.97.*SBc.*TwK.^4; %Radiation energy loss to hut. Zhu,wang
and deltour
qhutRGain=qWRloss.*He;

%.*.*.*.*.*.*.*.*.*.*.*Final heat
balance.*.*.*.*.*.*.*.*.*.*.*.*.*.*.*.*.*.*.*.*.*.*.*.*
qHutIO=(ThutOut-ThutIn)/(HutR*HutThickness);
```

```
qPond=qWRgain-qWRloss-qCair-qEair;
qHutOutside=qS.*0.5+qhutSky-qhutRwsky-qCairOut-qHutIO; %Sun covers
only 50% of hut
qHutInside=qHutIO+qhutRGain-qhutRloss-qCairIn;

Q1=qHutOutside.*TotalHutOuterArea.*3600;
Q2=qHutInside.*TotalHutInnerArea.*3600;
Q3=qWr + qPond.*A.*3600; %W./m2 to J.h

end;
tsT=x;
dy(1,1) = Q1 ./ (TotalHutCapacity./2);
dy(2,1) = Q2 ./ (TotalHutCapacity./2);
dy(3,1) = Q3 ./ (C.*Vol); %Differential, nett flux into system
resulting in delta T
end
```

9.4. MatLab Sealed Hut Pond and Solar Heating Model Code

9.4.1. Main Code

```
%Dynamic Pond Thermal Model
%Dylan Bailey
%NMMU 2006 MSc 198443750

clc
%PoolVol=sum(prod(PoolDimensions));
%PoolArea=sum(prod(PoolDimensions(1:2,1:3)));

PEData=WODataImport('PEData 2005.txt',1);
%WOData=WODataImport('UMTATAData 2005.txt',0);

Humidity=PEData{7};
Wind=PEData{2};
Temperature=PEData{6};
GlobalRadiation=PEData{11};
DiffuseRadiation=PEData{12};

uDamping=1; %Wind damping
SolarDamping=1; %Solar Damping

%Humidity=WOData{9};
%Wind=WOData{6};
%Temperature=WOData{5};


PEHumidity=StepMeans(Humidity,12,1);
PEWind=StepMeans(Wind,12,1);
PETemperature=StepMeans(Temperature,12,1);
PERadiation=StepMeans(GlobalRadiation,12,1);
PEDiffuseRadiation=StepMeans(DiffuseRadiation,12,1);

%if sim==1 PERadiation=IdealRadiation; end;
%IdealRadiation=ModelForecast(PERadiation);

PEWind=PEWind.*uDamping;
PERadiation=PERadiation.*SolarDamping;

Twi=0;
Tw=0;
```

```
hold off;
%Model Simulation
global tsT;
[nsn n]=size(PETemperature);
tsT=0;
sn=1;
n=8758;

Tin(1:n)=20;
Vin(1:n)=0;

tstep=sn:1:n;
h=odeset('MaxStep',1);
%Tdp=DPTemperature(tstep);
Ti = [PETemperature(sn) PETemperature(sn) PETemperature(sn)
PETemperature(sn)]; %Initial temperature
[t,y] = ode113(@ClosedHutThermalSystem, tstep, [Ti], h
,PETemperature,PEWind,PEHumidity,PERadiation.*4000,PEDiffuseRadiation
,Tin,Vin);
%%
hold off
tstep=1:1:336;%729.84 hrs per month
%plot(PETemperature(tstep),'c');
%hold on
plot(y(tstep,:))

for month=1:12
    hrmnth=floor(n/12);
    step=((hrmnth*(month-1))+1):1:(hrmnth*month);
Stats(1,month)=max(y(step,4));
Stats(2,month)=min(y(step,4));
Stats(3,month)=mean(y(step,4));
Stats(4,month)=std(y(step,4));

Stats(5,month)=max(PETemperature(step));
Stats(6,month)=min(PETemperature(step));
Stats(7,month)=mean(PETemperature(step));
Stats(8,month)=std(PETemperature(step));

Stats(9,month)=max(y(step,3));
Stats(10,month)=min(y(step,3));
Stats(11,month)=mean(y(step,3));
Stats(12,month)=std(y(step,3));

end;
```

9.4.2. ClosedHutThermalSystem Function Code

```
%1-D Thermal system solved with a system of linear differential
equations.
%Calculates heat fluxes between pool and ambient environment
%Dylan Bailey
%NMMU MSc 2006
%198443750

%Closed poor-ventilated organic material hut model. Assumes inside
humidity
%always 95%

%RCSystem ODE
```

```
function dy = ClosedHutThermalSystem(x,y,Ta,W,H,GSR,DR,Tin,Vin)
global tsT;

% Constants
%Hut Characteristics
HutR=26.6; %Thermal Resistance walls and roof
He=0.9; %Emittance walls and roof

HutRadius=2.5;
HutHeight=2.2;
RoofRadius=HutRadius+0.4;
HutWallOutside = 2 * pi * HutRadius;
HutThickness=0.300;
HutWallInside = 2 * pi * (HutRadius-HutThickness/2);

HutWallOutsideArea=HutWallOutside*HutHeight;
HutWallInsideArea=HutWallInside*HutHeight;

RoofOutsideArea = (pi * RoofRadius) * sqrt(RoofRadius^2 +
RoofRadius^2);
RoofRadius=RoofRadius-HutThickness;
RoofInsideArea = (pi * RoofRadius) * sqrt(RoofRadius^2 +
RoofRadius^2);

RoofVol=RoofInsideArea*HutThickness;
WallVol=HutWallInsideArea*HutThickness;

Density=0.64699/(0.0375*0.42*0.42); %mean mass/mean volume kg/m3,
from experiments
Capacity=(925.21/0.64699); %J/kg.`C, capacity from experiments

HutMass=(RoofVol+WallVol)*Density;
TotalHutCapacity=Capacity*HutMass;
TotalHutInnerArea=RoofInsideArea+HutWallInsideArea;
TotalHutOuterArea=RoofOutsideArea+HutWallOutsideArea;

InnerHutFloorArea=pi*HutRadius^2;
InnerHutVolume=InnerHutFloorArea*HutHeight;
AirCapacity=1.205*1000;
InnerHutCapacity=InnerHutVolume*AirCapacity;

%A few other necessary constants
Cw=4181; %Water specific heat J/kg.K
C=Cw*1000; %One cubic meter water thermal capacity J/K
A=pi*2^2;
Vol=A*1;
SBc=5.67*10^-8; %Stefan-Boltzman Constant
Wk=0.024; %Conductivity air W/m.K
d=1/400; %Characteristic Length A/P m
a1=0.362/24;
a2=0.214;
Lhvw=2260872; %Latent heat of vaporization for water J/kg
hec=0.00027778; %Scale from hours to seconds
uDamp=0.005; %Air movement damping inside hut

if x==tsT %t already evaluated? Then no flux for this run...
    Q1=0;
    Q2=0;
    Q3=0;
    Q4=0;
else %Otherwise, calculate heat flux between pool and environment
```

```
t=int16(x); %Proper time step. Matrix indices need real logical
values.
H(t)=95;

%Extract current temperatures
ThutOut=y(1);
ThutIn=y(2);
ThutAir=y(3);
Tw=y(4);

%Convert temperatures to kelvin
TaK=Ta(t)+273;
TwK=Tw+273;
ThutOutK=ThutOut+273;
ThutInK=ThutIn+273;
ThutAirK=ThutAir+273;

%************Solar Heating************
%Unglazed solar collector 3m2. Simplified solar heating model
SHe=0.35; %Solar efficiency
TSthresh=833; %Threshold GSR for thermosiphon to start
TSrate=70/3333; %Flow rate with GSR
SHSA=3; %Solar Heater Surface Area
SHWV=0.002*SHSA; %Water volume of solar collector in m3
if GSR(t)>TSthresh Win=(GSR(t).*TSrate)/1000; %Flow rate once GSR
threshold is met
else
    Win=0;
end;
qSHin=GSR(t).*0.9.*SHSA; %q input into solar collector
qWg=(qSHin*SHe)/SHWV; %Energy gain per m3 w/m3
qWr=qWg*Win; %Nett energy gain to pond W

%if Tw>25 qWr=0;
%end;

%******POND NODE FLUXES*******

%Psychrometrics
SVP=2.718.^(77.3450 + 0.0057.*ThutAirK - 7235./ThutAirK) /
ThutAirK.^8.2; %Saturation vapour pressure Pa
PropH=H(t)./100;
VP=SVP.*PropH; %Vapour Pressure Pa
B = (log((VP./100) ./ 6.108)) ./ 17.27;
Td = (237.3 .* B) ./ (1 - B); %Dewpoint Temperature

%Evaporation
I=a1.*(1+a2.*W(t).*uDamp).*(SVP./100-VP./100);%Meyers Formula
qEair=hec.*Lhvw.*I; %Heat loss due to evaporation W./m2

%Convection
Nu=Nusselt(d,Tw,ThutAir,W(t).*uDamp); %Nusselt determination
qCair = Nu.*Wk.*((Tw-ThutAir)./d); %Heat loss due to convection J

%.*.*.*.*.*.*.*.*.*.*.*Hut Node
Fluxes.*.*.*.*.*.*.*.*.*.*.*.*.*.*.*.*.*.*.*.*
%Convection outside
Nu=Nusselt(d,ThutOut,Ta(t),W(t)); %Nusselt determination
qCairOut = Nu.*Wk.*((ThutOut-Ta(t))./d); %Heat loss due to convection
J
```

```
%Radiation with sky
Tsky=0.0552.*TaK.^1.5; %Absolute radiation temperature of sky. Zhu,
wang and deltour
qhutSky=SBc.*Tsky.^4; %Radiation energy gain from sky
qhutRwsky=He.*SBc.*ThutOutK.^4; %Radiation energy loss to sky.
Zhu,wang and deltour
qS=GSR(t).*He; %Solar energy gain. Zhu, wang and deltour; Cathcart
and wheaton; Klemetson & Rogers

%Air Replacement
qAr=(TaK*AirCapacity*(W(t)*uDamp*InnerHutFloorArea))-
(ThutAirK*AirCapacity*(W(t)*uDamp*InnerHutFloorArea));%Heat flux from
air replacement

%Convection Inside
Nu=Nusselt(d,ThutIn,ThutAir,W(t).*uDamp); %Nusselt determination
qCairIn = Nu.*Wk.*((ThutIn-ThutAir)./d); %Heat loss due to convection
J

%.*.*.*.*.*.*.*.*.*Radiation balance between pool and hut
nodes.*.*.*.*.*.*.*.*.*.*.*.*
%From hut to pool
qhutRloss=He.*SBc.*ThutInK.^4; %Radiation energy lost from hut
qWRgain=qhutRloss.*0.97; %Radiation energy gain to pool

%From pool to hut
qWRloss=0.97.*SBc.*TwK.^4; %Radiation energy loss from pool
qhutRGain=qWRloss.*He; %Radiation energy gain to hut

%.*.*.*.*.*.*.*.*.*.*Final heat
balance.*.*.*.*.*.*.*.*.*.*.*.*.*.*.*.*.*.*.*.*.*.*
qHutIO=(ThutOut-ThutIn)/(HutR*HutThickness);
qPond=qWRgain-qWRloss-qCair-qEair;
qHutOutside=qS.*0.5+qhutSky-qhutRwsky-qCairOut-qHutIO; %Sun covers
only 50% of hut
qHutInside=qHutIO+qhutRGain-qhutRloss-qCairIn;

Q1=qHutOutside.*TotalHutOuterArea.*3600;
Q2=qHutInside.*TotalHutInnerArea.*3600;
Q3=(qAr+qCairIn.*TotalHutInnerArea+qCair.*A).*3600;
Q4=(qWr + qPond.*A).*3600; %W./m2 to J.h

end;
tsT=x;
dy(1,1) = Q1 ./ (TotalHutCapacity./2);
dy(2,1) = Q2 ./ (TotalHutCapacity./2);
dy(3,1) = Q3 ./ InnerHutCapacity;
dy(4,1) = Q4 ./ (C.*Vol); %Differential, nett flux into system
resulting in delta T
end
```